Foxo3-mediated physiological cell competition ensures robust tissue patterning throughout vertebrate development

(Foxo3 を介した生理的な細胞競合が、
脊椎動物個体における発生ロバストネスを支える)

by

Kanako Matsumoto

A Dissertation
Submitted to the Graduate School of Science
Osaka University
In partial fulfillment for the degree of Ph.D.

January 2025

Table of contents

1. Abbreviation

ANOVA: Analysis of variance

BMP: Bone morphogenetic protein

Cas9: CRISPR-associated protein 9

cDNA: Complementary DNA

Cdon: Cell-adhesion molecule-related/down-regulated by Oncogenes

CRISPR: Clustered regularly interspaced short palindromic repeats

DIG: Digoxigenin

DMSO: Dimethyl sulfoxide

dpf: Day post-fertilisation

d2EGFP: Destabilized enhanced green fluorescent protein

DV: Dorsoventral

ELuc: Emerald luciferase

Epi: Epiblast

ExE: Extra-embryonic ectoderm

FITC: Fluorescein isothiocyanate

Foxo3: Forkhead Box Protein O3

HCR: Hybridisation chain reaction

hpf: Hour post-fertilisation

KO: Knockout

KSOM: Potassium simplex optimised medium

MO: Morpholino oligos

mRNA: Messenger RNA

NAC: N-acetyl-l-cysteine

ns: Not significantly different

OTM: Optimal TCF motif

PBS: Phosphate-buffered saline

PBST: Triton X-100 in PBS

Pcdh19: Protocadherin 19

PCR: Polymerase chain reaction

Ptch1: Patched

Puma: p53 upregulated modulator of apoptosis

qPCR: Quantative polymerase chain reaction

RNA-seq: RNA-sequence

ROS: Reactive oxygen species

SBE: Smad binding element

SEM: Standard error of the mean

sgRNA: Single guide RNA

Shh: Sonic Hedgehog

Smo: Smoothened

Tg: Transgenic

TGF-β: Transforming growth factor-β

TSS: Transcription start site

VisEn: Visceral endoderm

2. Abstract

Unfit cells with defective signalling or gene expression are eliminated through competition with neighbouring cells. However, the physiological roles and mechanisms of cell competition in vertebrate remain unclear. In addition, the universal mechanisms regulating diverse cell competition are unknown. By zebrafish imaging analyses, we reveal that cell competition ensures robust patterning of spinal cord and muscle through elimination of cells with unfit sonic hedgehog-activity, driven by cadherin-mediated communication between unfit and neighbouring fit cells and subsequent activation of the Smad-Foxo3-reactive oxygen species axis. We identify Foxo3 as a common marker of loser cell in various types of cell competition in zebrafish and mice. Foxo3-mediated physiological cell competition is required to eliminate various naturally generated unfit cells and the consequent precise patterning during zebrafish embryogenesis and organogenesis. Given the implication of Foxo3 downregulation in age-related diseases, cell competition may be a defence system to prevent abnormalities throughout development and adult homeostasis.

3. Publication List

Paper

This dissertation contains matrial from the following paper:

(1) **Matsumoto, K.**[#], Akieda, Y.[#], Haraoka, Y., Hirono, N., Sasaki, H. & Ishitani, T. Foxo3-mediated physiological cell competition ensures robust tissue patterning throughout vertebrate development. *Nature Communications*, **15**, 10662 (2024) doi: 10.1038/s41467-024-55108-x

[#] These authors contributed equally to this work.

I am preparing a Review article submission related to the above research theme as follows:

(2) **Matsumoto, K.**, & Ishitani, T.

The longevity factor Foxo3 mediates "unfit" cell elimination to ensure healthy body construction. *Cell Structure and Function* (2025)

Others

I have contributed to several other papers and books during my Ph.D., but since they cover different topics, they are not included as part of this dissertation.

(1) Murakami, A., Kawamura, K. [#], **Matsumoto, K.** [#], Okamura, H. & Tominaga, K. "Circadian clock couples to maternal behavior but not feeding behavior in lactating mice." *iScience*, under revision

[#] These authors contributed equally to this work.

(2) Atala, A. & Zhang, Y. (Eds.) *Body-on-a-Chip: Essentials and Applications* (to be published June 15th, 2025), ISBN-13: 978-0443161100

Chapter6 - Recent Trends in Microfluidic Platform for Body-on-a-chip systems Takayama, S. (Senior Author), Kamei, K., **Matsumoto, K.**, Matsunaga, Y., Park M.

* Authors are listed in alphabetical order by last name.

Once again, these are **NOT** included in this dissertation.

4. Introduction

4.1 Background

Animal development is highly reproducible and repeatedly generates tissues and organs with the same function. An appropriate number of cells with specific functions must be located at the correct positions to construct functional tissues and organs. Such spatial cell arrangements are regulated by genetic information and the corresponding biochemical signals[1,2]. For instance, the classic French-flag model posists that activity gradients of morphogen signalling, such as Wnt/β-catenin, sonic hedgehog (Shh), bone morphogenetic protein (BMP), fibroblast growth factor (FGF) and nodal signalling pattern developing tissues and axes[1,3] (Fig 4.1.1).

However, dynamic morphogenesis, including active rapid cell proliferation, migration, and rearrangement during development, may induce replication errors and cellular signalling perturbations, generating unfit cells in developing tissues. Recent advances in single-cell analyses have revealed frequent generation of cells with somatic mutations or chromosome segregation errors during normal human and mouse embryogenesis[4–7]. Our previous zebrafish imaging analysis also showed frequent occurrence of unfit cells with abnormal Wnt/β-catenin activity in normal embryos[8]. Considering the fact that developing animals achieve reproducible construction of functional tissues and organs, they must possess systems to overcome the generation of such unfit cells. However, the mechanisms underlying robust tissue development are not completely understood.

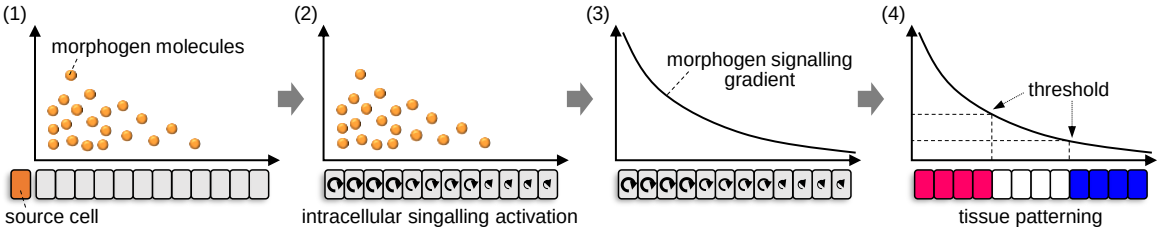

Fig 4.1.1: Wolpert's classical French-flag model.

(1) Morphogen secretion: Source cells secrete morphogen molecules, which diffuse across the tissue.
(2) Signal reception and interpretation: Cells within the tissue respond the morphogen molecules and activate intracellular signalling in a concentration-dependent manner.
(3) Gradient formation: Over time, a stable morphogen signalling gradient across the tissue is formed.
(4) Cell fate determination: Based on their position within the gradient, cells adopt different fates, resulting in a spatial pattern within the tissue.

4.2 Overview of cell competition

Cell competition may support conquering unfit cell appearance during animal development. Cell competition is a cell-cell interactive process in which cells with relatively higher fitness eliminates those with lower fitness. Cells with lower fitness are viable in a homogeneous population; however, when these populations are mixed, the less-fit cells are selectively removed from the population. This phenomenon was first described by Morata and Ripoll nearly 50 years ago, while they were studying the effects of heterozygous ribosomal protein gene mutations, also known as 'Minute' mutations, in *Drosophila*. Flies homozygous for the mutation (*M/M*), lacking both alleles of Minute gene, were lethal. However, heterozygous mutant flies (*M/+*) were viable despite a developmental delay due to their slower proliferation rate, and they were able to develop into fully functioning organisms. Interestingly, while *M/+* cells survived in non-mosaic conditions, they were progressively eliminated in mosaic flies when wild-type (+/+) cells were also present in growing tissues. Further studies revealed that *M/+* cells undergo caspase-dependent apoptotic elimination when in contact with wild-type cells[9] . These findings indicate that cells can compare their fitness with neighbouring cells, and subsequently remove less-fit cells (Fig. 4.2.1).

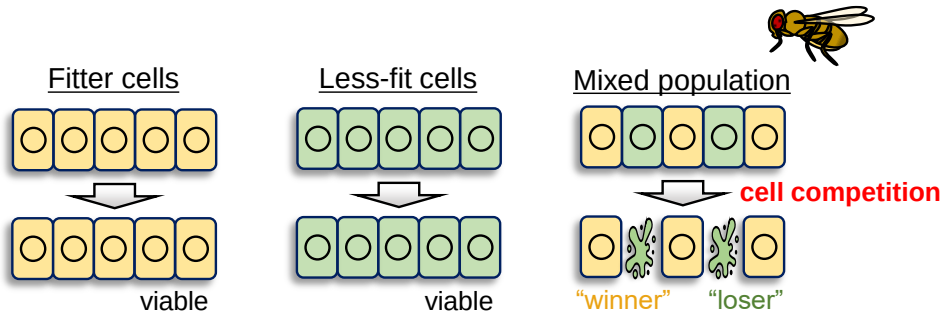

Fig 4.2.1: The basics of cell competition.
During cell competition, less-fit cells, which would be viable in a homogenous environment, are eliminated when surrounded by their fitter counterparts.

4.3 Supercompetition

Support for the idea that cell competition is based on relative fitness, rather than absolute fitness, comes from the discovery of 'supercompetition,' a phenomenon where even wild-type cells are outcompeted by fitter neighbors. This was first demonstrated in the *Drosophila* imaginal wing disc, where Myc-overexpressing (Myc-high) cells induced apoptosis in surrounding wild-type (Myc-low) cells[10,11]. Conversely, wild-type (Myc-high) cells can eliminate Myc mutant (Myc-low) cells in mosaics[12]. These results emphasize that the outcome of cell competition is driven by relative fitness differences between competing cells.

4.4 Cell competition as a tumour-supression mechanism

Cell competition phenomena have also been observed in mammalian cultured cells. Notably, mammalian epithelia can eliminate sporadically emerging oncogenic cells through communication with neighbouring normal cells. In Madin–Darby canine kidney (MDCK) cell cultures, mosaically introduced oncogenic cells with abnormal Ras and Src activities were apically extruded via interaction with the surrounding normal cells[13,14]. This neighbouring cells-mediated elimination of oncogenic cells is termed epithelial defence against cancer (EDAC)[15]. Collectively, these findings suggest that cell competition is evolutionarily conserved from insects to mammals. However, most studies on cell competition have been conducted using *Drosophila* and cultured cells. Moreover, these studies typically rely on genetic models that overexpress or mutate specific genes. Consequently, the understanding of 'physiological cell competition', especially in vertebrates, remains elusive.

4.5 Cell competition supports robust early embryogenesis

Recent studies have been gradually revealing that cell competition plays a critical role in vertebrate early embryonic development. In the mouse pre-implantation epiblast, TEAD and its co-activator YAP are essential for maintaining pluripotency. Over time, nuclear YAP levels become highly variable among cells in the embryo. Cells with relatively low

nuclear YAP levels spontaneously emerge but are eliminated through competitive interactions with neighbouring, fitter cells[16]. Similarly, in the post-implantation epiblast, unfit cells with relatively low Myc expression or mitochondrial defects spontaneously arise during early mouse embryogenesis; however, these cells are also removed through cell competition[17,18]. Furthermore, cell competition corrects the noisy Wnt/β-catenin morphogen gradient, which patterns the zebrafish embryonic anterior–posterior axis, by eliminating cells with abnormally high or low Wnt/β-catenin[8]. Notably, inhibition of cell competition induces the accumulation of Wnt-unfit cells, thereby disturbing embryonic patterning[8]. These findinds have highlightened the roles of cell competition during robust early embryogenesis. However, while the functions of cell competition in undifferentiated embryonic cells are becoming clear, the roles and mechanisms of cell competition in differentiating cells, such as those whitin organs where pluripotency is significantly reduced, remain unclear.

4.6 Molecular mechanisms of cell competition

Various factors, such as cells with abnormal Myc, YAP, Wnt/β-catenin, and Ras activity, or mutations in ribosomal protein genes/Minute drive competitive interactions with neighbouring normal cells[8,13,14,16–20]. Because different abnormalities can stimulate distinct signalling and gene expression pathways, unfit cells with different anomalies are eliminated through distinct mechanisms. Interstingly, recent studies on *Drosophila* have revealed shared mechanisms of cell competition. For example, activation of Flower-Azot signalling[21,22], Toll receptor signalling[23,24], and autophagy[25] is commonly involved in Myc- and Minute-induced cell competition. However, these mechanisms do not always function in other competition contexts[22,26]. Thus, it remains unknown whether a universal machinery exists that regulates diverse types of cell competition or whether distinct systems are employed depending on the context.

4.7 Contribution of this dissertation

In this study, we explored the role of physiological cell competition and the conserved machinery involved in vertebrate development using zebrafish imaging. We discovered cell competition-mediated correction of sonic hedgehog (Shh) morphogen gradients as previously unidentified roles of physiological cell competition during organogenesis in differntiating cells and deciphered that Cadherin-Smad-Foxo3-reactive oxygen species (ROS) signalling mediates this cell competition. Moreover, we identified Foxo3 as an evolutionally conserved common marker of unfit cells eliminated by various vertebrate cell competitions driven by Wnt, Shh, Ras, Myc, Yap, and ribosomal proteins. By analysing Foxo3 expression and function, we found that physiological cell competition-mediated elimination of endogenous unfit cells is essential in precise embryogenesis and organogenesis in vertebrates.

5. Results

5.1 Apoptosis supports precise neural and muscle patterning

We examined the effects of apoptosis inhibition on the spinal cord and muscle development in zebrafish to elucidate the role of cell competition-mediated apoptotic elimination of unfit cells during organogenesis. In the vertebrate spinal cord, various neural progenitor cells (e.g. p0, pMN, and floor plate) distinguished by specific transcription factors (*dbx1b*, *olig2*, and *foxa2*, respectively)[27–31] form stripe-like patterns along the dorsoventral (DV) axis (Fig. 5.1.1 a, b). In zebrafish muscle primordia, slow muscle precursors are at the periphery of the somites, whereas fast muscle precursors are located on the medial side[32]. Muscle pioneer cells are adjacent to the notochord[33] (Fig. 5.1.1 c, d). Inhibiting apoptosis by overexpressing *bcl2a* mRNA, which encodes an anti-apoptotic protein, induced ectopic expression of the intermediate neural marker *dbx1b* and the ventral neural markers *olig2* and *foxa2* in the ventral and dorsal areas, respectively (Fig. 5.1.1 b). Abnormal reductions in these markers were also observed (Fig. 5.1.1 b). In the muscle primordium, the precise induction of fast and slow muscle fibres and muscle pioneer cells was disturbed, and some of these were mislocated (Fig. 5.1.1 e-g). Consistent with this abnormal neural and muscle patterning, some apoptosis-inhibited larvae exhibited abnormal morphogenesis (Fig. 5.1.1 h), and even morphologically normal larvae showed poor locomotion (Fig. 5.1.1 i). We also generated a transgenic zebrafish line carrying HS:GFP-zBcl2a, which inhibited apoptosis in a heat shock-dependent manner (Fig. 5.1.2 a) to examine the role of apoptotic elimination during organogenesis. Blocking apoptosis during organogenesis also induced organ patterning distortion (Fig. 5.1.1 b, c), suggesting that apoptosis is required for precise spinal cord and muscle patterning.

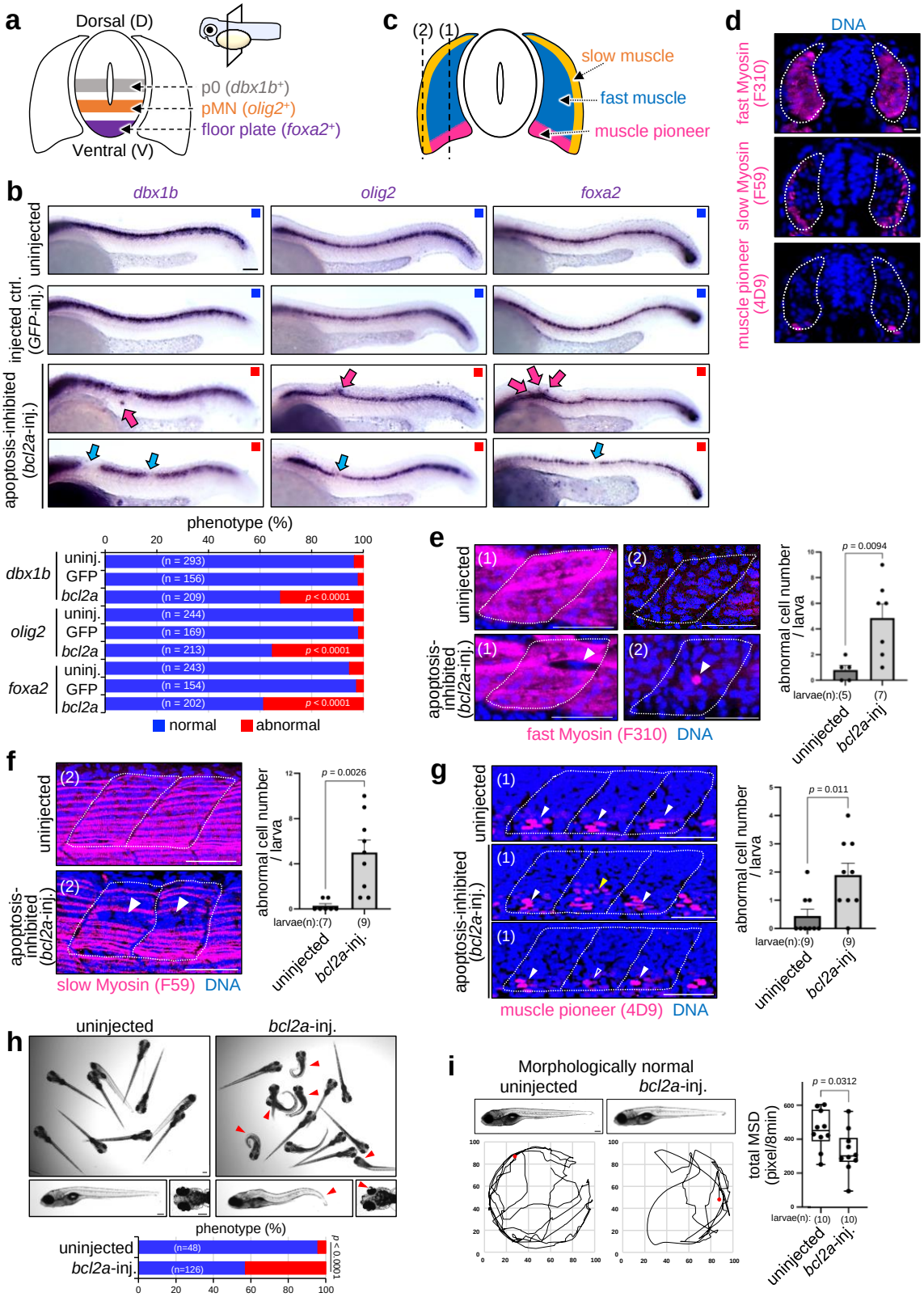
a
Dorsal (D)
Ventral (V)
p0 (dbx1b+)
pMN (olig2+)
floor plate (foxa2+)
c
(2) (1)
slow muscle
fast muscle
muscle pioneer
d
DNA
fast Myosin (F310)
slow Myosin (F59)
muscle pioneer (4D9)
b
dbx1b
olig2
foxa2
uninjected
injected ctrl. (GFP-inj.)
apoptosis-inhibited (bcl2a-inj.)
phenotype (%)
uninj.
GFP
bcl2a
(n = 293)
(n = 156)
(n = 209)
p < 0.0001
(n = 244)
(n = 169)
(n = 213)
(n = 243)
(n = 154)
(n = 202)
normal
abnormal
e
uninjected
apoptosis-inhibited (bcl2a-inj.)
fast Myosin (F310) DNA
p = 0.0094
abnormal cell number / larva
larvae(n):(5) (7)
uninjected
bcl2a-inj.
f
slow Myosin (F59) DNA
p = 0.0026
larvae(n):(7) (9)
g
muscle pioneer (4D9) DNA
p = 0.011
larvae(n):(9) (9)
h
uninjected
bcl2a-inj.
phenotype (%)
(n=48)
(n=126)
p < 0.0001
i
Morphologically normal
total MSD (pixel/8min)
p = 0.0312
larvae(n): (10) (10)

Fig 5.1.1: Apoptosis is essential for precise spinal cord and muscle patterning.
a Schematic illustration of the expression patterns of *dbx1b* (a p0 neural progenitor marker), *olig2* (a pMN neural progenitor marker), and foxa2 (a floor plate progenitor marker) in the spinal cord. **b** Inhibiting apoptosis distorts dorso-ventral (DV) patterning in the spinal cord. The panels show whole-mount in situ hybridisation of *dbx1b*, *olig2*, and *foxa2* in wild-type (uninjected), injected control (*GFP* mRNA-injected) and apoptosis-inhibited (*bcl2a* mRNA-injected) 24 hours post-fertilisation (hpf) larvae. In abnormal larvae, *dbx1b*, *olig2*, and *foxa2* were ectopically activated or inactivated in discontinuous regions. The bottom graph shows the percentages of larvae with normal or abnormal expression patterns in uninjected, *GFP* mRNA- or *bcl2a* mRNA-injected (apoptosis-inhibited) larvae. Scale bar = 100 μm. The chi-square test was used for statistical analysis. **c** Schematic illustration of muscle cell pattern. The labels (1) and (2) in **e-g** correspond to the images of sections indicated as (1) and (2) in **c**. **d** Representative confocal images show whole-mount immunostaining of fast myosin (F310), slow myosin (F59), or muscle pioneer (4D9) (magenta) in dorsal muscle primordia. Scale bar = 10 μm. **e-g** Apoptosis inhibition distorts gene expression patterns in the muscle primordia. The panels show whole-mount immunostaining for fast myosin (F310, fast muscle cells) (**e**), slow myosin (F59, slow muscle cells) (**f**), and muscle pioneer (4D9, muscle pioneer cells) (**g**), respectively (magenta). In abnormal larvae, fast myosin, slow myosin, and muscle pioneer proteins are ectopically expressed or are absent. Scale bar = 100 μm. Bar plots on the right show the mean + SEM of abnormal gene expressing-cell numbers in wild-type (uninjected) and apoptosis-inhibited larvae. An unpaired two-tailed *t*-test was used for the statistical analysis. **h** Apoptosis inhibition induces abnormal morphogenesis. The images show 5 days post-fertilisation (dpf) zebrafish larvae uninjected or injected with *bcl2a* mRNA (100 pg). Scale bar = 200 μm. Red arrows highlight the Shh-defectiveness-related phenotypes (e.g., shortened trunk and reduced eye size). The percentages of larvae with normal or abnormal morphology are graphed. The chi-square test was used. **i** Inhibiting apoptosis induces decreased locomotion. The images show 5 dpf control and apoptosis-inhibited larvae. Scale bar = 200 μm. Externally normal individuals were used in locomotion analysis. The bottom panels show the representative trajectories of control and apoptosis-inhibited larvae. The box plot shows the total mean square displacement (MSD) of each sample. Maximum and minimum: whiskers; medians: lines; 25^{th} and 75^{th} percentiles: boxes. Each dot represents one larva. An unpaired two-tailed *t*-test was used.

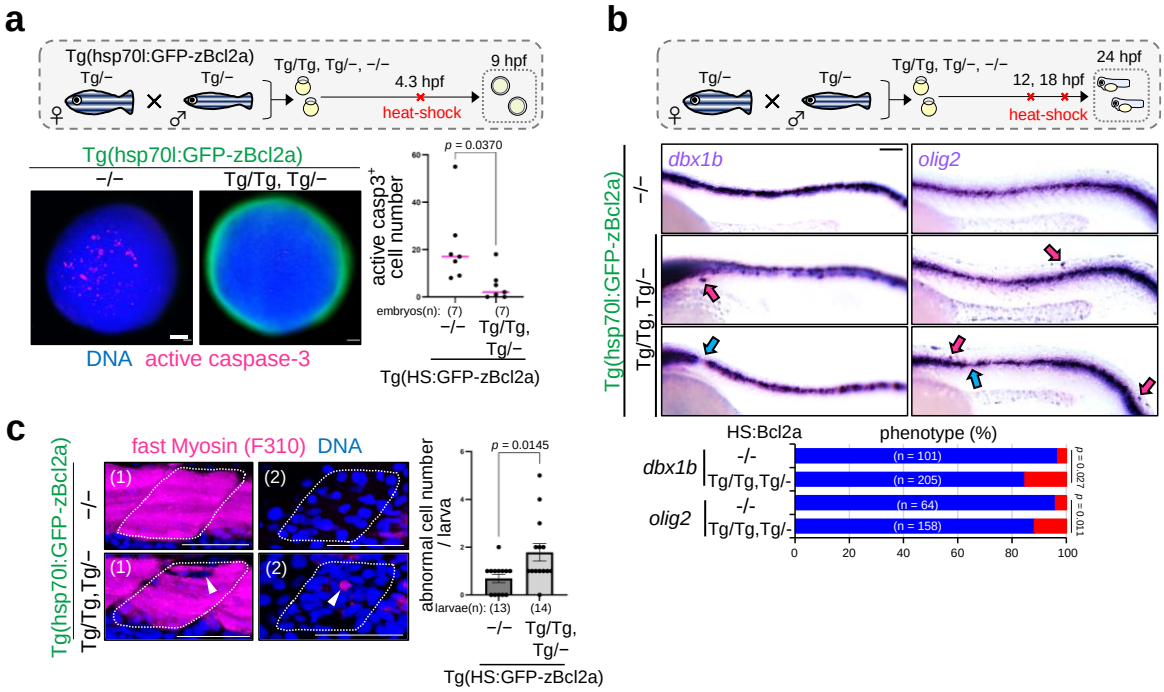

Fig 5.1.2: Blocking apoptosis during organogenesis also induce organ patterning distortion.

a Transient expression of Bcl2a inhibits apoptosis. Heterozygous Tg(hsp70l:GFP-zBcl2a) transgenic males and females were crossed. Collected embryos were exposed to heat-shock at 4.3 hpf and then collected at 9 hpf. Confocal images show active caspase-3 (magenta) in homozygote or heterozygote Tg(hsp70l:GFP-zBcl2a) mutants (Tg/Tg, Tg/-) versus their wild-type (-/-) siblings (green) (anterior to the top, ventral to the left). Scale bar = 100 μm. The caspase-3 active cell frequencies of each embryo are graphed. An unpaired two-tailed *t*-test was used. **b, c** Transient inhibition of apoptosis during organogenesis distorts the spinal cord (**b**) and muscle (**c**) patterning. Heterozygous Tg(hsp70l:GFP-zBcl2a) transgenic males and females were crossed. Collected embryos were exposed to heat shock at 12 and 18 hpf and collected at 24 hpf. Representative images showing the whole-mount in situ hybridisation of *dbx1b* and *olig2* (**b**) and immunostaining for fast myosin (**c**) in homozygote or heterozygote Tg(hsp70l:GFP-zBcl2a) mutants (Tg/Tg, Tg/-) versus their wild-type (-/-) siblings. Scale bar = 100 μm. The bottom graph in **b** shows the percentages of larvae with normal or abnormal expression patterns. The chi-square test was used for statistical analysis. The right graph in **c** shows the number of abnormal cells in each larva. An unpaired two-tailed *t*-test was used for the statistical analysis.

5.2 Shh-unfit cells undergo apoptotic elimination

Shh morphogen signalling forms an activity gradient along the DV axis and specifies the distinct fate of each cell in a signalling activity-dependent manner in the developing spinal cord and muscle primordia (Fig. 5.2.1 a)[33–36]. Therefore, we hypothesized that apoptosis eliminates abnormal cells with unfit Shh-activity during neural and muscle development. To test this hypothesis, we visualized Shh signalling in the Tg(8xGBS:d2EGFP) zebrafish line, which expresses destabilized enhanced green fluorescent protein (d2EGFP) upon activating the Gli transcription factor family downstream of Shh signalling[37] (Fig. 5.2.1 b). Unfit cells with abnormally high or low Shh signalling activity appeared spontaneously in the Shh activity-low (dorsal) or Shh activity-high (ventral) regions of the spinal cord and muscle primordia, respectively (Fig. 5.2.1 c, d). The number of unfit cells varied between larvae (left graphs in Fig. 5.2.1 e, f), suggesting that the appearance of these cells is not part of the developmental program but is the result of an error in the program. In addition, 38% of unfit cells (n = 11/29) in the spinal cord and 31% of unfit cells (n = 10/32) in the muscle were active caspase-3-positive (Fig. 5.2.1 c, d), suggesting that they undergo apoptosis. Moreover, apoptosis inhibition through *blc2a* overexpression blocked Shh-unfit cell elimination and enhanced their accumulation (Fig. 5.2.1 c-f). These data indicate that the apoptotic elimination of Shh-unfit cells is necessary for robust Shh morphogen gradient formation and precise neural and muscle patterning.

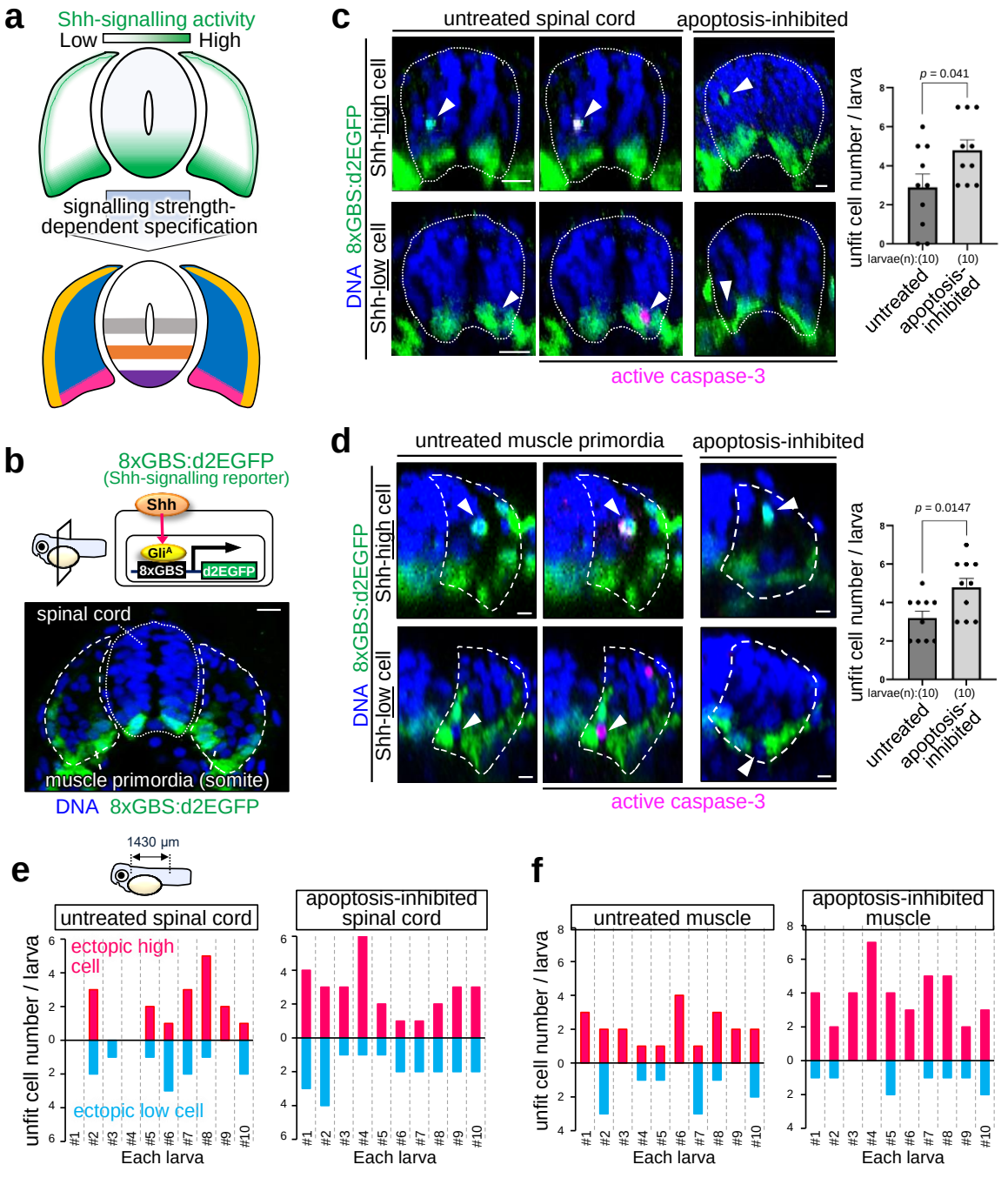

Fig 5.2.1: Shh-unfit cells are apoptotically eliminated.
a The strength of Shh signalling activity mediates distinct cell types specification in the spinal cord and muscle. **b** In a horizontal plane, 8xGBS:d2EGFP drives destabilised enhanced green fluorescent protein (d2EGFP) expression in response to Shh signalling activation in the developing spinal cord and muscle of reporter larvae (cross-sectional view with the dorsal on top, 24 hpf). The dotted line and dashed line represent the spinal cord and muscle primordia boundaries, respectively. Scale bar = 10 µm. **c, d** Caspase-3 activation in cells with impaired

Shh signalling activity during spinal cord (**c**) and muscle development (**d**). Whole-mount immunostaining of d2EGFP (green) horizonal plane and active caspase-3 (magenta) in Tg(8xGBS:d2EGFP) zebrafish larvae untreated or apoptosis-inhibited (*bcl2a* mRNA-injected). Arrowheads indicate cells with abnormal Shh signalling-reporter activity. Scale bar = 10 μm. The bar plots show the mean + SEM of unfit cell frequencies in untreated and apoptosis-inhibited larvae. An unpaired two-tailed t-test was used for the statistical analysis. **e, f** Inhibiting apoptosis enhances the Shh-unfit cell accumulation in the spinal cord (**e**) and muscle (**f**). The bar plots show unfit cell frequencies in untreated and apoptosis-inhibited larvae. Each larva has a different number of spontaneously appearing unfit cells with abnormally high or low Shh signalling activity.

5.3 Substantial difference in Shh-activity triggers apoptosis

We artificially introduced Shh-unfit cells expressing fluorescent proteins (e.g. mKO2 or GFP) into the zebrafish spinal cord and muscle primordia by injecting heat-shock-driven expression plasmids to confirm that developing organs possess a system for eliminating cells with unfit Shh activity through apoptosis. A low-dose injection of the plasmids induces a mosaic distribution of fluorescent cells surrounded by normal cells (Fig. 5.3.1 a). Shh-hyperactivated cells expressing constitutively active mutants of the Shh receptor Smoothened (SmoCA) and Shh-inactivated cells expressing the Shh negative regulator Ptch1 activated caspase-3, which gradually disappeared via DNA fragmentation. In contrast, cells expressing only mKO2 survived (Fig. 5.3.1 b-f). Bcl2a co-expression prevented SmoCA-expressing cell elimination (Fig. 5.3.1 d). Thus, developing organs can eliminate spontaneously appeared and artificially introduced Shh-defective cells. Furthermore, mosaically introduced SmoCA-expressing (Shh-high) cells or Ptch1-overexpressing (Shh-low) cells efficiently activated caspase-3 in the Shh signalling-low dorsal and signalling-high ventral regions, respectively (Fig. 5.3.2 a, b). These results suggest that a substantial difference in Shh activity between unfit and neighbouring normal cells triggers apoptosis. Forced Shh signalling activation through *SmoCA* expression or forced Shh signalling inactivation via treatment with the Shh signalling inhibitor Cylopamine[38] in whole tissues (Fig. 5.3.2 c, d) hindered Shh-high and Shh-low cells elimination, respectively (Fig. 5.3.2 e, f). These results indicate that a large difference in Shh signalling activity between unfit cells and neighbouring fit cells is essential to trigger unfit cell apoptosis. Intriguingly, when SmoCA-expressing (Shh-high) cells were clonally induced on the dorsal side of spinal cord, those at the clone's edge, surrounded by normal cells, underwent apoptosis efficiently (Fig. 5.3.2 g, h). However, the apoptosis efficiency in these cells decreased as the proportion of SmoCA cells in the surrounding adjacent cell population increased, and SmoCA cells inside the clone didn’t die (Fig. 5.3.2 g, h). These results suggest that simply being adjacent to cells with different Shh signalling activity is not enough to induce unfit cell apoptosis but being surrounded by cells with different signalling activity (being a minority in the population) is necessary for unfit cell death

induction. Notably, mosaic introduction of cells overexpressing the transcription factor Gli1 or the dominant negative form of the Gli3 transcription factor (Gli3R), which positively or negatively regulate Shh-target genes, respectively, could not activate caspase-3 (Fig. 5.3.1 b). As Smo and Ptch1 are transmembrane proteins, whereas Gli1 and Gli3 are signalling mediators that act in the cytoplasm and nucleus, the abnormal activity of Shh signalling at the membrane appears to trigger unfit cell elimination.

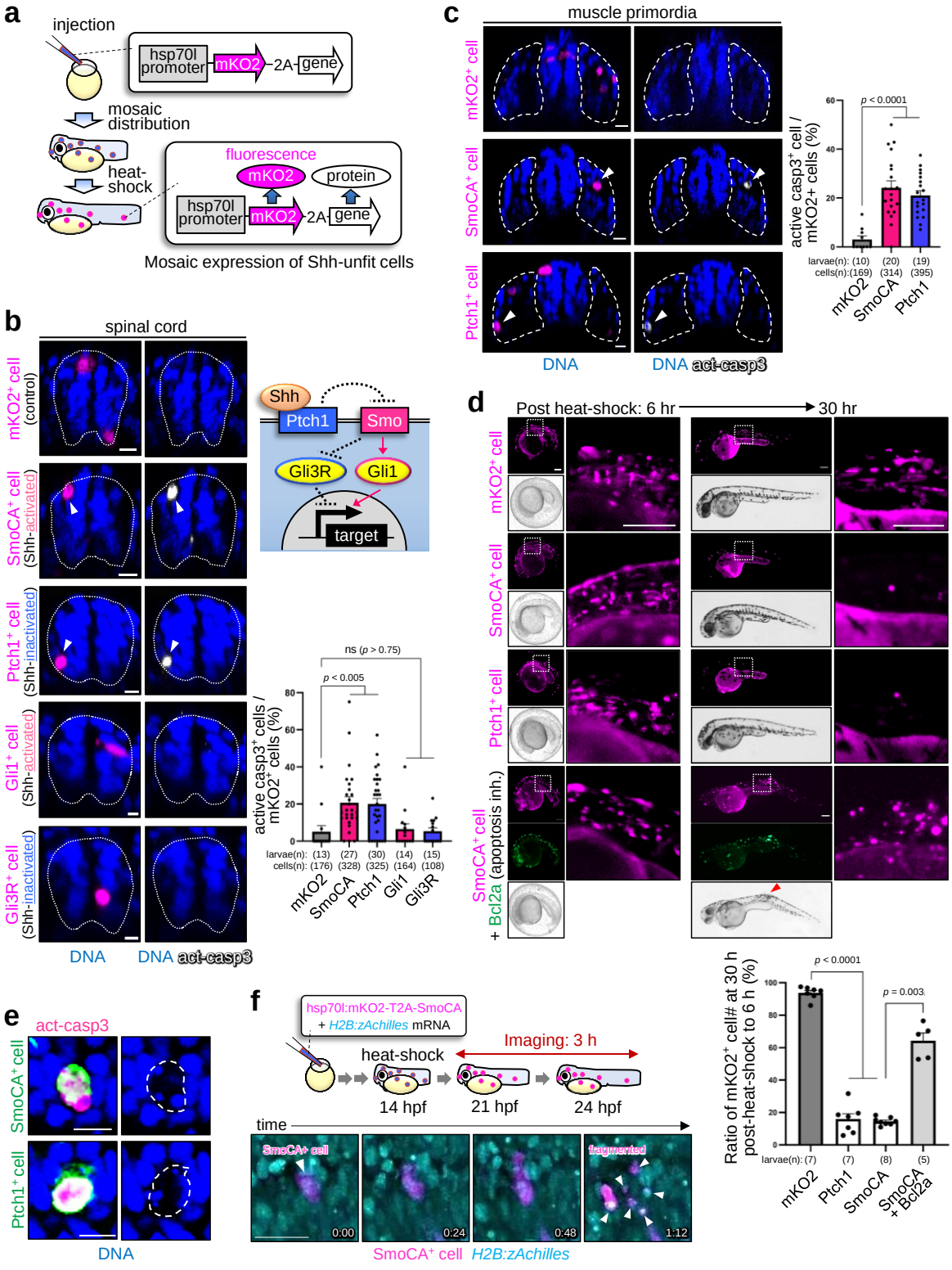
a
injection
hsp70l promoter
mKO2
2A-
gene
mosaic distribution
heat-shock
fluorescence
protein
Mosaic expression of Shh-unfit cells
b
spinal cord
mKO2+ cell (control)
SmoCA+ cell (Shh-activated)
Ptch1+ cell (Shh-inactivated)
Gli1+ cell (Shh-activated)
Gli3R+ cell (Shh-inactivated)
DNA
DNA act-casp3
Shh
Ptch1
Smo
Gli3R
Gli1
target
ns (p > 0.75)
p < 0.005
active casp3+ cells / mKO2+ cells (%)
larvae(n): (13) (27) (30) (14) (15)
cells(n): (176) (328) (325) (164) (108)
mKO2
SmoCA
Ptch1
Gli1
Gli3R
c
muscle primordia
mKO2+ cell
SmoCA+ cell
Ptch1+ cell
DNA
DNA act-casp3
p < 0.0001
active casp3+ cell / mKO2+ cells (%)
larvae(n): (10) (20) (19)
cells(n):(169) (314) (395)
mKO2
SmoCA
Ptch1
d
Post heat-shock: 6 hr
30 hr
mKO2+ cell
SmoCA+ cell
Ptch1+ cell
SmoCA+ cell + Bcl2a (apoptosis inh.)
e
act-casp3
SmoCA+ cell
Ptch1+ cell
DNA
f
hsp70l:mKO2-T2A-SmoCA + H2B:zAchilles mRNA
heat-shock
Imaging: 3 h
14 hpf
21 hpf
24 hpf
time
SmoCA+ cell
fragmented
0:00
0:24
0:48
1:12
SmoCA+ cell H2B:zAchilles
p < 0.0001
p = 0.003
Ratio of mKO2+ cell# at 30 h post-heat-shock to 6 h (%)
larvae(n): (7) (7) (8) (5)
mKO2
Ptch1
SmoCA
SmoCA + Bcl2a

Fig 5.3.1: Artificially introduced Shh-unfit cells undergo apoptotic elimination.
a Schematic diagram of the experimental introduction of abnormal fluorescent Shh signalling cells into zebrafish larvae in a mosaic manner through heat shock induction. **b, c** Artificially introduced SmoCA-expressing (Shh-activated) or Ptch1-overexpressing (Shh-inactivated) cells underwent apoptosis, but Gli1- or Gli3R-expressing cells did not undergo apoptosis in the spinal cord (**b**) and muscle (**c**). Confocal microscopy images show whole-mount immunostaining of active caspase-3 (grey) in mosaic larvae expressing mKO2 alone or with SmoCA, Ptch1, Gli1, or Gli3R (magenta). Arrowheads indicate caspase-3 active cells. Scale bar = 10 μm. Bar plots show the mean + standard error (SEM) of the $mKO2^+$ and caspase-3-active cell frequencies. Two-tailed one-way ANOVA was used for the statistical analysis. **d** Abnormal Shh-activity cells gradually disappear over time. Larvae with artificially introduced cells expressing mKO2 alone or with SmoCA or Ptch1 (magenta) with or without an apoptosis inhibitor Bcl2a (green). Fluorescent and bright-field images after heat-shock induction. Scale bar = 200 μm. The bar plots show the ratio of $mKO2^+$ (Ptch1, SmoCA, or SmoCA and Bcl2a) cell number at 30 h post-heat-shock to that at 6 h (%) (mean + SEM). Each dot represents one larva. An unpaired two-tailed *t*-test was used. **e, f** DNA fragmentation occurs in Shh-unfit cells. In **e**, DNA fragmentation occurs in caspase-3 active membrane GFP-tagged SmoCA- or Ptch1-expressing cells. The representative confocal fluorescent images show GFP (green), active caspase-3 (magenta), and DNA (blue). Dashed lines represent the GFP^+ cell boundary. Scale bar = 10 μm. In **f**, top diagram shows the schematic illustration of the experimental time course to observe $SmoCA^+$ cell fragmentation. $SmoCA^+$-expressing (magenta) mosaic embryos were injected with zAchilles-tagged histone cluster (*H2B:zAchilles*) mRNA (cyan) to visualise nuclear signals. The timing relative to first image is indicated in white text. Scale bar = 50 μm.

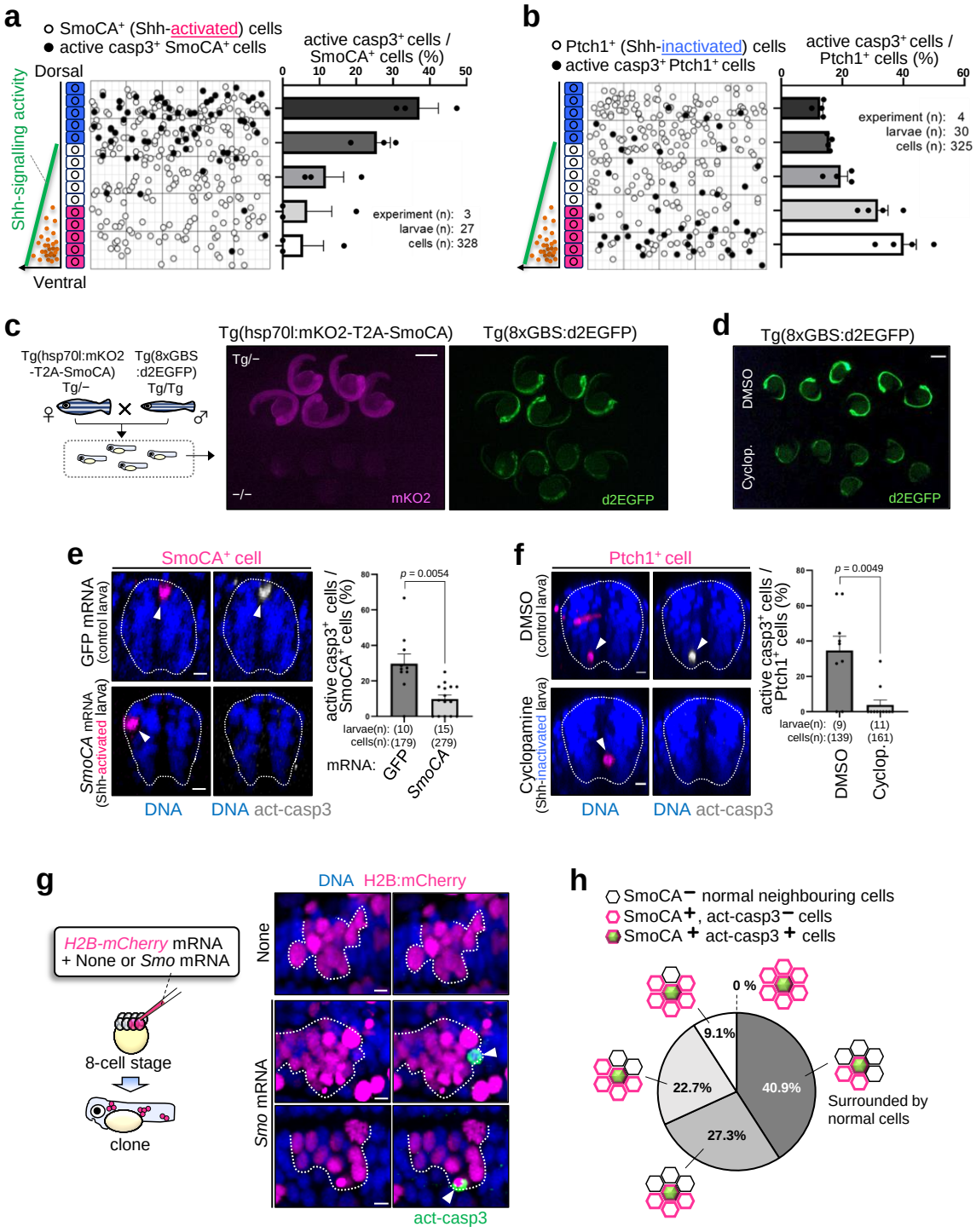

Fig 5.3.2: Substantial differences in Shh-activity trigger apoptosis.
a, b Cells causing substantial noise in the Shh gradient efficiently underwent apoptosis. The left panels show maps of artificially introduced SmoCA- or Ptch1-expressing cells in the zebrafish spinal cord. The graphs on the right show the mean + SEM of mKO2^{+} and caspase-

3-active cell frequencies within a divided range along the dorso-ventral (DV) axis. **c** Ubiquitous SmoCA expression upregulates Shh signalling. Heterozygous Tg(hsp70l:mKO2-T2A-SmoCA) transgenic fish were crossed with homozygous Tg(8xGBS:d2EGFP). Collected embryos were exposed to heat shock at 14 hpf and imaged at 24 hpf. The top fluorescent live image shows the mKO2 fluorescence of heterozygous Tg(hsp70l:mKO2-T2A-SmoCA) mutants (Tg/-,top) and their wild-type siblings (-/-, bottom). Bottom fluorescent live image showing GFP fluorescence of Tg(8xGBS:d2EGFP) in heterozygote Tg(hsp70l:mKO2-T2A-SmoCA) mutants (Tg/-,top) or wild-type siblings (-/-, bottom). Scale bar = 1000 μm. **d** Cyclopamine treatment downregulates Shh signalling. Fluorescent live image show Tg(8xGBS:d2EGFP) larvae treated with DMSO (control, top) or 30 μM cyclopamine (Shh signalling (Smo) inhibitor, bottom). Each solution was added at 18 hpf. Scale bar = 1000 μm. **e, f** Alleviation of Shh activity difference between Shh-unfit cells and neighbouring normal cells blocks Shh-unfit cell elimination. Shh-activated or -inactivated larvae were prepared by injecting *SmoCA* mRNA (**e**) or cyclopamine treatment (**f**). Representative confocal images showing whole-mount immunostaining of $SmoCA^+$ or $Ptch1^+$ cell (magenta) and active caspase-3 (grey). Scale bar = 10 μm. The bar plot shows the mean + SEM of $SmoCA^+$ or $Ptch1^+$ caspase-3-active cell frequencies. An unpaired two-tailed *t-test* was used. **g, h** Local comparison between neighbouring cells mediate the elimination of Shh-unfit cells. The schematic diagram in **g** shows the experimental introduction of SmoCA clones into zebrafish spinal cord. Confocal images show whole-mount immunostaining of larvae expressing *H2B-mCherry* without or with *SmoCA* (magenta) and active caspase-3 (green). Scale bar = 10 μm. The pie chart in **h** shows the proportion of SmoCA-expressing and non-expressing neighbouring cells around caspase-3 positive SmoCA-expressing cells. Note that there are no caspase-3 positive, SmoCA-expressing cells where all neighbouring cells are SmoCA-expressing cells.

4. N-cadherin mediates unfit cell sensing

We then explored the mechanisms underlying unfit cell elimination. In early embryos, Wnt/β-catenin signalling post-translationally stabilizes E-cadherin, shaping a membrane E-cadherin protein level gradient. Spontaneously emerging Wnt/β-catenin-unfit cells alter E-cadherin levels, leading to a substantial difference in membrane cadherin levels (cadherin imbalance) between unfit and neighbouring normal cells. This cadherin imbalance stimulates unfit cell apoptosis through TGF-β-type Smad activation, ROS production, and Bcl2 protein reduction[8]. We hypothesized that a similar Cadherin-Smad-ROS-Bcl2 system might also be involved in eliminating Shh-unfit cells. N-cadherin (Cdh2) forms a dorsal-to-ventral gradient that inversely correlates with Shh signalling in the developing spinal cord[39] (Fig. 5.4.1 a). Nevertheless, the molecular relationship between N-cadherin and Shh signalling remains unclear. Remarkably, forced Shh signalling activation by injecting *SmoCA* mRNA or Shh signalling inactivation by Cyclopamine treatment reduced or increased N-cadherin protein levels, respectively (Fig. 5.4.1 b, c). Mosaic introduction of Shh-unfit cells overexpressing SmoCA or Ptch1 decreased or increased membrane N-cadherin protein levels, respectively (Fig. 5.4.1 d). In contrast, neither forced activation nor inhibition of Shh activity affect *n-cadherin* mRNA levels (Fig. 5.4.1 e, f). In addition, unift Shh activity did not change *n-cadherin* mRNA levels (Fig. 5.4.1 g). These findings suggest that Shh signalling negatively regulates N-cadherin levels post-translationally. The mosaic introduction of Gli1 or Gli3R did not affect N-cadherin protein levels (Fig. 5.4.1 d), suggesting that Shh signalling controls N-cadherin levels through Ptch1 and Smo receptors but not transcription factors (Fig. 5.4.1 h). Unfit Shh activity-induced cadherin imbalance is possibly involved in unfit cell sensing. Consistent with this idea, partial N-cadherin knockdown through injecting *n-cadherin* antisense morpholino (MO), which blocks N-cadherin protein expression[39,40] (Fig. 5.4.2 a), reduced apoptotic elimination of Shh-high and -low cells (Fig. 5.4.2 b, c). Moreover, mosaically introduced N-cadherin-overexpressing cells efficiently activated caspase-3 in the N-cadherin-low ventral region (Fig. 5.4.2 d), indicating that cadherin imbalance sufficiently induces apoptosis. Importantly, partial knockdown of N-cadherin caused *olig2* mis-expression in developing

spinal cord (Fig. 5.4.2 ed), suggesting that N-cadherin mediate elimination of naturally generated unfit cells. Besides N-cadherin, Cdh11 is also expressed in the developing spinal cord[39,41]. Partial Cdh11 knockdown through injecting *cdh11* MO[39] did not affect the apoptotic elimination of Shh-unfit cells (Fig. 5.4.2 f). These results indicate that the difference in membrane N-cadherin levels between unfit and neighbouring fit cells is involved in Shh-unfit cell sensing.

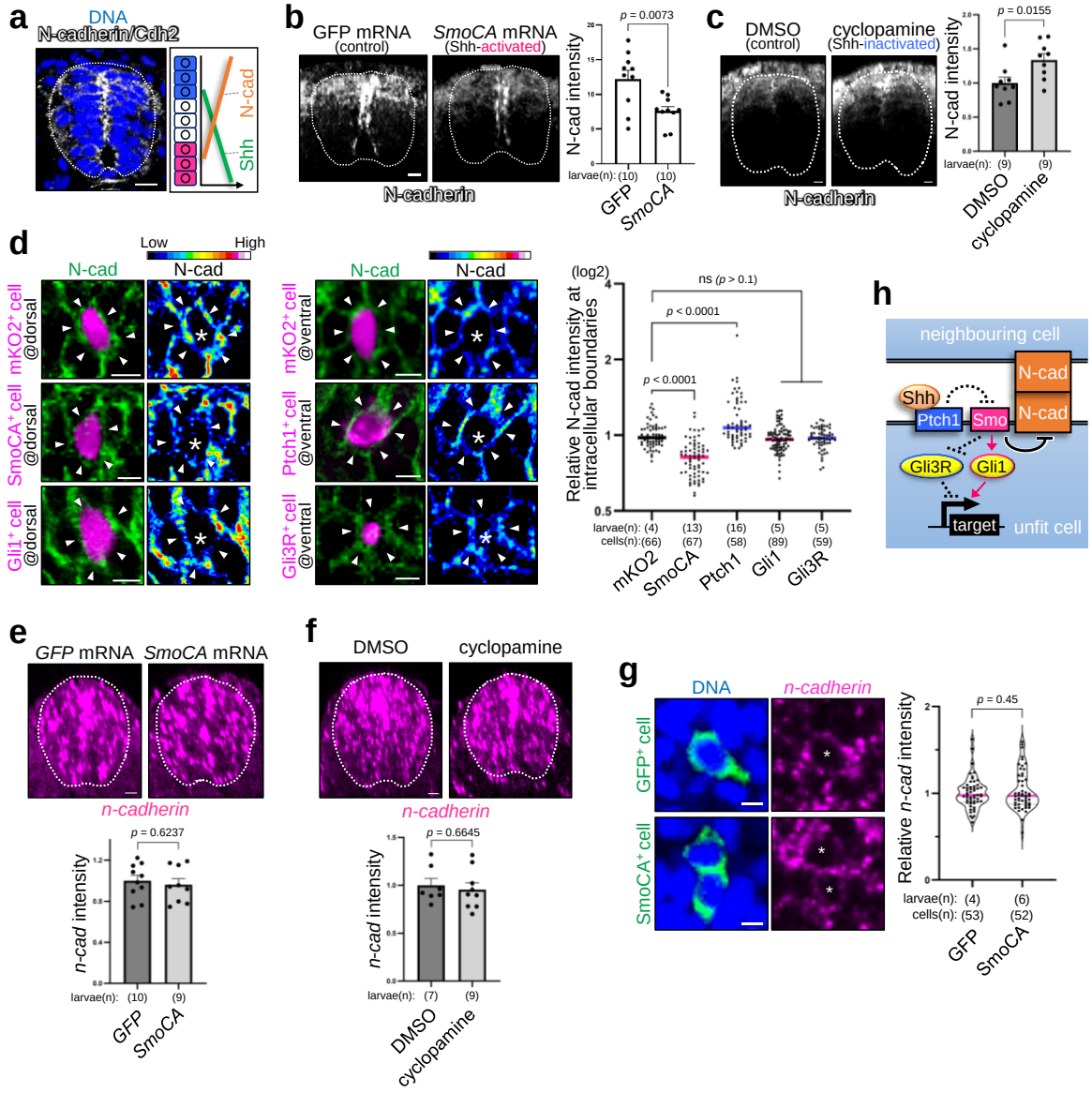

Fig 5.4.1: N-cadherin is post-translationally regulated by Shh signalling.
a N-cadherin/Cdh2 levels inversely correlate with Shh activity. Representative images show whole-mount immunostaining for N-cadherin (grey). Scale bar = 10 μm. **b, c** Activating or inactivating Shh signalling reduces or N-cadherin levels, respectively. Shh-activated or -inactivated larvae were prepared by *SmoCA*-mRNA injection (**b**) or cylopamine treatment (**c**). Scale bar = 10 μm. The mean + SEM of N-cadherin intensity of each larva is graphed. An unpaired tow-tailed *t*-test was used for the statical analysis. **d** Mosaic introduction of SmoCA- or Ptch1-expressing cells altered endogenous N-cadherin levels. Confocal images show whole-mount immunostaining for N-cadherin (green) and mosaic expression of mKO2 alone or with SmoCA, Ptch1, Gli1, or Gli3R (magenta). The fluorescence intensity of intercellular N-cadherin staining between mKO2$^+$ cells and neighbouring wild-type cells was normalised to the intercellular fluorescence intensity between wild-type cells. Each dot represents an mKO2$^+$ cell. Two-tailed one-way ANOVA was used. **e, f** Activating or inactivating Shh signalling throughout

the spinal cord did not alter the endogenous *n-cadherin* mRNA levels. Shh-activated or -inactivated larvae were prepared via *SmoCA*-mRNA injection (**e**), or cyclopamine treatment (**f**), respectively. Left confocal images show whole-mount in situ hybridisation of *n-cadherin* (magenta). Scale bar = 10 μm. The right graph shows the relative fluorescent intensity of *n-cadherin*. Each dot represents one larva. An unpaired two-tailed *t*-test was used. **g** Mosaic introduction of unfit Shh-activity (SmoCA) cells did not alter the endogenous *n-cadherin* mRNA level. Left confocal images showing whole-mount in situ hybridisation of *n-cadherin* (magenta) and mosaically introduced membrane GFP alone or with SmoCA (green). Scale bar = 10 μm. The right graph shows the fluorescent intensity of *n-cadherin* between GFP^+ cells and neighbouring wild-type cells, normalised to the fluorescence intensity between wild-type cells. Each dot represents one GFP^+ cell. Fluorescent intensity in two intercellular areas per cell was measured. An unpaired two-tailed *t*-test was used. **h** Schematic illustration of the Shh signalling pathway and N-cadherin regulation.

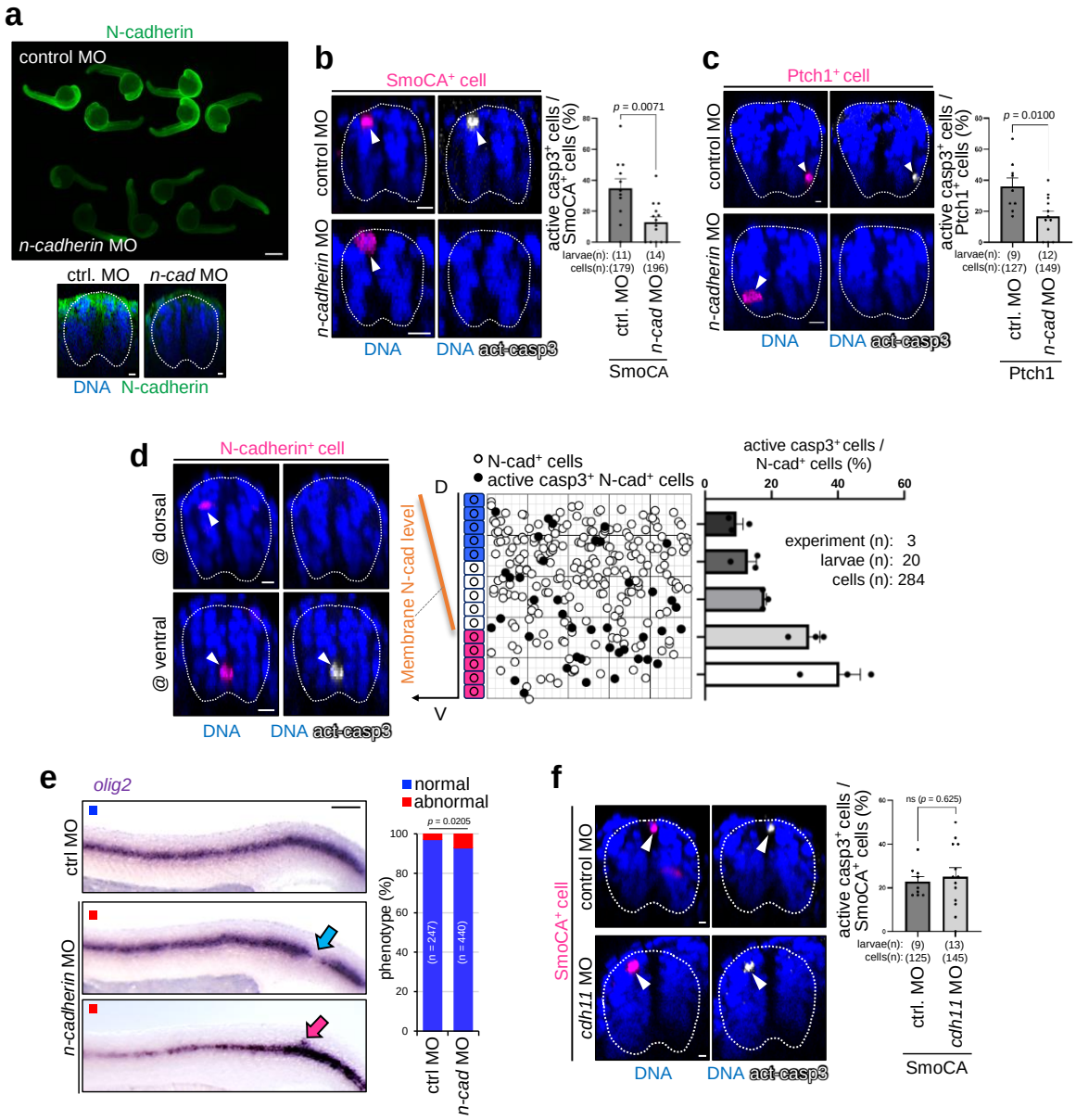

Fig 5.4.2: N-cadherin mediates the sensing of Shh-unfit cells.
a Partial knockdown of *n-cadherin* in zebrafish larvae. The top fluorescent image show anti-N-cadherin (green) immunostaining of larvae injected with 1 ng of control MO (upper) or *n-cadherin* MO (lower). Scale bar = 500 µm. The bottom images are cross-section views of the spinal cord. Scale bar = 10 µm. *n-cadherin* MO reduced endogenous N-cadherin levels. **b, c** Partial N-cadherin knockdown by injecting low-dose *n-cadherin* oligo morpholino (MO) blocks SmoCA- (**b**) or Ptch1- (**c**)-expressing cell elimination. Scale bar = 10 µm. The graphs on the right show the mean + SEM of mKO2$^+$ (SmoCA, Ptch1) and caspase-3-active cell frequencies. An unpaired two-tailed *t*-test was used for the statistical analysis. **d** Cells causing excess noise in N-cadherin-gradients efficiently underwent apoptosis. Confocal images show whole-mount immunostaining of mosaically introduced N-cadherin-overexpressing cells (magenta) and active caspase-3 (grey). Scale bar = 10 µm. The middle panel shows maps of N-cadherin cells

artificially introduced into the spinal cord. The right graph indicates the mean + SEM of $mKO2^+$ and caspase-3-active cell frequencies within a divided range along the DV axis. **e** Cadherin-mediated elimination of unfit cells is required for precise tissue patterning of the spinal cord. Representative images showing the whole-mount in situ hybridisation of *olig2* in control or *n-cadherin* MO-injected larvae. Scale bar = 100 μm. The graph shows the percentages of larvae with normal or abnormal expression patterns. The chi-square test was used for statistical analysis. **f** Partial *cdh11* knockdown by injecting low-dose *cdh11* MO did not block SmoCA-expressing cell elimination. Scale bar = 10 μm. The right graph shows the mean + SEM of $SmoCA^+$, caspase-3 active cell frequencies. An unpaired two-tailed *t*-test was used.

5. Smad-ROS pathway mediates Shh-unfit cell elimination

We then examined the involvement of Smad-ROS signalling in Shh-unfit cell elimination. SBE-Luc, which expresses luciferase in response to TGF-β-type Smad-dependent signalling, was activated in Shh-high and -low cells in the spinal cord (Fig. 5.5.1 a) and muscles (Fig. 5.5.1 b). Mosaically introduced N-cadherin-overexpressing cells also activated SBE-luc (Fig. 5.5.1 c), potentially indicating that TGF-β-type Smad signalling mediates unfit cell-killing downstream of cadherin. Inhibiting TGF-β-type Smad signalling by co-expression of Smad3b dominant negative mutants (Smad3bDN) in unfit cells or injecting *smad4a* MO[42] reduced unfit cell apoptosis (Fig. 5.5.1 d-g). Mosaically introduced Shh-high and -low cells triggered DNA oxidation in the spinal cord (Fig. 5.5.2 a) and muscles (Fig. 5.5.2 b). Treatment with N-acetyl-l-cysteine (NAC), a ROS scavenger, prevented cell oxidation (Fig. 5.5.2 c) and cell elimination (Fig. 5.5.2 d-g), demonstrating that the Smad-ROS pathway mediates unfit cell elimination (Fig. 5.5.2 h). Moreover, knockdown of Smad signalling with low dose of *smad4a* MO induced unfit cells with ectopic activation and inhibition of *olig2* expression in the developing spinal cord (Fig. 5.2.2 i), whereas it did not affect the width of *olig2*-expressing area (Fig. 5.5.2 j). These results suggest that Smad signalling mediates the elimination of unfit cells under physiological conditions. In addition, Bcl2 overexpression prevented apoptosis (Fig. 5.5.2 k, l), suggesting that Bcl2 is involved in the elimination of Shh-unfit cells. Our data collectively demonstrate that cadherin-mediated communication between Shh-unfit and neighbouring fit cells induces apoptosis in unfit cells by activating the Smad-ROS-Bcl2 axis.

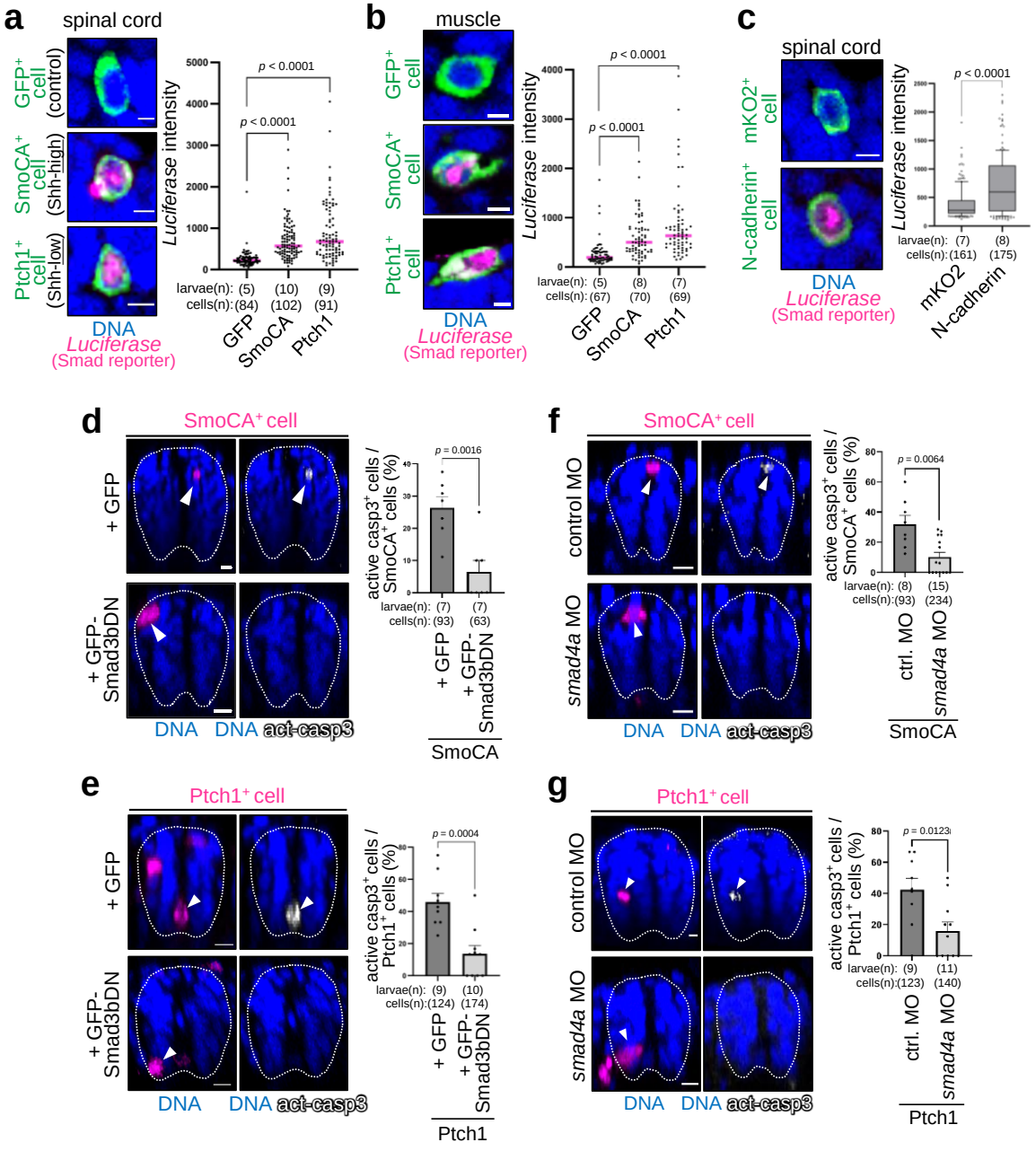

Fig 5.5.1: Smad signalling mediates the killing of Shh-unfit cells.
a, b Shh-unfit cells activate the Smad2/3/4-dependent reporter gene (SBE-Luc) in the spinal cord (**a**) and muscle (**b**). Confocal images show whole-mount fluorescent in situ hybridisation of *luciferase* mRNA (magenta) in mosaic larvae expressing membrane GFP alone or with SmoCA or Ptch1 (green). Scale bar = 10 μm. The *luciferase* intensity of each GFP$^+$ cell is plotted. Two-tailed one-way ANOVA was used. **c** N-cadherin imbalance induces TGF-β-Smad signalling-mediated killing of unfit cells. Representative images show whole-mount fluorescent in situ hybridisation of *luciferase* mRNA (magenta) in mosaic larvae expressing membrane mKO2 alone or with N-cadherin (green). Scale bar = 10 μm. The *luciferase* intensity of each mKO2$^+$

cell is graphed. A two-tailed *t*-test was used. **d-g** Smad signalling inhibition blocks SmoCA- or Ptch1-expressing cell death. Confocal images show whole-mount immunostaining of active caspase-3 (grey) in mosaic larvae expressing mKO2 with SmoCA or Ptch1 (magenta), injected with GFP or GFP-Smad3bDN (**d**, **e**), or control MO or *n-cadherin* MO (**f**, **g**). Scale bar = 10 μm. The graphs on the right show the mean + SEM of $mKO2^{+}$ (SmoCA, Ptch1) and caspase-3-active cell frequencies. An unpaired two-tailed *t*-test was used for the statistical analysis.

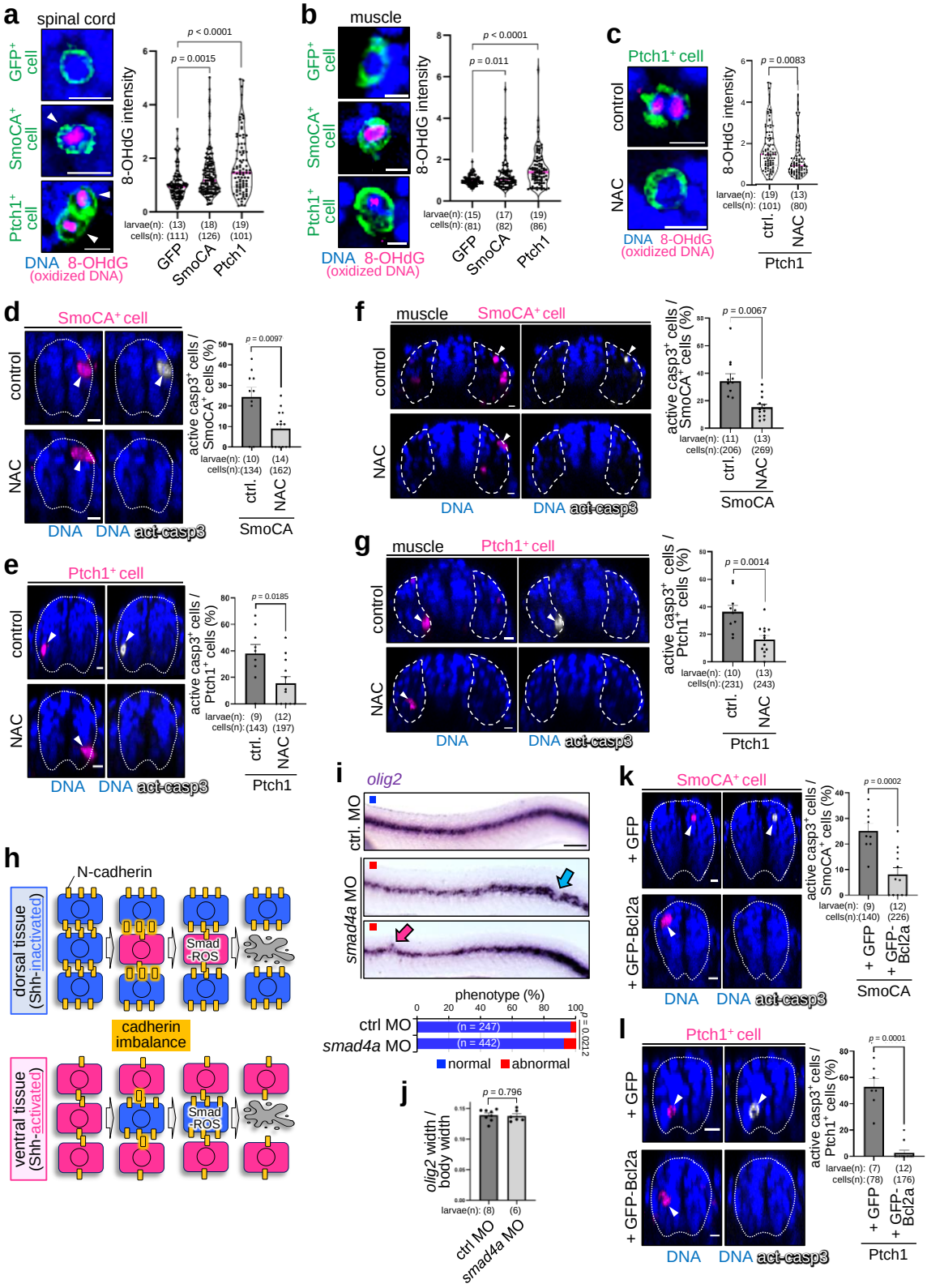
a
spinal cord
GFP+ cell
SmoCA+ cell
Ptch1+ cell
DNA 8-OHdG (oxidized DNA)
8-OHdG intensity
p < 0.0001
p = 0.0015
larvae(n): (13) (18) (19)
cells(n): (111) (126) (101)
GFP
SmoCA
Ptch1
b
muscle
p < 0.0001
p = 0.011
larvae(n): (15) (17) (19)
cells(n): (81) (82) (86)
c
Ptch1+ cell
control
NAC
p = 0.0083
larvae(n): (19) (13)
cells(n): (101) (80)
ctrl.
NAC
Ptch1
d
SmoCA+ cell
active casp3+ cells / SmoCA+ cells (%)
p = 0.0097
larvae(n): (10) (14)
cells(n): (134) (162)
DNA
DNA act-casp3
SmoCA
e
Ptch1+ cell
active casp3+ cells / Ptch1+ cells (%)
p = 0.0185
larvae(n): (9) (12)
cells(n): (143) (197)
f
muscle
SmoCA+ cell
p = 0.0067
larvae(n): (11) (13)
cells(n): (206) (269)
g
muscle
Ptch1+ cell
p = 0.0014
larvae(n): (10) (13)
cells(n): (231) (243)
h
N-cadherin
dorsal tissue (Shh-inactivated)
Smad -ROS
cadherin imbalance
ventral tissue (Shh-activated)
i
olig2
ctrl. MO
smad4a MO
phenotype (%)
ctrl MO (n = 247)
smad4a MO (n = 442)
normal
abnormal
p = 0.0212
j
p = 0.796
olig2 width / body width
larvae(n): (8) (6)
ctrl MO
smad4a MO
k
SmoCA+ cell
+ GFP
+ GFP-Bcl2a
p = 0.0002
larvae(n): (9) (12)
cells(n): (140) (226)
SmoCA
l
Ptch1+ cell
p = 0.0001
larvae(n): (7) (12)
cells(n): (78) (176)
Ptch1

Fig 5.5.2: Cadherin-Smad-ROS pathway mediates the killing of Shh-unfit cells.
a, b Shh-unfit cells activate reactive oxygen species (ROS) production in the spinal cord (**a**) and muscle (**b**). Confocal images show whole-mount immunostaining for 8-OHdG (magenta) in mosaic larvae expressing membrane GFP alone or with SmoCA or Ptch1 (green). Scale bar = 10 μm. Violin plots show the 8-OHdG intensity of each GFP^+ cell. Two-tailed one-way ANOVA was used. **c** NAC treatment reduced ROS production in Shh-unfit cells. The representative images show whole-mount immunostaining of 8-OHdG (magenta) in mosaic larvae expressing membrane GFP with Ptch1 (green) treated with D2W (control) or N-acetyl-l-cysteine (NAC, a ROS scavenger). Scale bar = 10 μm. Violin plots show the 8-OHdG intensity of each GFP^+ cell. An unpaired two-tailed *t-test* was used. **d-g** ROS inhibition blocks SmoCA- or Ptch1-expressing cell death in the spinal cord (**d, e**) and muscle (**f, g**). Confocal images show whole-mount immunostaining of active caspase-3 (grey) in mosaic larvae expressing mKO2 with SmoCA or Ptch1 (magenta), treated with D2W or NAC. Scale bar = 10 μm. The graphs on the right show the mean + SEM of $mKO2^+$ (SmoCA, Ptch1) and caspase-3-active cell frequencies. An unpaired two-tailed *t*-test was used for the statistical analysis. **h** Schematic diagram showing the elimination of Shh-unfit cells. **i** Cadherin-Smad-ROS axis-mediated elimination of unfit cells is required for precise tissue patterning of the spinal cord. Representative images showing the whole-mount in situ hybridisation of *olig2* in control or *smad4a* MO-injected larvae. Scale bar = 100 μm. The graph shows the percentages of larvae with normal or abnormal expression patterns. The chi-square test was used for statistical analysis. **j** Smad signalling inhibition does not expand the *olig2*-expressing area. The graph shows the ratio of *olig2*-expressing width to body width in ctrl or *smad4* MO-injected larvae. An unpaired two-tailed *t*-test was used. **k, l** Bcl2a overexpression blocked SmoCA- or Ptch1-expressing cell apoptosis. Confocal images show whole-mount immunostaining of active caspase-3 (grey) in mosaic larvae expressing mKO2 with SmoCA or Ptch1 (magenta), injected with GFP or GFP-Bcl2a. Scale bar = 10 μm. The graphs on the right show the mean + SEM of $mKO2^+$ (SmoCA, Ptch1) and caspase-3-active cell frequencies. An unpaired two-tailed *t*-test was used for the statistical analysis.

6. *Foxo3b* is a common mediator of cell competition

We have elucidated that the Cadherin-Smad-ROS-Bcl2 pathway is used in cell competition-mediated Wnt- and Shh-unfit cell elimination, indicating a common molecular mechanism underlying cell competition. Our previous RNA-seq analysis (GSE133526 [https://www.ncbi.nlm.nih.gov/geo/query/acc.cgi?acc=GSE133526]) identified *foxo3b*, *sesn3*, *lnx1*, and *tcima* as genes specifically upregulated in unfit cells with abnormally high Wnt/β-catenin-activity[8] (Table 5.6.1). These four genes were upregulated in Wnt/β-catenin-high unfit cells and Wnt/β-catenin-low, Shh-high, and Shh-low unfit cells (Fig. 5.6.1 a-d), indicating that these genes may be common regulators of unfit cell elimination. *foxo3b* encodes a transcription factor[43,44], and a Foxo3's target gene *sesn3*[45] is also upregulated in unfit cells. In addition, a GSEA reanalysis in unfit cells (Mosaic β-catCA) compared to control cells (Ubiquitous β-catCA) (GSE133526)[8] revealed that upregulation of apoptosis-related gene set including *puma* and *apaf1*, which are known target genes of Foxo3[46–51], was detected in unfit cells (Table 5.6.2; Fig. 5.6.2 a-c). Therefore, we hypothesized that Foxo3b transcriptional activity may play an essential role in the behaviour of unfit cells. Introduction of the dominant-negative mutant of *foxo3b* (Foxo3bDN) into Wnt- and Shh-defective cells significantly blocked their apoptotic elimination (Fig. 5.6.3 a, b), suggesting that *foxo3b* is essential for their elimination. We also generated *foxo3b* knockout (KO) zebrafish (hereinafter called "*foxo3b*-/-") using genome editing (Fig. 5.6.3 c, d). In *foxo3b*-/- mutant, 4,283bp including *foxo3b* Exon 1 and 2 was deleted, but we confirmed that this deletion did not affect the expression of *foxo3b*-neighbouring gene (Fig. 5.6.3 e). As expected, Wnt- and Shh-unfit cell elimination was blocked in this mutant (Fig. 5.6.3 f, g). Mosaic introduction of cells expressing a constitutively active Smad3b mutant (Smad3bCA) sufficiently induced *foxo3b* upregulation (Fig. 5.6.3 h). Consistent with the above findings, Smad3bDN co-expression blocked the *foxo3b* upregulation in Shh-unfit cells (Fig. 5.6.3 h), suggesting that *foxo3b* is transcriptionally upregulated downstream of Smad activation. In contrast, ROS inhibition via NAC treatment did not block *foxo3b* upregulation (Fig. 5.6.3 h), but introduction of Foxo3bDN prevented DNA oxidation in Shh-defective cells (Fig. 5.6.3 i). These results

suggest that Foxo3b mediates Smad-induced ROS production. To confirm that *foxo3b* transcriptional upregulation occurs upstream of apoptosis induction, we examined the relationship between *foxo3b* and apoptosis inducers, including Puma[46–48] and Caspase-8 (the initiator caspase of extrinsic apoptosis)[52,53]. The mRNA levels of *puma* were elevated in both β-catCA-expressing (Wnt-high) cells and Foxo3-hyperactivated cells expressing constitutively active mutants of Foxo3 (Foxo3CA)[54,55] (Fig. 5.6.4 a), suggesting that *puma* is upregulated downstream of Foxo3 in unfit cells. Consistent with this, artificially introduced Puma[46–48] and Caspase-8 (the initiator caspase of extrinsic apoptosis)[52,53] efficiently induced apoptosis (Fig. 5.6.4 b), but did not lead to *foxo3b* upregulation (Fig. 5.6.4 c). Furthermore, inhibiting apoptosis through *bcl2a* did not impair *foxo3b* upregulation in β-catCA cells (Fig. 5.6.4 c, d). These results indicate that *foxo3b* is activated upstream of apoptosis induction in unfit cells. Thus, Shh- and Wnt-defective cells are eliminated by activating the Smad-Foxo3-ROS axis.

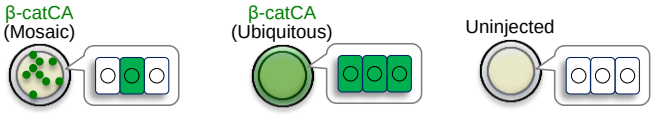

Akieda et al., 2019

βcatCA mosaic vs ubiquitous

βcatCA mosaic vs uninjected

Zebrafish proteins which have homology to *Drosophila azot*. (*azot*-like)

gene	baseMean	Log2FoldChange	*p*-value	gene	Log2FoldChange	*p*-value
foxo3b	5.9266704	**2.494590872**	4.34E-08	***foxo3b***	**2.674598467**	4.37E-08
sesn3	17.278078	**1.951765885**	0.000015	***sesn3***	**1.937583235**	9.94E-06
lnx1	6.7947094	**2.778521291**	2.50E-09	***lnx1***	**2.133672836**	1.10E-05
tcima	10.9589133	**1.582915968**	0.00086	***tcima***	**1.042842995**	0.02260
cacfd1 (flower)	0.0910062	-0.002164567	0.98918	*cacfd1 (flower)*	-0.015131613	0.92457
calm1a	15.643381	-0.401164789	0.34012	*calm1a*	0.075788369	0.85579
calm1b	0.1730290	0.052558357	0.74320	*calm1b*	0.062057132	0.69925
calm2a	8.2954654	-0.392351523	0.41274	*calm2a*	-0.538298835	0.25008
calm2b	54.191142	0.180468109	0.53341	*calm2b*	0.06253069	0.82283
calm3b	19.507702	0.579798888	0.16402	*calm3b*	0.18280071	0.64762
calm3a	1.6246146	0.310982457	0.53173	*calm3a*	0.126599293	0.80221
cabp5a	0.0878618	0	1	*cabp5a*	0	1
cabp5b	0			*cabp5b*		
calml4a	0			*calml4a*		
aif1l	26.54092	-0.445381758	0.26198	*aif1l*	-0.013577453	0.97244
cabp1a	0			*cabp1a*		
cabp1b	0			*cabp1b*		
cabp2a	0			*cabp2a*		
cabp2b	0.5300300	0.070816072	0.80871	*cabp2b*	0.082584968	0.77829
cabp4	0.0205818	0	1	*cabp4*	0	1
calb1	0			*calb1*		
calb2a	0			*calb2a*		
calb2b	0.0360925	-0.052911664	0.73867	*calb2b*	0	1
calml4b	0			*calml4b*		
capsla	0			*capsla*		
capslb	0			*capslb*		
cetn2	0.0724904	-0.047314796	0.76641	*cetn2*	0	1
cetn3	0.8444536	0.018936367	0.96309	*cetn3*	-0.317967572	0.44230
cetn4	1.5490245	-0.382396306	0.42725	*cetn4*	-0.407795489	0.40352
cmlc1	0			*cmlc1*		
efcab11	1.3756486	-0.024517897	0.95828	*efcab11*	-0.258156891	0.58796
efhd1	4.0721404	-1.185893668	0.02466	*efhd1*	-0.903982956	0.08549
efhd2	3.8994649	0.06521826	0.90217	*efhd2*	0.628168085	0.23627
gpd2	0.0205818	0	1	*gpd2*	0	1
myl1	0			*myl1*		
myl4	0			*myl4*		
myl6	13.395310	0.052813139	0.90239	*myl6*	0.068888689	0.86967
myl9a	0.0349059	0	1	*myl9a*	-0.051143001	0.74763
myl12.2	2.2718792	0.578167572	0.26213	*myl12.2*	0.509406164	0.32930
myl13	0			*myl13*		
mylz3	1.7521163	-0.285209486	0.55663	*mylz3*	0.257090789	0.59775
rhbdl3	0.0163267	0	1	*rhbdl3*	0	1
scgn	0			*scgn*		
si:cabz01076231.1	0			*si:cabz01076231.1*		
slc25a24l	0			*slc25a24l*		
tnnc1a	0			*tnnc1a*		
tnnc1b	0			*tnnc1b*		
TNNC2 (1 of many)	0			*TNNC2* (1 of many)		
zgc:153867	8.2872163	0.686423203	0.15785	*zgc:153867*	0.159401893	0.73456
zgc:163073	0			*zgc:163073*		

Table 5.6.1: Unfit Wnt-high loser cells increase *foxo3b*, *sesn3*, *lnx1*, and *tcima* expression, but do not increase *flower* or *azot*-like gene expression.
The RNA-seq data of β-catCA-mosaically introduced (Mosaic), ubiquitously β-catCA-expressing (Ubiquitous), or uninjected zebrafish embryos (GEO accession code: GSE133526) were re-analysed. DESeq2 (version 1.10.1) was used for the statistical analysis.

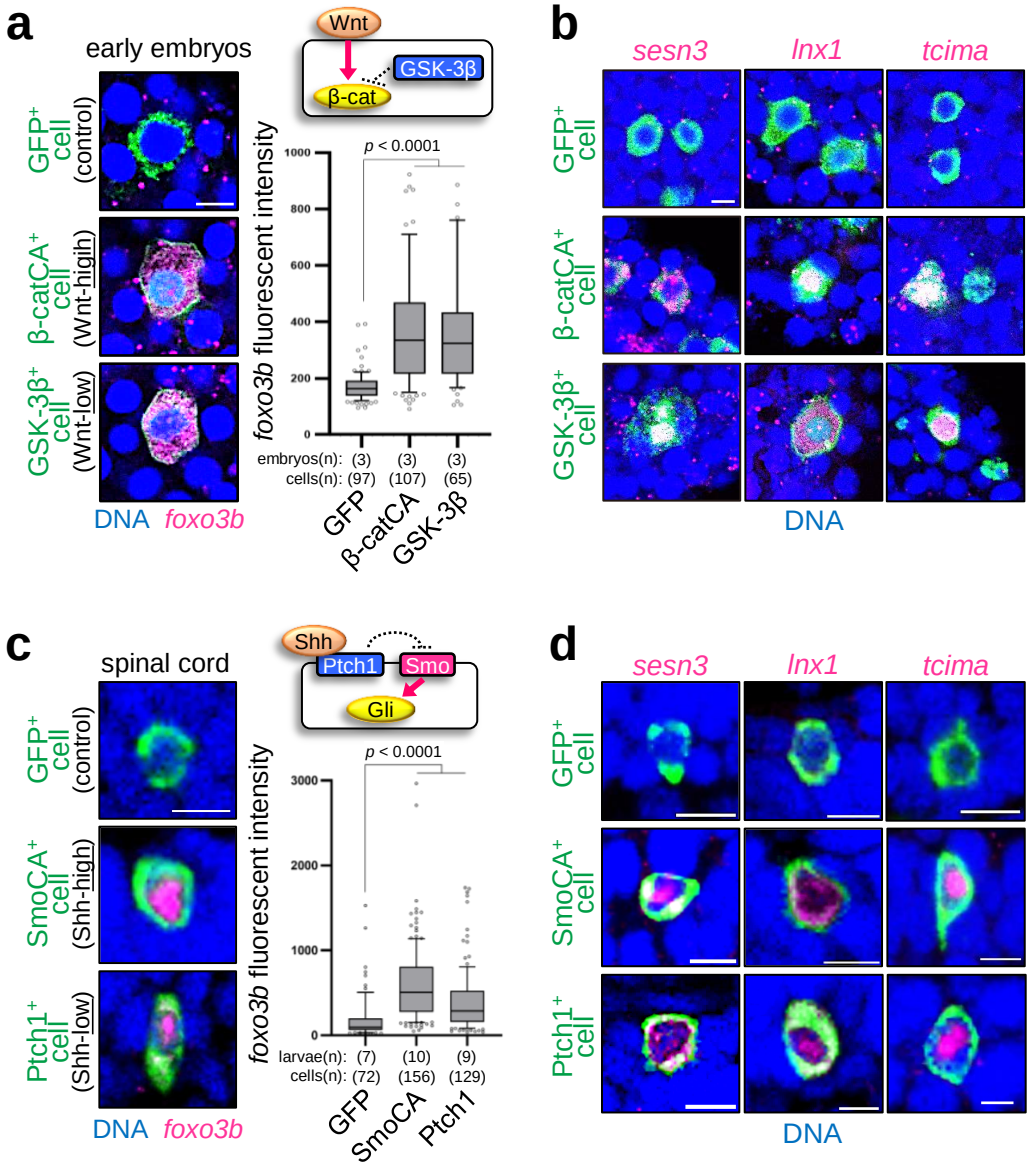

Fig 5.6.1: Exploration of universal cell competition markers.
a, c Artificially introduced Wnt-unfit cells into early embryos (9 hpf) (**a**) and Shh-unfit cells in the developing spinal cord (24 hpf) (**c**) strongly express *foxo3b*. Confocal images show whole-mount fluorescent in situ hybridisation of *foxo3b* mRNA (magenta) in GFP alone or with β-catCA, GSK-3β, SmoCA, or Ptch1 (green). Scale bar = 10 μm. *foxo3b* intensity of each GFP$^+$ cell was graphed. Maximum and minimum: whiskers; medians: lines; 10th and 90th percentiles: boxes. Two-tailed one-way ANOVA was used. **b, d** Artificially introduced Wnt-unfit cells in early embryos (**b**) and Shh-unfit cells in the developing spinal cord (**d**) strongly activate *sesn3*, *lnx1*, and *tcima*. Confocal images show whole-mount fluorescent in situ hybridisation of *sesn3* (left), *lnx1* (middle), and *tcima* (right) mRNA (magenta) in mosaic embryos/larvae expressing GFP alone, or with β-catCA, GSK-3β, SmoCA, or Ptch1 (green). Scale bar = 10 μm.

βcatCA mosaic vs ubiquitous

Pathway (Database: REACTOME)	Pathway_ID	NES	Padj
Eukaryotic Translation Initiation	R-DRE-72613	2.08001	0.01023
L13a-mediated translational silencing of Ceruloplasmin expression	R-DRE-156827	2.05762	0.01023
Degradation of beta-catenin by the destruction complex	R-DRE-195253	2.03937	0.01023
Cap-dependent Translation Initiation	R-DRE-72737	2.02995	0.01023
GTP hydrolysis and joining of the 60S ribosomal subunit	R-DRE-72706	2.00978	0.01023
Beta-catenin independent WNT signaling	R-DRE-3858494	2.00694	0.01023
Ribosomal scanning and start codon recognition	R-DRE-72702	1.9934	0.01023
Signaling by Wnt	R-DRE-195721	1.97791	0.01023
Translation	R-DRE-72766	1.93736	0.01023
MAPK6/MAPK4 signaling	R-DRE-5687128	1.90634	0.01023
Formation of a pool of free 40S subunits	R-DRE-72689	1.90185	0.01023
Nonsense Mediated Decay (NMD) independent of the Exon Junction Complex (EJC)	R-DRE-975956	1.86977	0.01023
Nonsense-Mediated Decay (NMD)	R-DRE-927802	1.83093	0.01023
Nonsense Mediated Decay (NMD) enhanced by the Exon Junction Complex (EJC)	R-DRE-975957	1.83093	0.01023
TCF dependent signaling in response to WNT	R-DRE-201681	1.77934	0.01023
Signaling by SCF-KIT	R-DRE-1433557	1.72446	0.01023
Fc epsilon receptor (FCERI) signaling	R-DRE-2454202	1.72286	0.01023
MAPK family signaling cascades	R-DRE-5683057	1.71894	0.01023
Keratinization	R-DRE-6805567	2.09985	0.01047
Activation of the mRNA upon binding of the cap-binding complex and eIFs, and subsequent binding to 43S	R-DRE-72662	1.97461	0.01217
Translation initiation complex formation	R-DRE-72649	1.97343	0.01217
Intrinsic Pathway for Apoptosis	R-DRE-109606	1.94965	0.01217
PCP/CE pathway	R-DRE-4086400	1.92924	0.01217
Stabilization of p53	R-DRE-69541	1.91207	0.01217
Formation of the ternary complex, and subsequently, the 43S complex	R-DRE-72695	1.90486	0.01217
p53-Dependent G1 DNA Damage Response	R-DRE-69563	1.88259	0.01217
p53-Dependent G1/S DNA damage checkpoint	R-DRE-69580	1.88259	0.01217
AUF1 (hnRNP D0) binds and destabilizes mRNA	R-DRE-450408	1.87923	0.01217
Signaling by Leptin	R-DRE-2586552	1.63011	0.01217
Processing of Capped Intron-Containing Pre-mRNA	R-DRE-72203	-1.7387	0.01217
mRNA Splicing	R-DRE-72172	-1.87573	0.01217
mRNA Splicing - Major Pathway	R-DRE-72163	-1.89966	0.01217
Adaptive Immune System	R-DRE-1280218	1.56811	0.01409
Asymmetric localization of PCP proteins	R-DRE-4608870	1.93637	0.01591
Autodegradation of the E3 ubiquitin ligase COP1	R-DRE-349425	1.92365	0.01591
Recruitment and ATM-mediated phosphorylation of repair and signaling proteins at DNA double strand breaks	R-DRE-5693565	1.93268	0.01597
DAP12 interactions	R-DRE-2172127	1.63858	0.01651
DAP12 signaling	R-DRE-2424491	1.63858	0.01651
DNA Repair	R-DRE-73894	1.60711	0.01651
Cytokine Signaling in Immune system	R-DRE-1280215	1.5981	0.01651
Signaling by PDGF	R-DRE-186797	1.59718	0.01651
G1/S DNA Damage Checkpoints	R-DRE-69615	1.84206	0.01809
DNA Damage/Telomere Stress Induced Senescence	R-DRE-2559586	1.91414	0.01828
Metabolism of folate and pterines	R-DRE-196757	1.93662	0.01838
Downstream signal transduction	R-DRE-186763	1.60302	0.01838
DNA Double Strand Break Response	R-DRE-5693606	1.93612	0.01884
Regulation of RAS by GAPs	R-DRE-5658442	1.83987	0.01884
Degradation of DVL	R-DRE-4641258	1.82984	0.01884
FBXL7 down-regulates AURKA during mitotic entry and in early mitosis	R-DRE-8854050	1.80526	0.01884
Apoptosis	R-DRE-109581	1.78614	0.01884
Programmed Cell Death	R-DRE-5357801	1.78614	0.01884
Signaling by the B Cell Receptor (BCR)	R-DRE-983705	1.6299	0.01884
Cellular responses to stress	R-DRE-2262752	1.5528	0.01884
The NLRP3 inflammasome	R-DRE-844456	1.74838	0.01942
Downstream signaling events of B Cell Receptor (BCR)	R-DRE-1168372	1.65266	0.01942
Interleukin-3, 5 and GM-CSF signaling	R-DRE-512988	1.59096	0.01942
FCERI mediated MAPK activation	R-DRE-2871796	1.58801	0.01942
Membrane Trafficking	R-DRE-199991	1.46272	0.01946
Autodegradation of Cdh1 by Cdh1:APC/C	R-DRE-174084	1.82662	0.01958
Cyclin A:Cdk2-associated events at S phase entry	R-DRE-69656	1.75569	0.01958
IGF1R signaling cascade	R-DRE-2428924	1.57234	0.01974
IRS-related events triggered by IGF1R	R-DRE-2428928	1.57234	0.01974
Signaling by Type 1 Insulin-like Growth Factor 1 Receptor (IGF1R)	R-DRE-2404192	1.56841	0.01974

Table 5.6.2: Apoptosis-related genes are enriched in Wnt-unfit cells.
A list of enriched gene sets (from the REACTOME database) in RNA-seq data (GSE133526), comparing unfit cells (Mosaic β-catCA) to control cells (Ubiquitous β-catCA), with Padj < 0.02. Red pathways are apoptosis-related pathways. DESeq2 (version 1.10.1) was used for the statistical analysis.

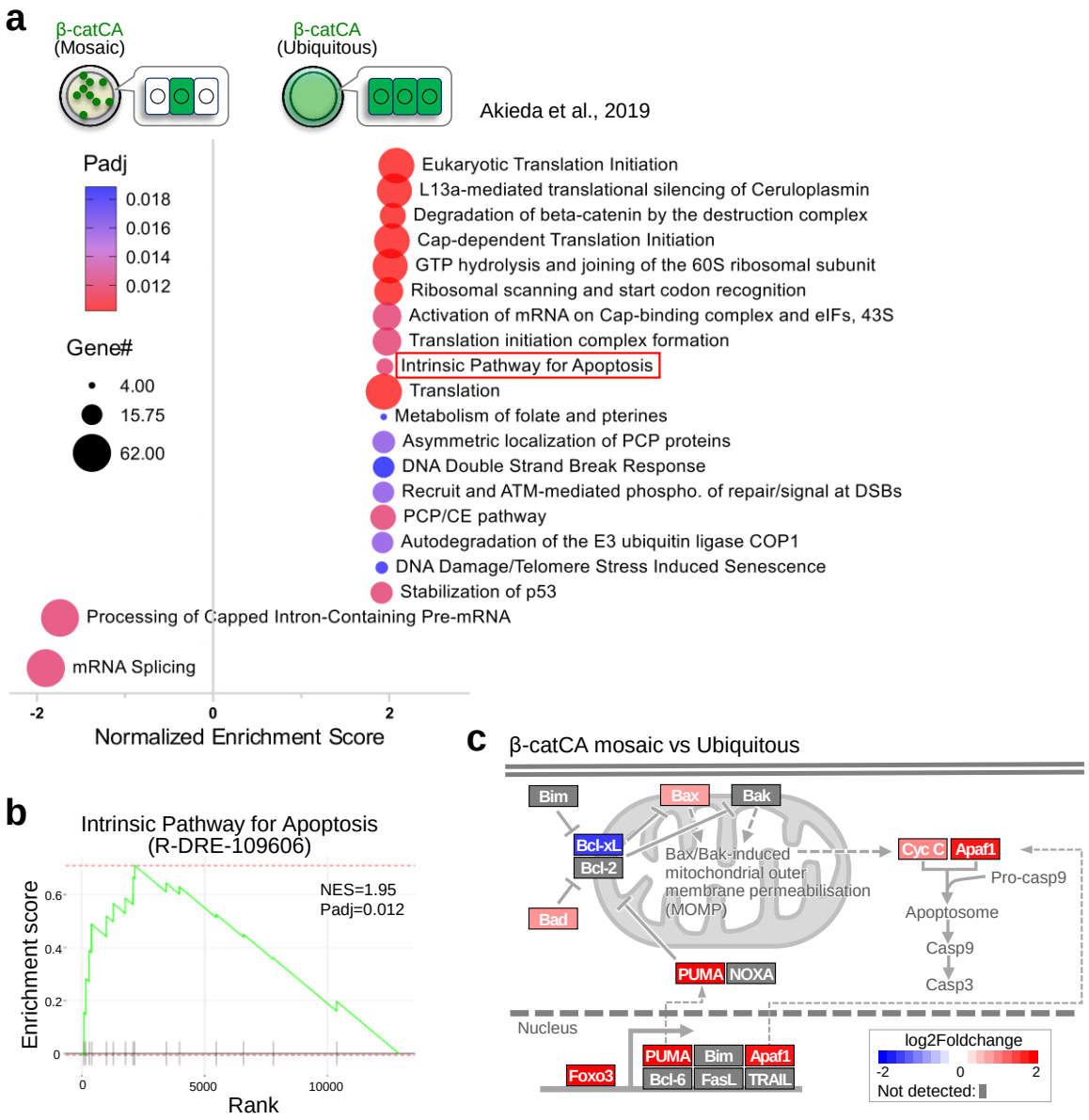

Fig 5.6.2: Apoptosis-related genes are enriched in Wnt-unfit cells.
a-c Gene set enrichment analysis against RNA-seq data (GSE133526) in unfit cells (Mosaic β-catCA) compared to control cells (Ubiquitous β-catCA) was performed. Bubble plot in **a** shows the top 20 enriched gene sets, excluding Wnt signalling-related gene sets. *p*-values were shown by different colour, the size of bubble indicate the gene count of each pathway. The enrichment plot in **b** shows the gene set for the Intrinsic Pathway for Apoptosis (R-DRE-109606), which is enriched in unfit cells (Mosaic βcatCA). The upper part shows the enrichment score, while the lower part shows the ranked gene list with black vertical line meaning for the genes of the set. The schematic diagram in **c** shows intracellular apoptotic pathway in unfit cells.

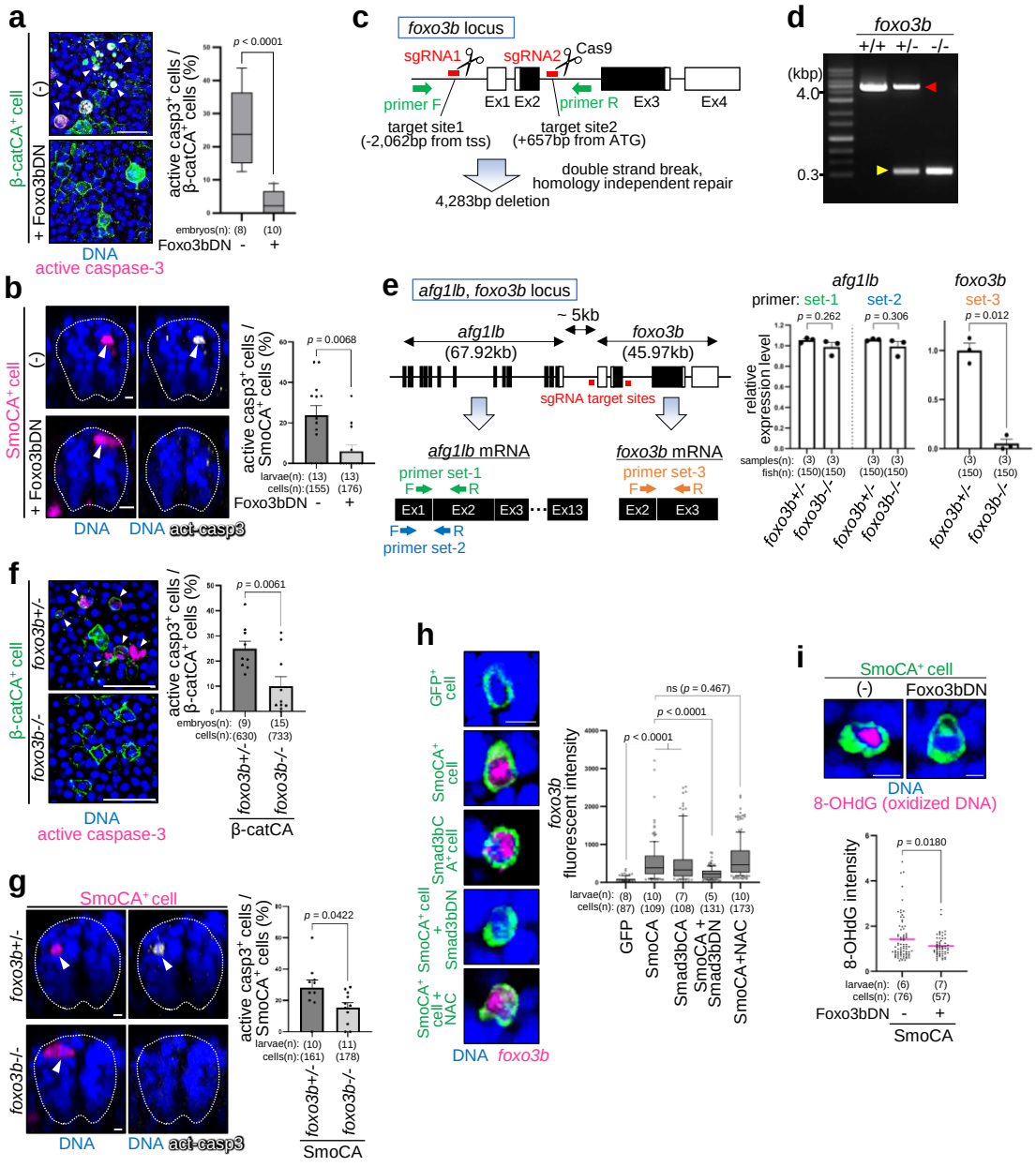

Fig 5.6.3: *foxo3b* is required for the elimination of Wnt- and Shh-unfit cells.
a, b Co-expression of Foxo3bDN blocks the elimination of cells expressing β-catCA (**a**) and SmoCA (**b**). Confocal images show whole-mount immunostaining of mosaic embryos expressing GFP-tagged β-catCA (green) (9 hpf) (**a**), mKO2-tagged SmoCA (magenta) (24 hpf) (**b**), and active caspase-3 (magenta in **a**, grey in **b**), with or without Foxo3bDN. Scale bar = 100 μm in **a** and 10 μm in **b**. The graph on the right shows the GFP$^+$ or mKO2$^+$ (β-catCA $^+$, SmoCA$^+$) and caspase-3-active cell frequencies. An unpaired two-tailed *t*-test was used for the statistical analysis. **c** Schematic diagram of foxo3b-/- zebrafish generation. **d** Electrophoresis of PCR products obtained using primers described in **c** with genomic DNA from adult fish. The red arrowhead indicates the expected size of the PCR products. Yellow arrowheads indicate

shortened PCR products, suggesting that deletion had occurred in the *foxo3b* gene. **e** The expression of neighbouring genes is not affected in the *foxo3b-/-* mutant. Schematic diagram shows the *afg1lb* and *foxo3b* loci. Expression levels of *foxo3b* and *afg1lb* in *foxo3b* heterozygous (foxo3b+/-) or homozygous (foxo3b-/-) 24 hpf siblings analysed using qPCR with primer pairs described in the diagram. The β-actin gene was used as normalisation control. **f, g** Eliminating Wnt- and Shh-unfit cells require *foxo3b*. Representative confocal images show mosaic embryos expressing GFP-tagged β-catCA (green), mKO2-tagged SmoCA (magenta), and active caspase-3 (magenta in **f**, grey in **g**) in *foxo3b* heterozygous (foxo3b+/-) or homozygous (foxo3b-/-) mutants. Scale bar = 100 μm in **f**, 10 μm in **g**. The graph on the right shows the mean + SEM of β-catCA$^+$ or SmoCA$^+$, caspase-3 active cell frequencies. An unpaired tow-tailed *t*-test was used for the statical analysis. **h** Foxo3b upregulation is triggered downstream of Smad activation and upstream of ROS production. Confocal images show whole-mount in situ hybridisation of *foxo3b* mRNA (magenta) in mosaic larvae expressing GFP alone or with SmoCA, Smad3bCA, SmoCA with Smad3bDN (co-injection), or NAC-treated SmoCA (green). Scale bar = 10 μm. The *foxo3b* intensity of each GFP$^+$ cell is graphed. A two-tailed one-way ANOVA was used. **i** Foxo3b inhibition blocks ROS production in Shh-unfit cells. Representative images showing whole-mount immunostaining of 8-OHdG (magenta) in mosaic larvae expressing membrane GFP-tagged SmoCA with or without Foxo3bDN (green). Scale bar = 10 μm. The graph on the bottom shows the 8-OHdG intensity of each GFP$^+$ cell. An unpaired two-tailed *t-test* was used.

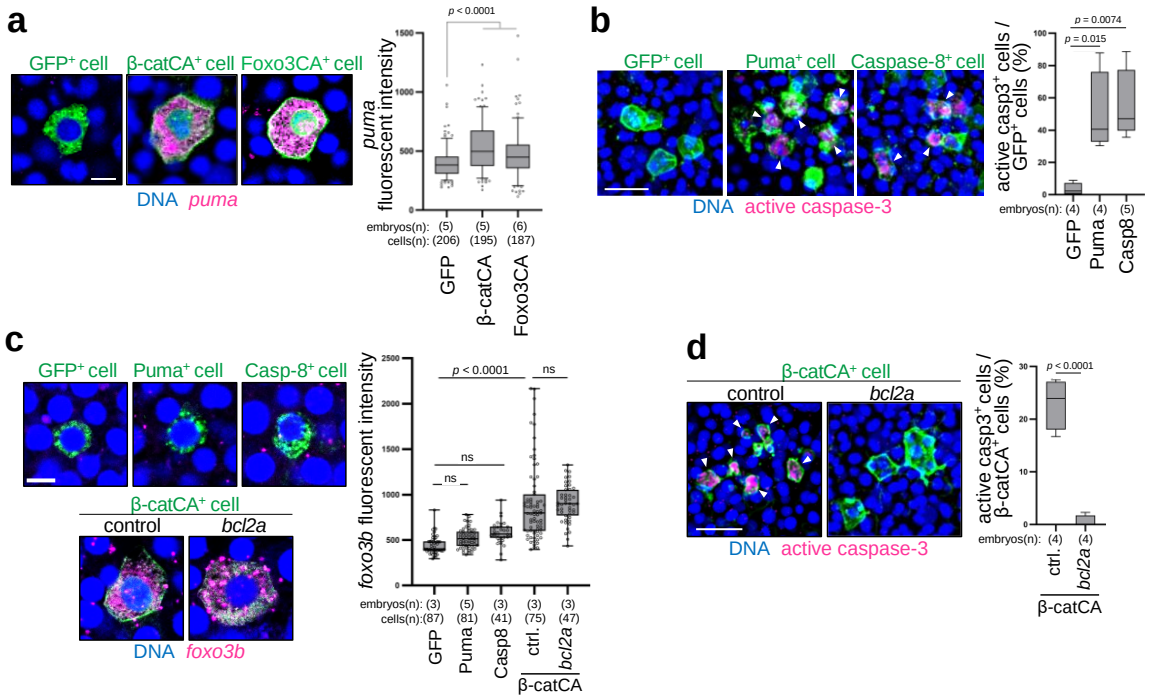

Fig 5.6.4: *foxo3b* is activated upstream of apoptosis induction in unfit cells.
a *puma* is involved in the elimination of Wnt-unfit cells. Representative images show whole-mount fluorescent in situ hybridisation of *puma* mRNA (magenta) in mosaic embryos (9 hpf) expressing GFP alone or with β-catCA or Foxo3CA. Scale bar = 10 µm. *puma* intensity of each GFP$^+$ cell was graphed. Each dot represents one GFP$^+$ cell. A two-tailed one-way ANOVA was used. **b** Pro-apoptotic protein Puma and the initiator extrinsic apoptosis Caspase-8 efficiently undergo apoptosis. Representative images show whole-mount immunostaining of mosaic embryos expressing GFP alone or with Puma or Caspase-8 (green) and active caspase-3 (magenta). Scale bar = 100 µm. The box plots on the right show the GFP$^+$ (Puma, Caspase-8) and caspase-3 active cell frequencies in each embryo. Maximum and minimum: whiskers; medians: lines; 25th and 75th percentiles: boxes. A two-tailed one-way ANOVA was used. **c** Apoptosis does not upregulate *foxo3b*. Representative images show whole-mount fluorescent in situ hybridisation of *foxo3b* mRNA (magenta) in mosaic embryos expressing GFP alone or with Puma, Caspase-8, or β-catCA co-injected with *Emerald luciferase* (ELuc, control) or *bcl2a* mRNA (green). Scale bar = 10 µm. *foxo3b* intensity of each GFP$^+$ cell was graphed. Each dot represents one GFP$^+$ cell. A two-tailed one-way ANOVA was used. **d** *bcl2a* overexpression blocks apoptosis of β-catCA-expressing cells. Confocal images show whole-mount immunostaining of active caspase-3 (magenta) in mosaic embryos expressing β-catCA (green) with *ELuc* (control) or *bcl2a* mRNA. Scale bar = 100 µm. β-catCA$^+$, caspase-3 active cell frequencies are graphed. An unpaired two-tailed *t-test* was used.

Next, we examined how *foxo3b* transcription is activated in unfit cells. Because Foxo3 binds to its own promoter and stimulates its expression via a positive autoregulatory feedback loop in human cell line[56], we tested the possibility that Foxo3 itself may be involved in *foxo3b* transcription in unfit cells. Mosaic introduction of cells-overexpressing wild-type Foxo3 activated endogenous *foxo3b* expression and apoptosis, and mosaic cells-expressing Foxo3CA activated them more strongly (Fig. 5.6.5 a, b). Thus, not only TGF-β-type Smad signalling but also Foxo3 activation can stimulates *foxo3b* expression. Considering these findings with the previous study which reported that Foxo3 and TGF-β-type Smads forms oligomer to control gene expression in the nucleus[57], it raises the possibility that Foxo3 and TGF-β-type Smads might cooperate to activates *foxo3b* expression in unfit cell elimination. Consistent with this idea, in Wnt/β-catenin-high unfit cells, nuclear localization of both Smad2 and Foxo3 was detected, whereas it was not in control cells (Fig. 5.6.5 c). Introduction of Foxo3bDN prevented Smad2 nuclear translocation in Wnt/β-catenin-high unfit cells (Fig. 5.6.5 d). In addition, mosaic introduction of Foxo3CA stimulated Smad2 nuclear localization (Fig. 5.6.5 d). Thus, Smads and Foxo3 translocate to the nucleus dependent on each other's activity in unfit cells. It is likely that downstream of communication between unfit and fit cells, Smads and Foxo3 proteins are activated, co-translocate into the nucleus, and cooperatively activate the transcription of *foxo*3. This *foxo*3 expression may enhance Foxo3 activity via a positive feedback loop and consequently activate the expression of apoptosis inducers, such as *puma* (Fig. 5.6.5 e).

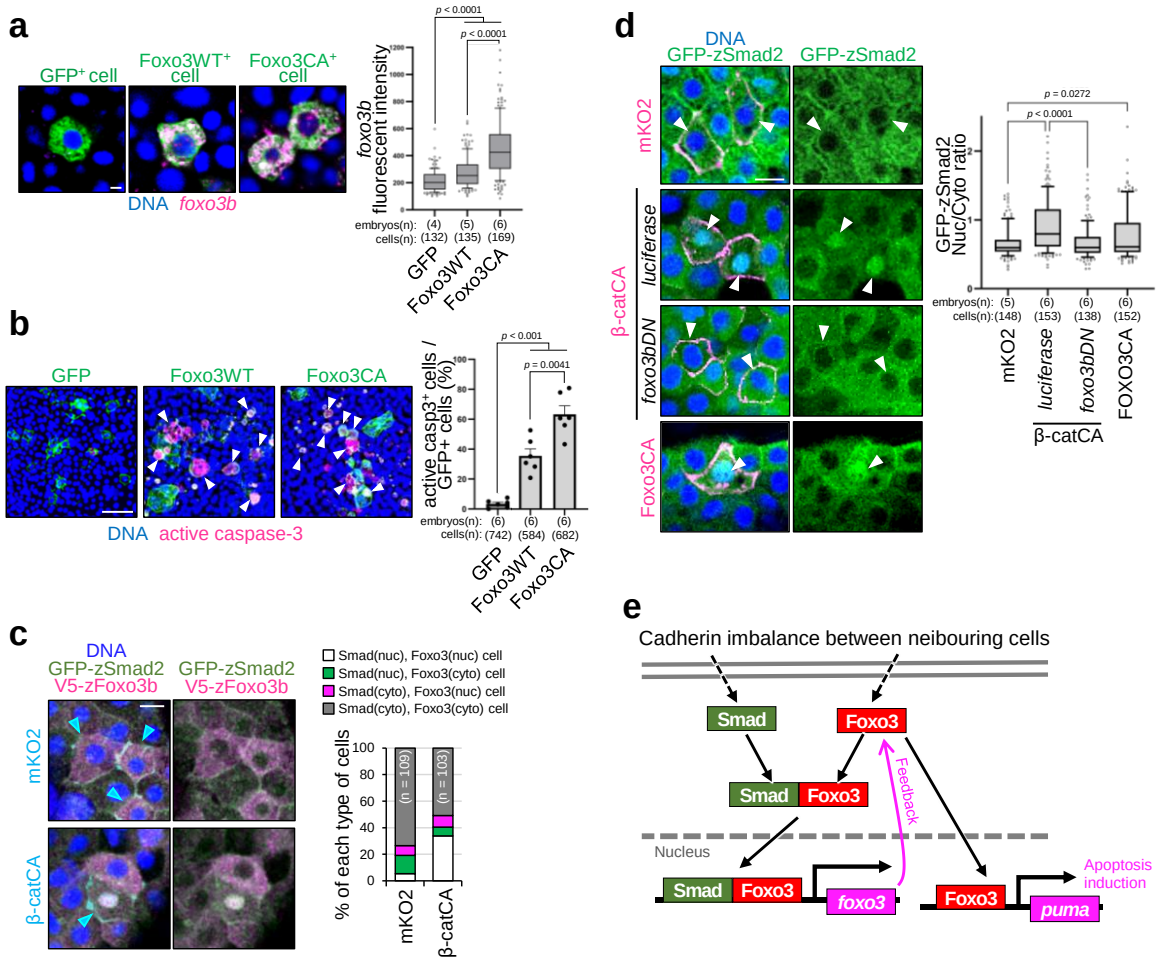

Fig 5.6.5: *foxo3b* is activated upstream of apoptosis induction in unfit cells.
a Foxo3 stimulates its expression via a positive auto-regulatory feedback loop. Representative images show whole-mount fluorescent in situ hybridisation of endogenous *foxo3b* mRNA (magenta) in mosaic embryos (9 hpf) expressing GFP alone or with Foxo3WT or Foxo3CA. Scale bar = 10 μm. *foxo3b* intensity of each GFP$^+$ cell was graphed. Each dot represents one GFP$^+$ cell. A two-tailed one-way ANOVA was used. **b** Mosaic introduction of Foxo3 induces apoptosis. Representative images show whole-mount immunostaining of mosaic embryos expressing GFP alone or with Foxo3WT or Foxo3CA (green) and active caspase-3 (magenta). Scale bar = 100 μm. The graph shows the mean + SEM of GFP$^+$ and caspase-3-active cell frequencies in each embryo. A two-tailed one-way ANOVA was used for analysis. **c** Smad2 and Foxo3 co-translocate into unfit cell nuclei. Representative images show whole-mount immunostaining of GFP-zSmad2 (green) and V5-zFoxo3b (magenta) in mosaic embryos expressing membrane mKO2 or mKO2-tagged β-catCA (cyan). Scale bar = 10 μm. Cyan arrows indicate mKO2-expressing cells. Bar chart on the right indicates percentage of each type of cells. **d** Smads and Foxo3 translocate to the nucleus dependent on each other's activity in unfit cells. Confocal images show whole-mount immunostaining of GFP-zSmad2 (green) in mosaic embryos expressing mKO2, β-catCA with *luciferase* or *foxo3bDN* mRNA, or Foxo3CA (magenta). Scale bar = 10 μm. Nuclear/cytoplasmic GFP-zSmad2 ratio in mKO2$^+$ cell is graphed. Maximum and minimum: whiskers; medians: lines; 25th and 75th percentiles: boxes.

An unpaired two-tailed *t-test* was used for analysis. **e** Schematic illustration of the Smad-Foxo3 signalling.

7. *foxo3b*-mediated unfit cell elimination is essential for precise development

Because unfit cells with abnormal Wnt/β-catenin, Shh activity, or *dbx1b* expression spontaneously appear during embryogenesis and organogenesis, we also confirmed that *foxo3b* expression was upregulated in naturally generated Wnt-, Shh-, or *dbx1b*-unfit cells (Fig. 5.7.1 a, b, c). We generated transgenic zebrafish Tg(*foxo3b*:GFP) and Tg(*foxo3b*:mCherry), which expresses GFP or mCherry in cells expressing endogenous *foxo3b* to examine *foxo3b*-positive unfit cells during development further (Fig. 5.7.1 d, e). *foxo3b*-positive cells appeared spontaneously in early embryos (Fig. 5.7.1 f, g) and in the developing spinal cord and muscle primordia (Fig. 5.7.1 h). The number and position of *foxo3b*-positive cells varied among the individuals (Fig. 5.7.1 f, h), indicating that *foxo3b* upregulation is not preprogramed. Moreover, some *foxo3b*-positive cells activated caspase-3 (Fig. 5.7.1 f-h), and the inhibition of apoptosis-induced *foxo3b*-positive cell accumulation (Fig. 5.7.1 i). These results suggest that *foxo3b* reporter zebrafish can be used to visualize naturally emerging unfit cells which are eliminated through cell competition.

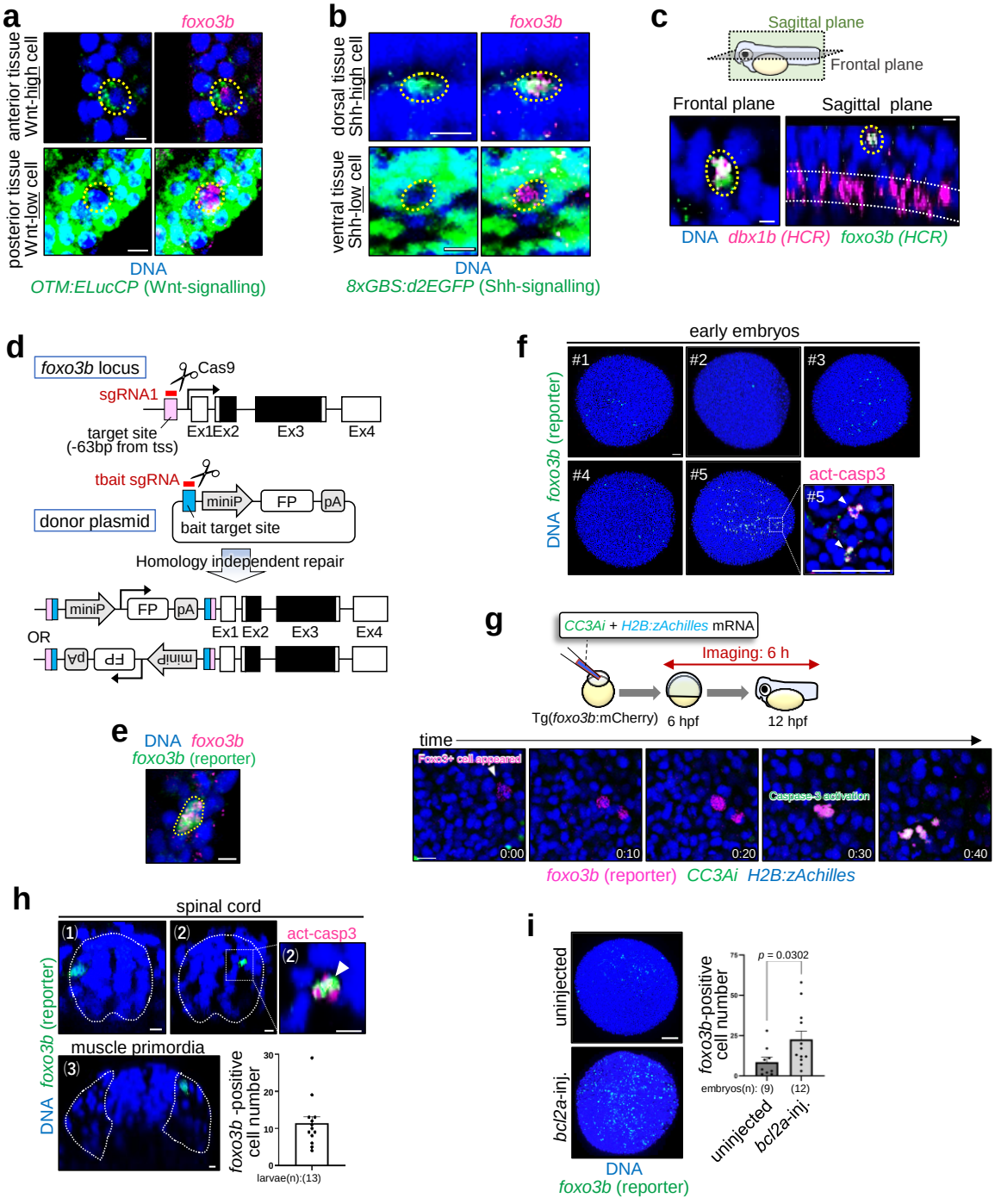

Fig 5.7.1: Naturally generated unfit cells upregulate *foxo3b* and undergo apoptosis.
a, b, c Endogenous *foxo3b* mRNA levels are upregulated in naturally generated Wnt- (**a**), Shh- (**b**), or *dbx1b* (**c**)-unfit cells. Confocal images in **a** and **b** show whole-mount fluorescent in situ hybridisation of *foxo3b* mRNA (magenta) in Tg(OTM:ELucCP*)* embryos (9 hpf) (**a**) or Tg(8xGBS:d2EGFP*)* larvae (24 hpf) (**b**) (green). Representative images in **c** show whole-

mount multiplex in situ hybridisation chain reaction (HCR) of *dbx1b* (magenta) and *foxo3b* (green) mRNA in 24 hpf larvae. Scale bar = 10 μm. Naturally occurring unfit cells are indicated by yellow dotted line circles. White dotted lines in sagittal plane in **c** show normally *dbx1b*-expressing region. **d** Schematic diagram of *foxo3b*-reporter transgenic zebrafish generation. FP stands for fluorescent protein, such as GFP or mCherry. **e** *foxo3b*:GFP reporter reflects the endogenous *foxo3b* in zebrafish. Representative images show fluorescent in situ hybridisation of endogenous *foxo3b* expression (magenta) in Tg(*foxo3b*:GFP) embryos. Yellow dot line surrounds *foxo3b* reporter (green) and endogenous *foxo3b* (magenta) double-positive cell. Scale bar = 10 μm. **f-i** Cells strongly expressing *foxo3b* naturally appear and undergo apoptosis during early embryogenesis (**f, g**) and organogenesis (**h**). Apoptosis inhibition induced *foxo3b*-positive cell accumulation (**i**). Representative images show whole-mount immunostaining of GFP (green) and active caspase-3 (magenta) in Tg(*foxo3b*:GFP). Scale bar = 100 μm in **f, i** and 10 μm in **h**. The number and the location of *foxo3b*-positive cells differ in each embryo. In **g** and **i**, the graphs show the mean + SEM of *foxo3b*-positive cell number in each individual. An unpaired two-tailed *t*-test was used. In **g**, top diagram shows the schematic illustration of the experimental time course to observe spontaneous appearance of foxo3b-positive cells and their apoptotic elimination. Tg(*foxo3b*:mCherry) mosaic embryos (magenta) were injected with mRNA of the caspase activity fluorescent biosensor/*CC3Ai* (green) and fluorescent-tagged histone cluster/*H2B:zAchilles* (blue). The timing relative to first image is indicated in white text. Scale bar = 50 μm.

To evaluate the Foxo3b function under physiological conditions, we inhibited Foxo3b using *foxo3b*DN mRNA. Overexpression of *foxo3b*DN did not affect the expression patterns of Wnt morphogen in early embryos and Shh morphogen in developing organs (Fig. 5.7.2 a, b), whereas it induced Wnt-unfit cell accumulation (Fig. 5.7.2 c) and ectopic activation or inactivation of a Wnt-target posterior gene *cdx4*[58] (Fig. 5.7.2 d) in early embryos, Shh-unfit cell accumulation (Fig. 5.7.2 e) and ectopic *olig2* activation or inactivation (Fig. 5.7.2 f) in the developing spinal cord, mis-patterning of fast muscles (Fig. 5.7.2 g) in muscles, abnormal larval morphogenesis (Fig. 5.7.2 h), and poor locomotion (Fig. 5.7.2 i). To further confirm physiological Foxo3b function, we generated a *foxo3b* KO zebrafish by optimising the CRISPR/Cas9-mediated genome editing system[59–61] (Fig. 5.7.3 a). We designed four short guide RNAs (sgRNAs) and confirmed that injection of these four sgRNAs, but not of a single sgRNA, induced deletion of the *foxo3b* gene efficiently in F0 generation (hereinafter, referred to as '*foxo3b* KO'). As a control, we injected four sgRNAs targeting *luciferase*, which did not result in any phenotypic abnormalities, to ensure that injection of sgRNAs and Cas9 mix had no side effects (Fig. 5.7.3 a-c). As expected, *foxo3b* KO yielded similar results to those obtained with *foxo3b* inhibition (Fig. 5.7.3 d-h). These suggest that *foxo3b* upregulation in unfit cells is essential for their elimination and precise tissue patterning (Fig. 5.7.3 i).

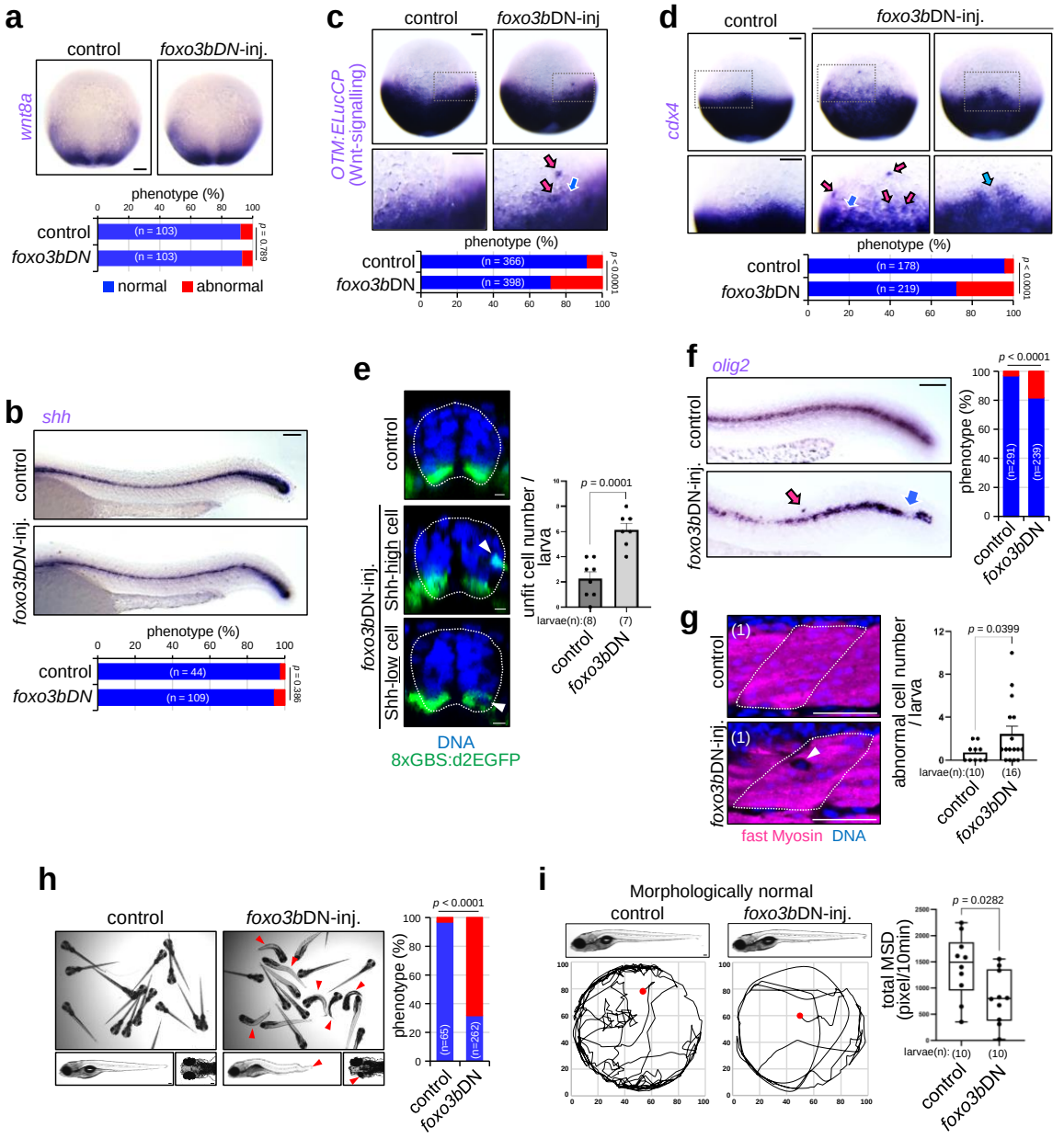

Fig 5.7.2: Foxo3-mediated physiological cell competition is required for the precise patterning during embryogenesis and organogenesis.

a, b *foxo3b* inhibition does not affect Wnt and Shh morphogen expression. Representative images show the whole-mount in situ hybridisation of *wnt8a* in early embryos (9 hpf) (**a**) and *shh* in larvae (24 hpf) (**b**) injected with *GFP* (control) or *foxo3b*DN mRNA. Scale bar = 100 µm. The bottom graphs show the percentages of embryos/larvae with normal or abnormal expression patterns. The chi-square test was used for statistical analysis. **c, e** *foxo3b* inhibition enhances the accumulation of Wnt- and Shh-unfit cells. Representative images show the whole-mount in situ hybridisation of *ELuc* in Tg(OTM:ELucCP) early embryos (**c**) or immunostaining of d2EGFP (green) in Tg(8xGBS:d2EGFP) larvae (**e**) uninjected (control) or

injected with *foxo3b*DN mRNA. Scale bar = 100 μm in **c** and 10 μm in **e**. The bottom graph in **c** show the percentages of embryos with normal or abnormal expression patterns. The chi-square test was used for statistical analysis. The bar plots in **e** show unfit cell frequencies in each larva. An unpaired two-tailed *t*-test was used for the statistical analysis. **d, f, g** *foxo3b*-mediated unfit cell elimination is required for precise tissue patterning of the early embryos (**d**), spinal cord (**f**), and muscles (**g**). Representative images showing the whole-mount in situ hybridisation of *cdx4* (**d**) or *olig2* (**d**) and immunostaining of fast myosin (**e**) in uninjected (control) and *foxo3b*DN mRNA-injected samples. Scale bar = 100 μm. The graphs in **d** and **f** show the percentages of embryos/larvae with normal or abnormal expression patterns. The chi-square test was used for statistical analysis. The graph to the right of **g** shows the number of abnormal cells in each larva. An unpaired two-tailed *t*-test was used for the statistical analysis. **h** Foxo3b inhibition induces abnormal morphogenesis. The images show 5 dpf zebrafish larvae uninjected (control) or injected with *foxo3b*DN mRNA. Scale bar = 100 μm. Red arrows highlight the Shh-defectiveness-related phenotypes (e.g., shortened trunk and reduced eye size). Percentages of larvae with normal or abnormal morphology are graphed. The chi-square test was used. **i** Inhibiting Foxo3b induces decreased locomotion. The images show 5 dpf uninjected (control) and *foxo3b*DN larvae. Scale bar = 100 μm. Note that externally normal individuals were used in locomotion analysis. The bottom panels show the representative trajectories of the control and *foxo3b*DN larvae. The box plot shows the total MSD of each sample. Maximum and minimum: whiskers; medians: lines; 25^{th} and 75^{th} percentiles: boxes. Each dot represents one larva. An unpaired two-tailed *t*-test was used.

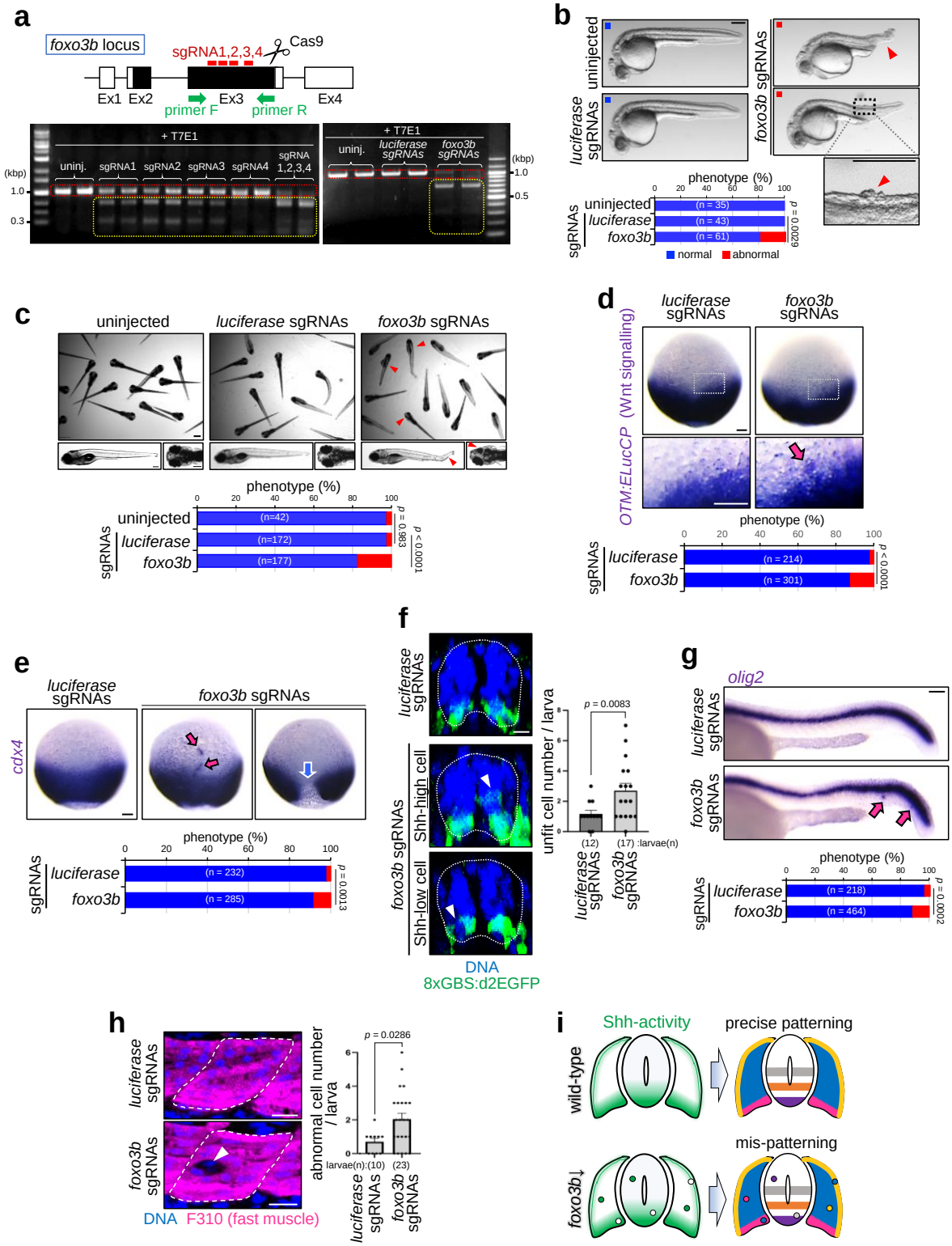
a
foxo3b locus
sgRNA1,2,3,4
Cas9
Ex1 Ex2 Ex3 Ex4
primer F
primer R
+ T7E1
uninj.
sgRNA1
sgRNA2
sgRNA3
sgRNA4
sgRNA 1,2,3,4
luciferase sgRNAs
foxo3b sgRNAs
(kbp)
1.0
0.3
0.5
b
uninjected
luciferase sgRNAs
foxo3b sgRNAs
phenotype (%)
(n = 35)
(n = 43)
(n = 61)
p = 0.0029
normal
abnormal
c
uninjected
luciferase sgRNAs
foxo3b sgRNAs
phenotype (%)
(n=42)
(n=172)
(n=177)
p = 0.983
p < 0.0001
d
luciferase sgRNAs
foxo3b sgRNAs
OTM:ELucCP (Wnt signalling)
phenotype (%)
(n = 214)
(n = 301)
p < 0.0001
e
luciferase sgRNAs
foxo3b sgRNAs
cdx4
phenotype (%)
(n = 232)
(n = 285)
p = 0.013
f
luciferase sgRNAs
foxo3b sgRNAs
Shh-high cell
Shh-low cell
DNA
8xGBS:d2EGFP
unfit cell number / larva
p = 0.0083
(12)
(17) :larvae(n)
g
olig2
luciferase sgRNAs
foxo3b sgRNAs
phenotype (%)
(n = 218)
(n = 464)
p = 0.0002
h
luciferase sgRNAs
foxo3b sgRNAs
DNA F310 (fast muscle)
abnormal cell number / larva
p = 0.0286
larvae(n):(10) (23)
i
Shh-activity
precise patterning
wild-type
mis-patterning
foxo3b↓

Fig 5.7.3: Foxo3 is required for the precise patterning during development.
a Injection with Cas9 protein and quadruple sgRNAs induce the deletion of the *foxo3b* gene. Total genomic DNA extracted from 24 hpf zebrafish uninjected or injected with single *foxo3b* sgRNA, quadruple *foxo3b* sgRNAs (sgRNA1, 2, 3, 4 shown in the top diagram), or quadruple *luciferase* sgRNAs (injected control) was amplified using PCR with the primers shown in the top diagram. DNA cleavages were detected using the T7E1 assay. Red dot line surrounds intact PCR products. The red dotted frame indicates the expected size of the PCR products. Yellow dot line surrounds shortened PCR products, indicating that the deletion had occurred in the *foxo3b* gene. **b, c** Foxo3b inhibition induces abnormal morphogenesis. The images show 30 hpf (**b**) and 5 dpf (**c**) zebrafish larvae uninjected or injected with *luciferase* or *foxo3b* sgRNAs. Scale bar = 200 μm. Red arrows highlight the Shh-defectiveness-related phenotypes (e.g. shortened trunk, tumour-like cell masses, and reduced eye size). Percentages of larvae with normal or abnormal morphology are graphed. The chi-square test was used. **d, f** *foxo3b* inhibition enhances Wnt- and Shh-unfit cell accumulation. Whole-mount in situ hybridisation of ELuc in Tg(OTM:ELucCP) embryos (**d**) or immunostaining of d2EGFP (green) in Tg(8xGBS:d2EGFP) larvae (**f**) injected with *luciferase* or *foxo3b* sgRNAs (*foxo3b* KO). Scale bar = 100 μm in **d** and 10 μm in **f**. The bar plots show unfit cell frequencies in each sample. The chi-square test and an unpaired two-tailed *t*-test were used for statistical analyses in **d** and **f,** respectively. **e, g, h** *foxo3b*-mediated unfit cell elimination is required for precise tissue patterning. Representative images show the whole-mount in situ hybridisation of *cdx4* (**e**) or *olig2* (**g**) and immunostaining for fast myosin (**h**) injected with *luciferase* or *foxo3b* sgRNAs. Scale bar = 100 μm in **e** and **g** and 10 μm in **h**. The bottom graph in **e** and **g** show the percentages of embryos/larvae with normal or abnormal expression patterns. The chi-square test was used for statistical analysis (**e**, **g**). The graph to the right of **h** shows the mean + SEM of abnormal gene expressing-cell frequencies in each larva. An unpaired two-tailed *t*-test was used for the statistical analysis. **i** Schematic illustration indicating that precise morphogen gradient formation and tissue patterning require *foxo3b* activity.

8. Foxo3 is a common marker of cell competition

In mice and zebrafish, Ras-hyperactivated cells are physically extruded from the epithelia through competitive communication with neighbouring normal cells[20,62] and cells expressing high levels of Myc protein kill neighbouring normal cells[8,17,63]. “Minute cell competition”, which is the most well-documented example of cell competition in *Drosophila* and drives competitive communication between wild-type cells and ribosomal protein gene *rps3*-mutated cells (“Minute” cells) and consequent apoptotic elimination of mutated cells[19], can also occur in zebrafish (Fig. 5.8.1 a, b). Surprisingly, *foxo3b* was upregulated in Minute cells enclosed with normal cells (Fig. 5.8.1 c), Ras-hyperactivated cells surrounded by normal cells (Fig. 5.8.1 d), and normal cells neighbouring Myc-high cells (Fig. 5.8.1 e), all of which are “loser cells” in cell competition. These results indicate that *foxo3b* is a common marker of loser cells in zebrafish competition.

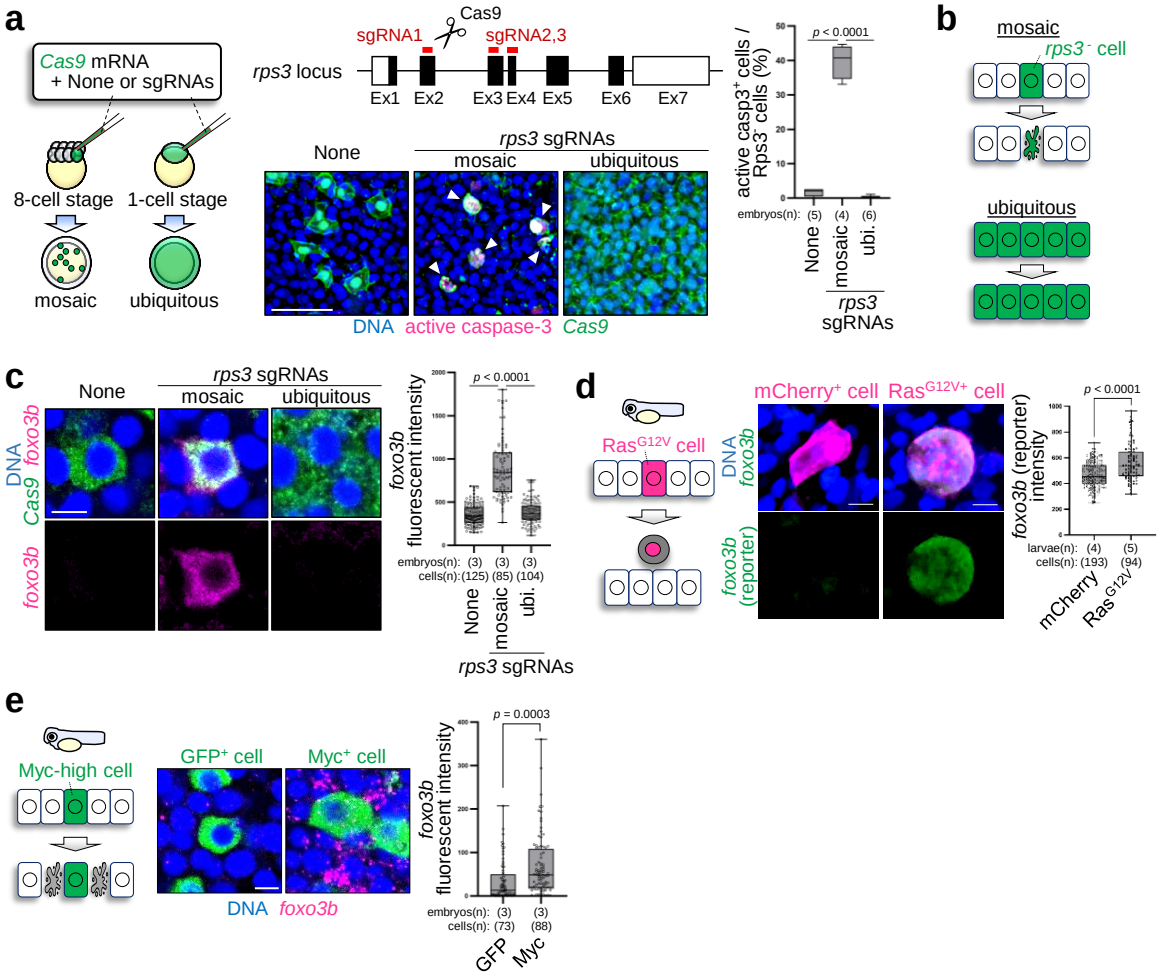

Fig 5.8.1: Foxo3b is a common marker of cell competition.
a Cell competition eliminates *rps3* mutant cells. The schematic diagram on the left shows the experimental introduction of *rps3* mutant cells into zebrafish embryos in a mosaic or ubiquitous manner using CRISPR/Cas9-mediated genome editing. Confocal images show whole-mount immunostaining of embryos (9 hpf) without *rps3* mutants (none) or with mosaic or ubiquitous *rps3* mutants (green) and active caspase-3 (magenta). Scale bar = 100 µm. The box plot on the right shows the mean + SEM of the GFP$^+$ and caspase-3 active cell frequencies. Maximum and minimum: whiskers; medians: lines; 25th and 75th percentiles: boxes. Two-tailed one-way ANOVA was used. **b** Schematic illustration indicating that *rps3* mutant cells are eliminated by competition with neighbouring normal cells. **c** *rps3* mutant cells upregulate *foxo3b*. Representative images show whole-mount in situ hybridisation of *foxo3b* mRNA (magenta) in embryos without *rps3* mutants (none) or with mosaic or ubiquitous *rps3* mutants (green). Scale bar = 10 µm. **d** Oncogenic Ras^{G12V} cells show upregulated *foxo3b* expression. Confocal images show endogenous *foxo3b* (green) expression in Tg(*foxo3b*:GFP) 24 hpf larvae expressing mCherry alone or with Ras^{G12V}. Scale bar = 10 µm. **e** Myc-surrounding cells upregulate *foxo3b*. Myc-high cells communicate with and induce apoptosis in the surrounding Myc-low cells. Representative images show whole-mount in situ hybridisation of *foxo3b* mRNA (magenta) in mosaic embryos (9 hpf) expressing GFP alone or with Myc. Scale bar = 10 µm. In **c**, **d**, **e**, the box plot on the right shows the mean + SEM of the *foxo3b* intensity of each GFP$^+$

cell (**c**), mCherry^{+} cell (**d**), and cells neighbouring GFP^{+} cell (**e**). Maximum and minimum: whiskers; medians: lines; 25th and 75th percentiles: boxes. An unpaired two-tailed one-way ANOVA was used.

We next examined whether Foxo3 is a cell competition marker in mice. Zebrafish have two duplicated *foxo3* copies (*foxo3a* and *foxo3b*), whereas mice only have one (*Foxo3*). Previous phylogenetic and functional analyses revealed that zebrafish *foxo3b* is highly orthologous to mouse *Foxo3*[44,64,65]. Therefore, we re-analysed the single-cell RNA-seq data of mouse loser cells in post-implantation epiblast (accession number E-MTAB-80-640 [https://www.ebi.ac.uk/biostudies/arrayexpress/studies/E-MTAB-8640/files])[18]. The presumptive loser cells expressed *Foxo3* (Fig. 5.8.2 a, b). We also examined *Foxo3* expression in loser cells with low nuclear YAP levels, which trigger competitive communication with neighbouring normal cells in the mouse pre-implantation epiblast[16]. Apoptosis inhibition through Z-VAD-FMK treatment increased the number of nuclear YAP-low loser cells in mouse epiblasts (Fig. 5.8.2 c-f). Foxo3 expression levels were low in nuclear YAP-low cells within DMSO-treated epiblasts, but in Z-VAD-FMK-treated epiblasts, Foxo3 expression levels in nuclear YAP-low loser cells increased, supporting our hypothesis that Foxo3 is upregulated in loser cells (Fig. 5.8.2 c-e, g, h), which is consistent with our hypothesis that the loser cells express high-level of Foxo3. Thus, Foxo3 may be a conserved common marker for less-fit cells in various cell competition contexts.

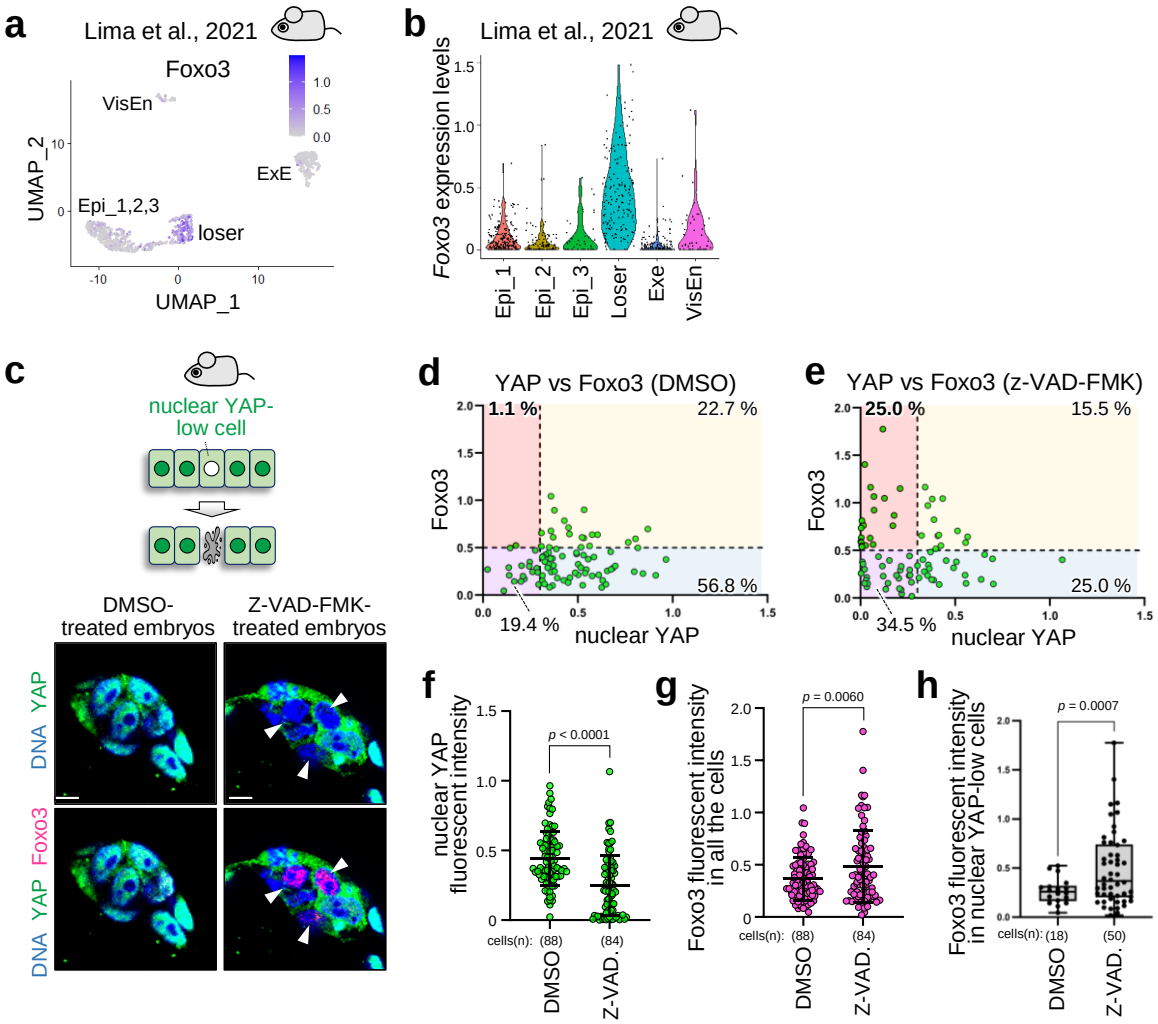

Fig 5.8.2: Foxo3 is a potential conserved common marker of cell competition.
a, b Loser cells in mouse post-implantation epiblast express *Foxo3.* The single-cell RNA-seq data of E5.5 mouse embryos cultured for 16 h with or without a caspase inhibitor (accession number E-MTAB-80-640) was re-analysed using Seurat 4.0.0. Six clusters, named Epiblast_1 (Epi_1), Epiblast_2 (Epi_2), Epiblast_3 (Epi_3), Loser, Extra-embryonic ectoderm (ExE), and Visceral endoderm (VisEn), were identified based on marker gene expression (**a**). The clusters Epi_1/Epi_2 and Epi_3 likely correspond to the Normal (winner) epiblast and Intermediate clusters, respectively. The graph in **b** shows *Foxo3* expression levels in each cluster. **c-h** Nuclear YAP-low loser cells in mouse pre-implantation epiblast express Foxo3. Representative images in **c** show whole-mount immunostaining for YAP (green) and Foxo3 (magenta) in DMSO-treated (control) or Z-VAD-FMK-treated (apoptosis-inhibited) embryos. Note that most of the cells in DMSO-treated embryos are nuclear YAP-high and Foxo3-low, but Z-VAD-FMK treatment increased nuclear YAP-low and Foxo3-high cells. Apoptosis inhibition induces nuclear YAP-low, Foxo3-high cell accumulation (**d-h**). Correlations between signals of nuclear YAP and Foxo3 in DMSO-treated (control) and Z-VAD-FMK-treated (apoptosis-inhibited) embryos are graphed in (**d**, **e**), and quantified nuclear YAP and Foxo3 signals in all the cells or quantified Foxo3 signals in nuclear YAP-low cells treated with DMSO or Z-VAD-FMK are graphed in **f**, **g, h**, respectively. The percentages of nuclear YAP-low and Foxo3-high cells

(upper left, orange), nuclear YAP-high and Foxo3-high cells (upper right, yellow), nuclear YAP-high and Foxo3-low cells (bottom right, light blue), and nuclear YAP-low and Foxo3-low cells (bottom left, pink) are shown in **d** and **e**. An unpaired two-tailed *t*-test was used.

6. Discussion

6.1 Summary and Conclusion

This study identified a previously unknown universal cell competition marker candidate in vertebrates and elucidated the novel roles and mechanisms of physiological cell competition during organogenesis: Shh-unfitness-driven cell competition. In zebrafish spinal cord and muscle development regulated by Shh morphogen gradients, unfit cells with abnormal Shh activity spontaneously appear and distort the morphogen gradient. Subsequently, unfit cells alter membrane N-cadherin protein levels, activate the Smad-Foxo3-ROS axis, and undergo apoptosis through communication with neighbouring normal cells (Fig. 6.1.1). In zebrafish and mouse, Foxo3 is upregulated in cells with abnormal morphogen signalling and in various less-fit cells, which are eliminated through cell competition. Thus, Foxo3 can be a common marker of cell competition in vertebrates.

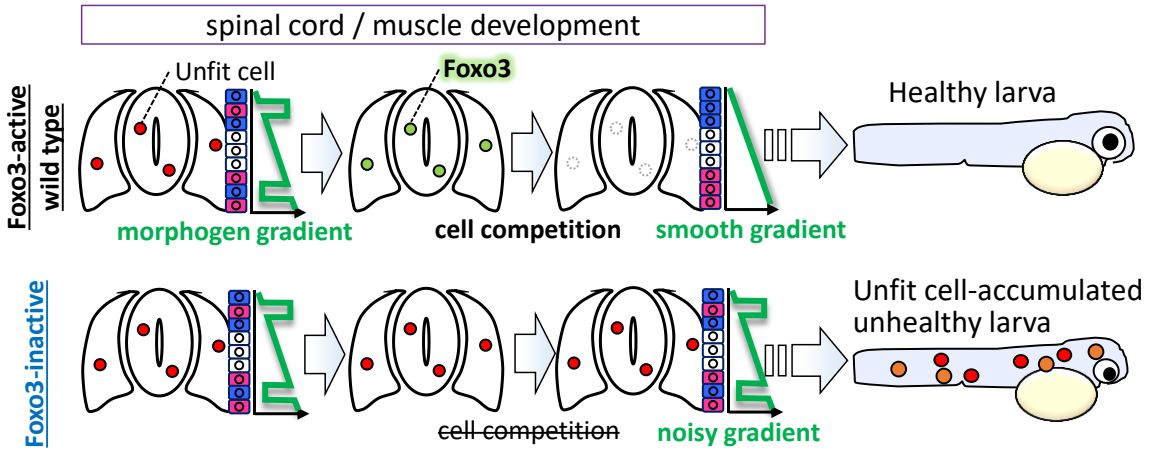

Fig 6.1.1: Foxo3-mediated physiological cell competition eliminates unfit cells to achieve robust oraganogenesis.
Although cells with unfit Shh activity spontanously emerge, Foxo3-mediated physiological cell competition eliminated unfit cells and achieve precise patterning of the spinal cord and muscle tissues.

Moreover, we demonstrated that the morphogen gradients, specifically those involving Wnt and Shh signalling, are not merely established through passive diffusion, as described in the classic French-flag model, but are actively manitained by the removal of unfit cells. While morphogen gradients are not entirely precise, they enable cells with similar properties to be specified in close proximity. However, during developmental process, cells that introduce noise into the morphogen gradients spontaneously emerge. Competitive communication-mediated elimination of these unfit cells correct such noises, thereby ensuring precise cell fate specification. Therefore, we propose that robust tissue patterning requires the interplay between morphogen gradients and cell competition.

6.2 Future perspectives

Physiological roles of cell competition in vertebrate development

Artificially introduced cells with abnormal Myc or Axin2 activity trigger competitive communication with neighbouring normal cells in developing mouse organs (i.e. the heart, skin, and brain)[66–68]. These facts suggest that developing tissues can eliminate unfit cells through cell competition. However, whether unfit cells are generated and drive cell competition during physiological organogenesis is poorly understood. This is partly due to the inherent difficulty in capturing spontaneously arising abnormal cells. In our zebrafish model, which is well-suited for imaging analyses, we have previously captured the emergence of unfit cells during embryogenesis[8]. In this study, we visualized abnormal cell appearance and endogenous cell competition in vertebrate organogenesis and elucidated their regulatory mechanisms. Furthermore, we demonstrated that eliminating these unfit cells is essential for proper organogenesis. Thus, we have revealed the physiological significance of cell competition during organogenesis.

Cell competition-mediated morphogen gradient correction

Drosophila imaginal discs, that form bone morphogenetic proteins (BMP) morphogen gradients, can eliminate artificially introduced cells with abnormally high or low BMP activity[69,70]. Zebrafish embryonic tissue eliminates naturally and artificially generated cells with unfit Wnt/β-catenin signalling activity through cell competition to correct noisy Wnt/β-catenin morphogen gradients and achieve precise anterior-posterior patterning[8]. This study demonstrates that cell competition-mediated elimination of Shh-unfit cells ensures the precise Shh morphogen gradient formation and robust spinal cord and muscle patterning. These findings indicate that cell competition-mediated morphogen gradient correction may function irrespective of the morphogen type, supporting robust tissue patterning. Because morphogen gradients are also formed in adult organs[71–73], this correction system may be involved in tissue homeostasis and regeneration. Regarding elimination mechanisms, Wnt- and Shh-unfit cells are eliminated via cadherin-mediated communication with neighbouring fit cells and Smad-Foxo3-ROS axis activation. How Shh

morphogen signalling controls N-cadherin protein levels remain elusive. As N-cadherin levels are regulated in the plasma membrane, investigating the endocytic processes of cadherins may offer intriguing perspectives. It might be interesting to focusing on Cell-adhesion molecule-related/down-regulated by Oncogenes (Cdon) protein as a possible mediator of this process because Shh signaling negatively regulates Cdon expression, and Cdon positively regulates membrane-localization of N-cadherin and in developing zebrafish spinal cord[74]. Thus, our studies indicate that dose-dependent morphogen signalling activation in morphogen-receiving cells and cadherin-mediated intercellular coordination is required to precisely form morphogen gradients and consequent tissue patterns.

Mechano-gradients and unfit cell elimination

In our study, we demonstrated that both abnormally high and low Shh-unfit ells activate the Smad-Foxo3-ROS axis. From the perspective of chemical signal transduction, interpreting how opposite chemical signals converge to activate the same downstream pathways is significant challenge. Interstingly, from a mechanical signalling perspective, we recently succeeded in clarifying part of the mechanisms underlying the elimination of both abnormally high and low Wnt-unfit cells in zebrafish early embyos[75]. In summary, we discovered that (1) the gradients of Wnt/β-catenin morphogen signalling activity are converted into mechano-gradients' generated by the actomyosin contractile activity; (2) cells with abnormally high and low Wnt signalling activity, which introduce noise in morphogen gradients, induce local deformation of the mechano-gradients, and thereby activates mechanosensitive calcium channels in the neighbouring fit cells, leading them to secrete AnnexinA1 for killing the unfit cells. We propose that a similar mechanism may operate during organogensis, integrating chemical and mechanical signalling to ensure robust tissue patterning.

Cell competition- and cell sorting-mediated morphogen gradient correction

In addition to cell competition, cadherin-mediated cell sorting contributes to morphogen gradient correction during spinal cord development in zebrafish[39]. In the spinal cord, strong Shh signalling activation induces protocadherin 19 (Pcdh19) transcription, whereas moderate Shh signalling levels induce the transcriptional activation of type-II cadherin Cdh11. Because of this Shh activity-dependent cadherin transcription and preferential homophilic cadherin binding, cells with unfit Shh activity migrate to areas with fitter Shh-activity[39]. However, the significance of multiple systems for morphogen gradient correction and differential utilization in developing tissues is unknown. To clarify this, identifying specific regulatory factors governing cell sorting is critical.

This study demonstrated that cell competition is crucial for robust spinal cord development by inhibiting cell competition through blocking apoptosis or *foxo3* activity. Furthermore, forced cell competition inhibition led to the accumulation of Shh-high cells in the Shh-high ventral region (Fig. 6.2.1 a, b), indicating that ectopically generated and surviving Shh-high cells may have migrated to the Shh-high fit area. Additionally, apoptosis inhibition mainly led to the increase of physiologically emerged Shh-high cells, whereas Shh-low cells did not show a significant increase (Fig. 5.2.1 e, f). This may be because the unfit cells with abnormally low Shh signalling activity are more prone to migrate under apoptosis inhibition. These findings also suggest that cell competition and sorting-mediated systems mutually influence one another. Considering the efficient activation of the apoptosis-mediated system in cells only causing substantial noises in morphogen gradients, the "unfitness" of unfit cells can determine the system they use. For example, minor and fluctuating noise may be repaired by sorting, whereas severe and persistent noise may be eliminated through cell competition. Notably, the types of cadherins and their regulatory mechanisms differ between these two systems. Cdh11 and Pcdh19, which are transcriptionally regulated by the Shh morphogen gradient, mediate sorting[39], whereas N-cadherin, which is post-translationally regulated by the Shh morphogen, mediates cell competition. Investigating this distinction may provide insight into the underlying switching mechanisms.

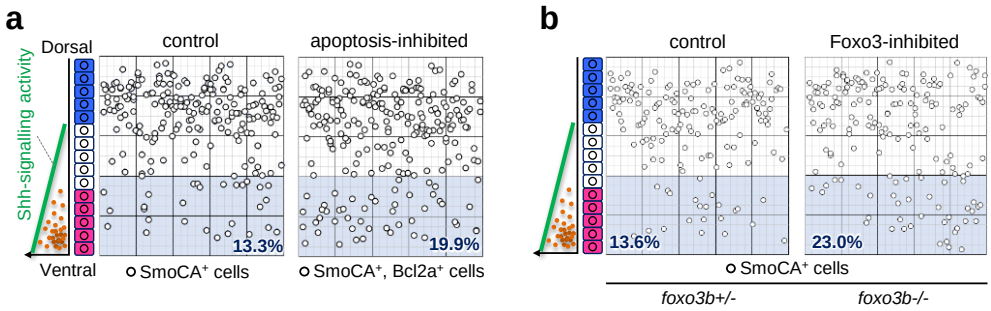

Fig 6.2.1: Forced cell competition inhibition induces the accumulation of Shh-high SmoCA$^+$ cells in the Shh-high ventral region.
a, b The panels in **a** show the maps of artificially introduced cells expressing SmoCA without (left) or with Bcl2a (right) in the zebrafish spinal cord. The panels in **b** show the maps of artificially introduced cells expressing SmoCA in the spinal cord of *foxo3b+/-* or *foxo3b-/-* mutants. The percentages of SmoCA$^+$ cells in the Shh-high ventral area are shown at the bottom.

Universal molecular mechanisms of cell competition

The universal mechanisms regulating diverse types of cell competition remain unknown. Transcriptomic analysis indicated that the Flower-Azot pathway is specifically activated in loser cells in *Drosophila*[21,22]. However, our previous RNA-seq data did not show *flower* or *azot*-like gene upregulation in Wnt-unfit cells (GEO accession code: GSE133526)[8] (Table. 5.6.1), indicating that the Flower-Azot pathway might not be a universal machinery of cell competition in vertebrates. This study identified several genes encoding common regulator candidates, including *foxo3b*, *sesn3*, *tcima*, and *lnx1*. *foxo3b* is commonly upregulated in cells that lose cell competition driven by Wnt, Shh, Ras, Myc, and ribosomal proteins in zebrafish. In addition, less-fit cells in mice also upregulated *Foxo3*, suggesting that Foxo3 is a potential marker of cell competition in vertebrates.

However, how different cellular fitness leads to *foxo3* expression in unfit cells, and what is the specific functional role of Foxo3 in each context is still unclear and requires further investigation. This study shows that, at least in unfit cells with abnormal Wnt

signalling activity, Smads and Foxo3 proteins seem to cooperatively translocate into nucleus and activate *foxo3* gene expression. A similar mechanism would be used in Shh-unfit cell apoptosis, because Smad activation and *foxo3* upregulation are required for this process. On the other hand, we previously shown that Myc-mediated cell competition occurs in a Smad-independent manner[7]. It is well-known that Foxo family proteins can associate with a variety of unrelated transcription factors to regulate target gene expression[76–78]. Therefore, it would be interesting to investigate the possibility that Foxo3 might bind to different transcription factors depending on the type of cellular unfitness, thereby inducing *foxo3* expression in the nucleus.

Foxo3 and the role of physiological cell competition in tissue integrity

Because less-fit cells appear sporadically, analysing when and where cell competition occurs is challenging. In this study, we generated a Tg(*foxo3b*:GFP) and Tg(*foxo3b*:mCherry) reporter to visualize the spatiotemporal dynamics of *foxo3b* expression from embryogenesis to organogenesis, enabling us to understand the spatiotemporal dynamics and roles of physiological cell competition. However, Foxo3 is involved in various signalling pathways (e.g. cell metabolism, DNA damage repair, and stress resistance)[43,79], and therefore, to attain a more accurate understanding of physiological cell competition, integrating additional factors such as *sesn3*, *tcima*, *lnx1*, and others would be advantageous. This approach would allow us to precisely detect naturally generated unfit cells, thereby understanding the importance of physiological cell competition and elucidating the causes of the "abnormality" of unfit cells.

Cells with abnormal Shh and Wnt signalling activities or Foxo3 dysregulation can be the origin of tumorigenesis[80–85]. Therefore, cell competition-mediated elimination of unfit cells might support robust tissue development and serve as a mechanism to suppress cancer initiation. Additionally, Foxo3 is well-known for its associations with ageing and age-related diseases. For instance, genetic variations in Foxo3 are associated with longevity[86–88], whereas the decreased activity of Foxo3 is implicated in the progression of age-related diseases[89]. We also show that a part of *foxo3b*-/- zebrafish, which appeared phenotypically

normal during embryonic and larval development, exhibited deformities as they aged (Fig. 6.2.2). Foxo3 may sustain the robustness of tissue homeostasis through cell competition throughout life. Interestingly, a previous study reported that *foxo3b*-null zebrafish have lower survival rates under hypoxic stress[90]. Possibly, this vulnerability to hypoxia might be partly due to poor-quality cells, which would normally be removed through cell competition, persisting in these *foxo3*-deficient zebrafish. Thus, it would be interesting to investigate the role of this system in health maintenance, stress tolerance, and the prevention of aging. Our findings reveal a novel facet of Foxo3 that has already been recognized as an anti-ageing factor.

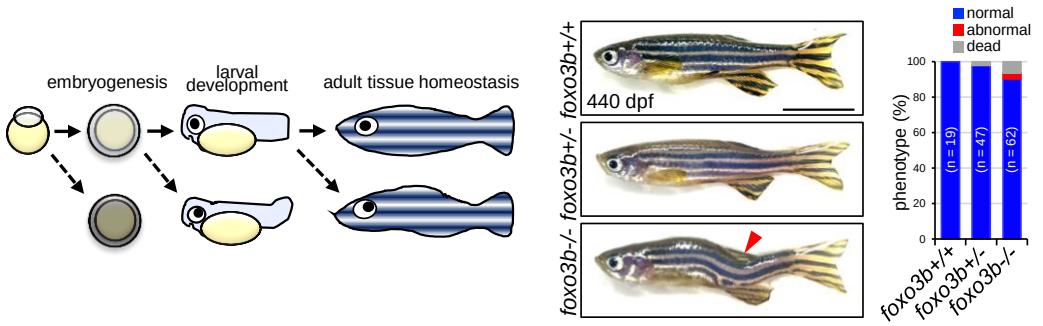

Fig 6.2.2: Foxo3 may sustain the robustness of tissue homeostasis via cell competition throughout life.
Representative images show wild-type (*foxo3b*+/+), heterozygous (*foxo3b*+/-), or homozygous (*foxo3b*-/-) 440 dpf male siblings. Note that we placed phenotypically normal larvae into tanks and analysed their phenotypes as they aged. Percentages of individual with normal or abnormal phenotypes, as well as those that died, are graphed. Scale bar = 1000 μm.

Materials and Methods

Ethical approval

All experimental animal care was performed following institutional and national guidelines and regulations. The study protocol was approved by the Institutional Animal Care and Use Committee of Osaka University (RIMD Permit# Biken-AP-R02-04, FBS Permit# FBS-20-001). The study was conducted following the ARRIVE guidelines.

Zebrafish maintenance

Adult zebrafish were maintained under a 14 h light/10 h dark cycle at 28.5°C. Wild-type strains (AB) and the following transgenic lines were used: Tg(8xGBS:d2EGFP)[37], Tg(OTM:ELuc-CP)[8], Tg(hsp70l:mKO2-T2A-SmoCA), Tg(hsp70l:GFP-zBcl2a), Tg(*foxo3b*:GFP), Tg(*foxo3b*:mCherry), *foxo3b-/-*, and Tg(*krt4p:gal4*)[91]. One-cell stage embryos were used for cell injection to generate transgenic fish or mosaic embryos and larvae, with the larvae processed at 24 h post-fertilization (hpf).

Plasmids

8xGBS:d2EGFP was constructed by inserting the SmaI fragment of 8x3'Gli-BS-δ51-LucII[92], including Gli-biding sequence (Gli-BS), between the Tol2 excision site and a minimal promoter (miniP, AGAGGGTATATAATGGAAGCTCGACTTCCAG), which is derived from pGL4 (Promega, Madison, WI, USA), of XhoI/EcoRI-digested pT2-TCF-mini-d2EGFP[93]. The half-life of d2EGFP protein is relatively short (about approximately 2 h), which was used as a fluorescent reporter in 8xGBS:d2EGFP, and this property facilitates the detection of dynamic changes during Shh signaling *in vivo*.

The *hsp70l* promoter was subcloned into a pTol2 vector (a gift from Dr K. Kawakami) to prepare heat-shock promoter-driven plasmids. mKO2 or membrane-tagged (GAP43-fused) GFP and T2A were then subcloned into the pTol2-hsp70l promoter plasmid. These plasmids expressed mKO2 or GAP43-GFP in response to heat shock. PCR-amplified cDNA encoding signalling modulator proteins were subcloned downstream of T2A in

pTol2-hsp70l:mKO2 (or GAP43-GFP)-T2A plasmids to generate plasmids expressing mKO2 or GAP43-GFP with signalling modulator proteins.

The Shh signalling activators included a constitutively active mutant of mouse Smoothened (SmoCA), in which Trp539 was replaced with Leu (a gift from Dr P. Beachy, Addgene plasmid #37673; Cambridge, MA, USA)[94] and human wild-type Gli1 (a gift from Dr B. Vogelstein; Addgene plasmid #16419)[95]. Shh signalling inhibitors included mouse wild-type Ptch1 (a gift from Dr P. Beachy, Addgene plasmid #120889)[96] and the dominant-negative form of Gli3R (a gift from Dr B. Vogelstein; Addgene plasmid #16420)[95]. Other signalling regulators were as follows: N-cadherin; Smad3bDN, in which Pro401, Ser421 and Ser423 were substituted with His, Ala, and Ala, respectively[97]; constitutively active zebrafish Smad3b mutant (Smad3bCA), in which Ser421 and Ser423 were substituted with Asp; *foxo3b*DN (N-terminus-truncated zebrafish foxo3b)[98]; GFP-fusion zebrafish Bcl2a (GFP-Bcl2a); human Puma (a gift from Dr B. Vogelstein; Addgene plasmid #16588)[48]; and zebrafish Caspase-8. Wnt/β-catenin signalling activator (N-terminus-truncated mouse β-catenin, β-catCA) and Wnt/β-catenin signalling inhibitor (human wild-type GSK-3β) have been previously described[8]. To prepare UAS promoter-driven plasmids expressing constitutively active human H-Ras (Ras^{G12V}) mutants, Gly12 was substituted with Val (pTol2-UAS-mCherry-T2A-Ras^{G12V}) as previously described[20].

cDNAs for signalling proteins were PCR-amplified and cloned into the multicloning site of the pCS2p+ vector for mRNA synthesis. The cloned proteins were caspase activity fluorescent biosensor/CC3Ai (a gift from Dr. B. Li, Addgene #78909)[99], mScarlet (a gift from Dr D. Gadella; Addgene plasmid #85042)[100], GFP, Cas9, human Bcl2a (a gift from Dr S. Korsmeyer, Addgene #8768)[101], mouse SmoCA, and zebrafish Foxo3b.

sgRNA synthesis

We selected target sequences for each gene that did not overlap with other genomic sequences using the CRISPR design tool CHOPCHOP (https://chopchop.cbu.uib.no/). The protocol for sgRNA synthesis was based on a previously reported method[102]. The oligonucleotides containing a T7 promoter sequence, target sequence, and the sgRNA

templates were PCR-amplified from sgRNA scaffold oligo[103] using the oligonucleotides and primer sgRNA-RV with PrimeSTAR Max (TaKaRa, Kusatsu, Japan) and purified using the NucleoSpin Gel and PCR Clean-up Kit (MACHEREY–NAGEL, Düren, Germany). sgRNAs were synthesized using the CUGA7 gRNA Synthesis Kit (Nippon Gene, Tokyo, Japan), and their concentrations were measured using a NanoDrop Lite spectrophotometer (Thermo Fisher Scientific, Waltham, MA, USA).

Generation of transgenic zebrafish

Plasmid DNA and Tol2 transposase mRNA were co-injected into one-cell stage wild-type zebrafish embryos to generate Tg(hsp70l:mKO2-T2A-SmoCA) and Tg(hsp70l:GFP-zBcl2a) zebrafish. To generate Tg(*foxo3b*:GFP) and Tg(foxo3b:mCherry) zebrafish, a donor plasmid containing a heat-shock promoter was co-injected into one-cell stage wild-type embryos and a short guide RNA (sgRNA) targeted for genome digestion, an sgRNA targeted for donor plasmid digestion, and the Cas9 protein (M0646, New England Biolabs, Ipswich, MA, USA)[104]. The sgRNA sequences were 5′-tcccgtacgcggaatccaggggg-3′ (*foxo3b* transcription start site (TSS) upstream target) and 5′-ggctgctgtcagggagctcatgg-3′ (tbait).

Two sgRNAs and Cas9 proteins were co-injected into one-cell-stage wild-type embryos to generate *foxo3b*$^{-/-}$ zebrafish. Two gRNAs were designed to delete the 2 kb upstream promoter region from the TSS and exon 2. The sgRNA sequences were as follows: 5′-catgcctcaacataggacagtgg-3′ (-2 kb from the TSS) and 5′-gaactgctgcctgtgtcacaagg-3′ (flanking region of exon2). Transgenic fish were then outcrossed with wild-type fish to produce founder lines. Heterozygous adult fish were crossed to obtain homozygous transgenic lines.

Clonal introduction of Shh-unfit cells

H2B-mCherry (100 pg) mRNA with or without *SmoCA* mRNA (400 pg) were injected into two blastomeres of an eight-cell stage embryo. This method introduces Shh-unfit cells at the patchy-clone level.

Mosaic introduction of Shh-unfit cells

Hsp70 promoter-driven plasmids (12.5–50 pg) were injected into one-cell stage embryos and maintained at 23.5°C until 14 hpf (10-somite stage). The larvae were then exposed to heat shock. After bringing larvae back to 28.5°C for 15 min, they were transferred to pre-warmed egg water at 37°C and kept at this temperature for 1 h. Subsequently, larvae were placed at 28.5°C, then fixed at 24 hpf for immunostaining or in situ hybridization. This method introduces Shh-unfit cells at the single-cell level but not at the patchy-clone level.

Mosaic introduction of Wnt-unfit cells

Hsp70 promoter-driven plasmids (5–17.5 pg) were injected into one-cell-stage embryos and maintained at 28.5°C until 4.3 hpf (dome stage). The embryos were then exposed to heat-shock at 37°C for 1 h. After the heat shock, embryos were placed at 28.5°C, then fixed at 9 hpf.

Mosaic introduction of oncogenic cells

UAS promoter-driven plasmids (7.5–25 pg) were injected into one-cell-stage Tg(*krt4p:gal4*) embryos, maintained at 25.5 °C, and fixed at 26–28 hpf.

foxo3b KO zebrafish in the F0 generation

Cas9 protein and four sgRNAs were injected into one-cell stage embryos to generate *foxo3b* KO zebrafish in the F0 generation[59–61]. The sgRNA sequences were as follows: 5′-ccggcgaagggccaaaaatgggg-3′, 5′- gacggaggcttcccggcgaaggg-3′, and 5′-ggattcagcaaccccatttttgg-3′, 5′- gcgtagacggtagttttgagagg-3′. As control, four *luciferase* sgRNAs were injected and their sequences were as follows: 5′- gggcatttcgcagcctaccgtgg-3′, 5′- ggcatgcgagaatctcacgcagg-3′, and 5′-tcggggaagcggttgccaagagg-3′, 5′-tttgtggacgaagtaccgaaagg-3′.

Mosaic or ubiquitous introduction of *rps3* mutant cells

Cas9 mRNA and sgRNAs were injected into a single blastomere of an eight-cell stage embryo to introduce mosaic mutants[105]. *Cas9* mRNA and sgRNAs were injected into one-cell stage embryos to generate ubiquitous mutants[105]. Three sgRNAs were injected to disrupt the *rps3* gene efficiently[59,61]. The sgRNA sequences were as follows: 5′-cgaggatggttattccggcgtgg-3′, 5′-cattcgtgagctgaccgctgtgg-3′, and 5′-tctctgcgctacaagctgctcgg-3′.

Time-lapse imaging and data analysis

For time-lapse confocal live imaging, larvae with mosaically introduced SmoCA cells (Supplementary Movie 1, 2) or Tg(foxo3b:mCherry) embryos (Supplementary Movie 3) were manually dechorionated using forceps and mounted in 1% low melting agarose with egg water onto glass bottom dishes. Live imaging was performed using an FV3000 confocal laser scanning microscope (Olympus, Tokyo, Japan). In Supplementary Movie 1, 2, two laser lines at 488 and 594 nm were used. The recording interval was 10 min. At each time point, 30 confocal slices were acquired along the z-axis. In Supplementary Movie 3, three lase lines at 445, 488, and 561 nm were used. The recording interval was 10 min. At each time point, 18 confocal slices were acquired along the z-axis.

Antibodies

Primary antibodies included anti-fast myosin (F310) (#AB_531863, 1/10; Developmental Studies Hybridoma Bank (DSHB), Iowa City, IA, USA); anti-slow myosin (F59) (#AB_528373, 1/10; DSHB,); anti-muscle pioneer (4D9) (#AB_528224, 1/5; DSHB); anti-N-cadherin (Cadherin2) (#125885, 1/1000; GeneTex, Irvine, CA, USA); chicken anti-GFP (#13970, 1/1000; Abcam, Cambridge, UK); rabbit anti-GFP (#A-11122, 1/500; Thermo Fisher Scientific); anti-active caspase-3 (#559565 (1/500; BD Bioscience, Franklin Lakes, NJ, USA) and #9661 (1/500; Cell Signaling, Mountain View, CA, USA)); anti-V5 tag (R960-25, 1/200; Invitrogen).

Secondary antibodies included AlexaFluor488-conjugated anti-chicken IgY (#A-78948, 1/1000; Invitrogen, Waltham, MA, USA) and anti-rabbit IgG (#A-11034, 1/500; Invitrogen); AlexaFluor594-conjugated anti-mouse IgG (#A-11032, 1/500; Invitrogen) and anti-rabbit IgG (#A-11037, 1/500; Invitrogen); AlexaFluor647-conjugated anti-rabbit IgG (#4414, 1/500; Cell Signaling Technology) and anti-mouse IgG (#A-21235, 1/500, Invitrogen).

mRNA and antisense oligo MO microinjection

Capped mRNA was synthesized using the SP6 mMESSEAGE mMACHINE kit (Ambion, Austin, TX, USA) and purified using Micro Bio-Spin columns (Zymo Research, Irvine, CA, USA). The synthesized mRNA was injected into one-cell-stage embryos. Antisense oligo MOs (Gene Tools, Philomath, OR, USA) were injected into one-cell stage embryos to perform knockdown experiments in zebrafish larvae. Standard control morpholino, 5′-CCT CTT ACC CTC AGT TAC AAT TTA TA-3′; N-cadherin (*n-cadherin*)[39,40], 5′-TCT GTA TAA AGA AAA GCG ATA GAG TT-3′ (1 ng); Smad4 (*smad4a*)[42], 5′-AAT CAT ACT CAT CCT TCA CCA TCA T-3′ (2 ng); Cadherin11 (*cdh11*)[39], 5′-TCT GTA TAA AGA AAC CGA TAG AGT T-3′ (2 ng) were injected. *n-cadherin* and *smad4a* MOs are translation-blocking morpholinos, and *cdh11* MO is a splicing-blocking morpholino. We adjusted the concentration of the MO to achieve a level of expression that was sufficiently reduced without causing severe morphogenetic defects.

Chemical treatment

Zebrafish larvae were treated with 30 μM Smo inhibitor Cyclopamine (Selleck Chemicals, Houston, TX, USA) to downregulate Shh signalling activity. Larvae were treated with 100 μM NAC (Sigma-Aldrich, St. Louis, MO, USA) to evaluate the effects of ROS on eliminating unfit cells. Each solution was added at 18 hpf.

Whole-mount immunostaining

At 9 hpf, embryos were fixed with pre-cooled 4% paraformaldehyde in phosphate-buffered saline (PBS) overnight at 4°C. At 24 hpf, larvae were dechorionated with 1 mg/ml pronase (Roche, Darmstadt, Germany) and fixed with 4% paraformaldehyde in PBS overnight at 4°C. The embryos and larvae were washed with 0.5% Triton X-100 (PBST) at least four times and blocked with 10% fetal bovine serum, 4% Block Ace (Megmilk Snow Brand, Tokyo, Japan), and 1% dimethylsulphoxide (DMSO) in 0.1% PBST for 1 h. The embryos and larvae were incubated with the primary antibodies overnight at 4°C, washed, and incubated with AlexaFluor-conjugated secondary antibodies with Hoechst33342 (H3570, 1/1000; Invitrogen) overnight at 4°C.

Immunostaining for anti-8-OHdG was performed as previously described with slight modifications[106]. Larvae were dechorionated at 24 hpf with 1 mg/ml pronase and fixed with pre-cooled 50% Bouin's solution in PBS overnight at 4°C. The larvae were washed with 0.5% PBST at least 12 times. After rinsing with 0.5% PBST, larvae were treated with 0.1% collagenase in 2% PBST at 28.5°C for 15 min. After rinsing with 0.5% PBST, larvae were treated with proteinase K (10 μg/mL) at room temperature for 12 min. After rinsing with 0.5% PBST, DNA was denatured using 4 N HCl for 12 min at 28.5°C. The pH was adjusted with 50 mM Tris-HCl for 5 min at 28.5°C. After rinsing with 0.5% PBST and blocking, larvae were incubated with anti-8-OHdG monoclonal antibody (15A3, sc-66036, 1/100; Santa Cruz Biotechnology, Dallas, TX, USA) and anti-GFP antibody overnight at 4°C, then washed and incubated with AlexaFluor-conjugated secondary antibodies and with Hoechst33342 overnight at 4°C. Stained larvae were visualized using an FV3000 confocal laser scanning microscope. Images were prepared and analysed using ImageJ software (NIH, Bethesda, MD, USA).

Whole-mount in situ hybridisation

RNA probe synthesis was performed as previously described[107]. The probes used were as follows: *n-cadherin*, *smoCA*, *dbx1b*, *olig2*, *foxa2*, *cdx4*, *foxo3b*, *sesn3*, *lnx1*, *tcima*, *puma*, *wnt8a*, *shh*, *GFP*, *Emerald luciferase* (ELuc), and *firefly luciferase* (Luc). SBE-Luc

(pGL4.48[luc2P/SBE/Hygro] vector) was purchased from Promega (Madison, WI, USA). Whole-mount in situ hybridization was performed as previously described[107]. Fluorescence in situ hybridization was performed as previously described[108]. digoxigenin (DIG)- or fluorescein isothiocyanate (FITC)-labelled RNA antisense probes were prepared from plasmids containing *n-cadherin*, *dbx1b*, *olig2*, *foxa2*, *cdx4*, *foxo3b*, *sesn3*, *lnx1*, *tcima*, *puma*, *wnt8a*, *shh*, *GFP*, *Emerald luciferase* or *firefly luciferase*. Images were obtained using an FV3000 confocal laser scanning microscope.

Whole-mount multiplex in situ hybridization chain reaction (HCR)

We followed the protocols suggested by Nepagene and previously described[109]. The probes used were as follows: *foxo3b* and *dbx1b* (probe sequences are shown in Table 3). Images were obtained using an FV3000 confocal laser scanning microscope.

Name	Sequence
foxo3b-left1-S23	GGGTGGTCGaaggactcgggcagaggccaagtgcat
foxo3b-left2-S23	GGGTGGTCGaatgccgttgtcctctccttcacccat
foxo3b-left3-S23	GGGTGGTCGaaagagtggagagcctgtgttctcctg
foxo3b-left4-S23	GGGTGGTCGaaagtctcttgtcaggggtgctctcta
foxo3b-left5-S23	GGGTGGTCGaactgttgctgtcgcctttgtctttga
foxo3b-left6-S23	GGGTGGTCGaactgttcatcactgctccgggaagtg
foxo3b-left7-S23	GGGTGGTCGaaccaggataggtgacaggcgtccact
foxo3b-left8-S23	GGGTGGTCGaaaatcgaccattaggttgtccgcctc
foxo3b-left9-S23	GGGTGGTCGaactggaggagctgctttgctgagact
foxo3b-left10-S23	GGGTGGTCGaatccattagttctgagcggattatgg
foxo3b-right1-S23	gtcattggatgcaggcttagccatgaaTCGAAGTCGTAT
foxo3b-right2-S23	aaattagttcttcggccaggcttggaaTCGAAGTCGTAT
foxo3b-right3-S23	ctgtggttgcggaagctgcctgagaaaTCGAAGTCGTAT
foxo3b-right4-S23	atccagtcatagatctgggacagtgaaTCGAAGTCGTAT
foxo3b-right5-S23	cggatggagttcttccaaccagctgaaTCGAAGTCGTAT
foxo3b-right6-S23	agaacggaagtcagtccagcacgataaTCGAAGTCGTAT
foxo3b-right7-S23	ctgagacatcatcaagctctggattaaTCGAAGTCGTAT
foxo3b-right8-S23	gcacctgtgtggcgatgttgtctaaaaTCGAAGTCGTAT
foxo3b-right9-S23	ctcggtcatcagcatggtgggctgtaaTCGAAGTCGTAT
foxo3b-right10-S23	tcaaagttaaaatccagtccatcggaaTCGAAGTCGTAT

Name	Sequence
dbx1b-left1-A161	GGTACGCGAaaggtggcgcaataacacttggcaaca
dbx1b-left2-A161	GGTACGCGAaaaagcagtagacatggcgacgtggact
dbx1b-left3-A161	GGTACGCGAaaggtgaacgccgattgtaacgctgga
dbx1b-left4-A161	GGTACGCGAaacctgttgctggaggagatgcacttg
dbx1b-left5-A161	GGTACGCGAaagacgcgagaatcgcattcactccaa
dbx1b-left6-A161	GGTACGCGAaatctttctgtccggcttgctgatgta
dbx1b-left7-A161	GGTACGCGAaacgccagacgacagaagttctctttc
dbx1b-left8-A161	GGTACGCGAaatcgagggcgacttgaagtgtaaatc
dbx1b-left9-A161	GGTACGCGAaatcgtgctgtgagtggccaagcaaaa
dbx1b-left10-A161	GGTACGCGAaattccgacgtcgcttaaatctggatt
dbx1b-right1-A161	gccgcagaaagctcggatacatggaaAGGTAGGTGTAA
dbx1b-right2-A161	ttgcggggagcttgatctttttgccaaAGGTAGGTGTAA
dbx1b-right3-A161	gtcctccacaaggaaactcgagtgcaaAGGTAGGTGTAA
dbx1b-right4-A161	gaggaggtagtgttcaaagttgtgaaaAGGTAGGTGTAA
dbx1b-right5-A161	ggtggtggtgaagcatttcgtgttgaaAGGTAGGTGTAA
dbx1b-right6-A161	ctttaagaccaagtttcgtcgccagaaAGGTAGGTGTAA
dbx1b-right7-A161	tcgtcggtaaagtttgttccctgcaaaAGGTAGGTGTAA
dbx1b-right8-A161	ctgagaagtctgagtgcttgctggaaaAGGTAGGTGTAA
dbx1b-right9-A161	tcgaagcattcctctcctcggcttcaaAGGTAGGTGTAA
dbx1b-right10-A161	tgagaaccgcctcatgttcaaacctaaAGGTAGGTGTAA

Table3: Sequences of HCR probes used in this study

Reverse transcription polymerase chain reaction

For qPCR analysis, cDNA was synthesized using the ReverTra Ace qPCR RT master mix with genomic DNA remover (#FSQ-301; Toyobo, Osaka, Japan). qPCR analysis was conducted on a Stratagene Mx3000P qPCR system using THUNDERBIRD SYBR qPCR Mix (#QPS-201; Toyobo) using the following conditions: 95°C (1 min), 45 cycles at 95°C (15 s) and 60°C (35 s). A standard curve was used to determine the relative mRNA abundance. The *β-actin* gene was used as a normalization control. The primers used were as follows: 5′-taaggcaagcagagggtgttc-3′ (*afg1lb* Fw1), 5′-ttctctgttgcgggtccttt-3′ (*afg1lb* Rv1), 5′-ttgaatcaacatggcggcg-3′ (*afg1lb* Fw2), 5′-gttgtcgaacaccctctgctt-3′ (*afg1lb* Rv2), 5′-gagcacccctgacaagagac-3′ (*foxo3b* Fw), 5′-gccggatggagttcttccaa-3′ (*foxo3b* Rv), 5′-tggactttgagcaggagatgggaa-3′ (*β-actin* Fw), 5′-aaggtggtctcatggataccgcaa-3′ (*β-actin* Rv).

Histology

Dechorionated larvae were fixed in 4% paraformaldehyde overnight at 4 °C, solidified in iPGell (Genostaff, Tokyo, Japan), placed in 10 and 20% sucrose/PBS until the tissues sank and 30% sucrose/PBS overnight at 4°C. iPGell-solidifed larvae were embedded in a Tissue-Tek optimal cutting temperature (OCT) freezing medium (Sakura Finetek, Tokyo, Japan). Slices (20-μm thick) were prepared using a Thermo Fisher Scientific HM525NX cryostat and stored at −80°C until used (Fig. 2d, Supplementary Fig. 1a).

Gene set enrichment analysis (GSEA)

GSEA against RNA-seq data of β-catCA-mosaically introduced (Mosaic) or ubiquitously β-catCA-expressing (Ubiquitous) zebrafish embryos (GEO accession code: GSE133526)[8] was performed using RaNA-seq[110].

Mouse maintenance

Adult mice were maintained under a 12 h light/12 h dark cycle at 22°C, 55% humidity. B6D2F1/Jcl (C57BL/6N x DBA/2N) F1 female mice were purchased from CLEA Japan, Inc. (Tokyo, Japan). Embryos were obtained from 3-week-old B6D2F1/Slc F1 female mice.

Mice were maintained under specific pathogen-free conditions at the Animal Facility of the Frontier of Biosciences, Osaka University. The Animal Care and Use Committee of the Graduate School of Frontier Biosciences, Osaka University, approved all mice experiments (FBS Permit# FBS-20-001).

Mouse embryo culture and inhibitor treatment

Mouse embryos were obtained from the intercrosses of B6D2F1/Jcl mice at the one- or two-cell stage using standard protocols[111] and were cultured in a well of a 72-well MiniTray (Nunc 136528) containing 10 μl of KSOM medium (ARK resource, Kumamoto, Japan) covered with 5 μl of mineral oil at 37℃ in a 5% CO_2 incubator. Embryos were cultured in KSOM containing 200 mM of Z-VAD-FMK (3118-v; Peptide Institute Inc., Osaka, Japan) and 0.4% DMSO from the early blastocyst stage to the late blastocyst stage to suppress apoptosis. Control embryos were cultured in KSOM containing 0.4% DMSO.

Immunofluorescent staining and image acquisition of mouse embryos

Embryo immunofluorescence staining was performed using a 72-well MiniTray (Nunc 136528), as previously described[16], with slight modifications. Embryos were fixed in 4% paraformaldehyde in PBS for 5 min at room temperature, washed and permeabilized twice with 0.1% Triton X-100 in PBS (0.1% PBST) for 1 min at room temperature. The embryos were then blocked with 2% donkey serum in 0.1% PBST (blocking solution) and incubated overnight with primary antibodies in a blocking solution at 4℃. After washing thrice in 0.1% PBST for 1 min, the embryos were incubated with the secondary antibodies and Hoechst33342 (H342, 1/1000; Dojindo, Jawa Tengah, Indonesia) in 0.1% PBST for over 1 h at room temperature. After two washes in PBS, the embryos were placed in a PBS drop on a glass-based dish, and confocal images were obtained using a Nikon A1 inverted confocal microscope (Tokyo, Japan). Images were analysed using NIS-Elements AR analysis (Nikon) or IMARIS software (Bitplane, Belfast, UK). The following antibodies were used: mouse monoclonal anti-YAP1 antibody (H00010413-MO1, 1/100; Abnova, Taipei, Taiwan), and rabbit monoclonal anti-FOXO3 (2497S, 1/100; Cell Signaling

Technology), Alexa Fluor Plus 488-conjugated donkey anti-mouse antibody (A32766, 1/1000; Thermo Fisher Scientific), Alexa Fluor Plus 555-conjugated donkey anti-rabbit antibody (A32794, 1/1000; Invitrogen), and Alexa Fluor Plus 647-conjugated donkey anti-goat antibody (A21447, 1/1000; Invitrogen).

Analysis of *Foxo3* expression in post-implantation embryo loser cells

Single-cell RNA-seq data from E5.5 mouse embryos cultured for 16 h with or without a caspase inhibitor (accession number E-MTAB-80-640)[18] were re-analysed using Seurat 4.0.0.[112]. Six clusters, Epiblast_1 (Epi_1), Epiblast_2 (Epi_2), Epiblast_3 (Epi_3), Loser, Extra-embryonic ectoderm (ExE), and Visceral endoderm (VisEn), were identified based on the expression of marker genes.

Statistical analyses

Larvae without severe morphological defects were selected for imaging in each experiment. Differences between groups were examined using a two-tailed unpaired Student's *t*-test, one-way analysis of variance (ANOVA), chi-square test in Prism 8 (GraphPad Software, San Diego, CA, USA) or Excel (Microsoft, Redmond, WA, USA), and DESeq2 (version 1.10.1) (The R Project for Statistical Computing). p values <0.05 were considered significant. The representative images and plots were reproduced in at least two or three or more independent experiments.

Refernece

1. Wolpert, L. Positional information and the spatial pattern of cellular differentiation. *Journal of Theoretical Biology* **25**, 1–47 (1969).
2. Davidson, E. H. Emerging properties of animal gene regulatory networks. *Nature* **468**, 911–920 (2010).
3. Schrier, A. F. & Talbot, W. S. Molecular Genetics of Axis Formation in Zebrafish. *Anu. Rev. Genet.* **39**, 561–613 (2005).
4. Ju, Y. S. *et al.* Somatic mutations reveal asymmetric cellular dynamics in the early human embryo. *Nature* **543**, 714–718 (2017).
5. Jonsson, H. *et al.* Multiple transmissions of de novo mutations in families. *Nat Genet* **50**, 1674–1680 (2018).
6. Mashiko, D. *et al.* Chromosome segregation error during early cleavage in mouse pre-implantation embryo does not necessarily cause developmental failure after blastocyst stage. *Sci Rep* **10**, 854 (2020).
7. Currie, C. E. *et al.* The first mitotic division of human embryos is highly error prone. *Nat Commun* **13**, 6755 (2022).
8. Akieda, Y. *et al.* Cell competition corrects noisy Wnt morphogen gradients to achieve robust patterning in the zebrafish embryo. *Nat Commun* **10**, 4710 (2019).
9. Moreno, E., Basler, K. & Morata, G. Cells compete for Decapentaplegic survival factor to prevent apoptosis in Drosophila wing development. *Nature* **416**, 755–759 (2002).
10. De La Cova, C., Abril, M., Bellosta, P., Gallant, P. & Johnston, L. A. Drosophila Myc Regulates Organ Size by Inducing Cell Competition. *Cell* **117**, 107–116 (2004).
11. Moreno, E. & Basler, K. dMyc Transforms Cells into Super-Competitors. *Cell* **117**, 117–129 (2004).
12. Johnston, L. A., Prober, D. A., Edgar, B. A., Eisenman, R. N. & Gallant, P. Drosophila myc Regulates Cellular Growth during Development. *Cell* **98**, 779–790 (1999).
13. Hogan, C. *et al.* Characterization of the interface between normal and transformed epithelial cells. *Nat Cell Biol* **11**, 460–467 (2009).
14. Kajita, M. *et al.* Interaction with surrounding normal epithelial cells influences

signalling pathways and behaviour of Src-transformed cells. *Journal of Cell Science* **123**, 171–180 (2010).

15. Kajita, M. & Fujita, Y. EDAC: Epithelial defence against cancer--cell competition between normal and transformed epithelial cells in mammals. *Journal of Biochemistry* **158**, 15–23 (2015).
16. Hashimoto, M. & Sasaki, H. Epiblast Formation by TEAD-YAP-Dependent Expression of Pluripotency Factors and Competitive Elimination of Unspecified Cells. *Developmental Cell* **50**, 139-154.e5 (2019).
17. Clavería, C., Giovinazzo, G., Sierra, R. & Torres, M. Myc-driven endogenous cell competition in the early mammalian embryo. *Nature* **500**, 39–44 (2013).
18. Lima, A. *et al.* Cell competition acts as a purifying selection to eliminate cells with mitochondrial defects during early mouse development. *Nat Metab* **3**, 1091–1108 (2021).
19. Morata, G. & Ripoll, P. Minutes: Mutants of Drosophila autonomously affecting cell division rate. *Developmental Biology* **42**, 211–221 (1975).
20. Haraoka, Y., Akieda, Y., Nagai, Y., Mogi, C. & Ishitani, T. Zebrafish imaging reveals TP53 mutation switching oncogene-induced senescence from suppressor to driver in primary tumorigenesis. *Nature Communications* **13**, 1417 (2022).
21. Rhiner, C. *et al.* Flower Forms an Extracellular Code that Reveals the Fitness of a Cell to its Neighbors in Drosophila. *Developmental Cell* **18**, 985–998 (2010).
22. Merino, M. M. *et al.* Elimination of Unfit Cells Maintains Tissue Health and Prolongs Lifespan. *Cell* **160**, 461–476 (2015).
23. Meyer, S. N. *et al.* An ancient defense system eliminates unfit cells from developing tissues during cell competition. *Science* **346**, 1258236 (2014).
24. Alpar, L., Bergantiños, C. & Johnston, L. A. Spatially Restricted Regulation of Spätzle/Toll Signaling during Cell Competition. *Developmental Cell* **46**, 706-719.e5 (2018).
25. Nagata, R., Nakamura, M., Sanaki, Y. & Igaki, T. Cell Competition Is Driven by Autophagy. *Dev Cell* **51**, 99-112.e4 (2019).

26. Katsukawa, M., Ohsawa, S., Zhang, L., Yan, Y. & Igaki, T. Serpin Facilitates Tumor-Suppressive Cell Competition by Blocking Toll-Mediated Yki Activation in Drosophila. *Current Biology* **28**, 1756-1767.e6 (2018).
27. Novitch, B. G., Chen, A. I. & Jessell, T. M. Coordinate regulation of motor neuron subtype identity and pan-neuronal properties by the bHLH repressor Olig2. *Neuron* **31**, 773–789 (2001).
28. Pierani, A. *et al.* Control of interneuron fate in the developing spinal cord by the progenitor homeodomain protein Dbx1. *Neuron* **29**, 367–384 (2001).
29. Park, H.-C., Mehta, A., Richardson, J. S. & Appel, B. olig2 Is Required for Zebrafish Primary Motor Neuron and Oligodendrocyte Development. *Developmental Biology* **248**, 356–368 (2002).
30. Gribble, S. L., Nikolaus, O. B. & Dorsky, R. I. Regulation and function of Dbx genes in the zebrafish spinal cord. *Dev Dyn* **236**, 3472–3483 (2007).
31. Lek, M. *et al.* A homeodomain feedback circuit underlies step-function interpretation of a Shh morphogen gradient during ventral neural patterning. *Development* **137**, 4051–4060 (2010).
32. Devoto, S. H., Melançon, E., Eisen, J. S. & Westerfield, M. Identification of separate slow and fast muscle precursor cells in vivo, prior to somite formation. *Development* **122**, 3371–3380 (1996).
33. Stickney, H. L., Barresi, M. J. & Devoto, S. H. Somite development in zebrafish. *Dev Dyn* **219**, 287–303 (2000).
34. Blagden, C. S., Currie, P. D., Ingham, P. W. & Hughes, S. M. Notochord induction of zebrafish slow muscle mediated by Sonic hedgehog. *Genes Dev.* **11**, 2163–2175 (1997).
35. Jessell, T. M. Neuronal specification in the spinal cord: inductive signals and transcriptional codes. *Nat Rev Genet* **1**, 20–29 (2000).
36. Dessaud, E., McMahon, A. P. & Briscoe, J. Pattern formation in the vertebrate neural tube: a sonic hedgehog morphogen-regulated transcriptional network. *Development* **135**, 2489–2503 (2008).
37. Ueda, Y., Shimizu, Y., Shimizu, N., Ishitani, T. & Ohshima, T. Involvement of sonic

hedgehog and notch signaling in regenerative neurogenesis in adult zebrafish optic tectum after stab injury. *J Comp Neurol* **526**, 2360–2372 (2018).

38. Incardona, J. P., Gaffield, W., Kapur, R. P. & Roelink, H. The teratogenic *Veratrum* alkaloid cyclopamine inhibits Sonic hedgehog signal transduction. *Development* **125**, 3553–3562 (1998).
39. Tsai, T. Y.-C. *et al.* An adhesion code ensures robust pattern formation during tissue morphogenesis. *Science* **370**, 113–116 (2020).
40. Lele, Z. *et al. parachute* / *n-cadherin* is required for morphogenesis and maintained integrity of the zebrafish neural tube. *Development* **129**, 3281–3294 (2002).
41. Franklin, J. L. & Sargent, T. D. Ventral neural cadherin, a novel cadherin expressed in a subset of neural tissues in the zebrafish embryo. *Dev. Dyn.* **206**, 121–130 (1996).
42. Sun, Y., Tseng, W.-C., Fan, X., Ball, R. & Dougan, S. T. Extraembryonic Signals under the Control of MGA, Max, and Smad4 Are Required for Dorsoventral Patterning. *Developmental Cell* **28**, 322–334 (2014).
43. Carter, M. E. & Brunet, A. FOXO transcription factors. *Current Biology* **17**, R113–R114 (2007).
44. Xie, X., Liu, J.-X., Hu, B. & Xiao, W. Zebrafish foxo3b Negatively Regulates Canonical Wnt Signaling to Affect Early Embryogenesis. *PLoS ONE* **6**, e24469 (2011).
45. Nogueira, V. *et al.* Akt Determines Replicative Senescence and Oxidative or Oncogenic Premature Senescence and Sensitizes Cells to Oxidative Apoptosis. *Cancer Cell* **14**, 458–470 (2008).
46. Han, J. *et al.* Expression of *bbc3* , a pro-apoptotic BH3-only gene, is regulated by diverse cell death and survival signals. *Proc. Natl. Acad. Sci. U.S.A.* **98**, 11318–11323 (2001).
47. Nakano, K. & Vousden, K. H. PUMA, a Novel Proapoptotic Gene, Is Induced by p53. *Molecular Cell* **7**, 683–694 (2001).
48. Yu, J., Zhang, L., Hwang, P. M., Kinzler, K. W. & Vogelstein, B. PUMA induces the rapid apoptosis of colorectal cancer cells. *Mol Cell* **7**, 673–682 (2001).
49. You, H. *et al.* FOXO3a-dependent regulation of Puma in response to cytokine/growth

factor withdrawal. *The Journal of Experimental Medicine* **203**, 1657–1663 (2006).

50. You, H., Yamamoto, K. & Mak, T. W. Regulation of transactivation-independent proapoptotic activity of p53 by FOXO3a. *Proc. Natl. Acad. Sci. U.S.A.* **103**, 9051–9056 (2006).
51. Tucka, J. *et al.* Akt1 Regulates Vascular Smooth Muscle Cell Apoptosis Through FoxO3a and Apaf1 and Protects Against Arterial Remodeling and Atherosclerosis. *ATVB* **34**, 2421–2428 (2014).
52. Boldin, M. P., Goncharov, T. M., Goltseve, Y. V. & Wallach, D. Involvement of MACH, a Novel MORT1/FADD-Interacting Protease, in Fas/APO-1- and TNF Receptor–Induced Cell Death. *Cell* **85**, 803–815 (1996).
53. Muzio, M. *et al.* FLICE, A Novel FADD-Homologous ICE/CED-3–like Protease, Is Recruited to the CD95 (Fas/APO-1) Death-Inducing Signaling Complex. *Cell* **85**, 817–827 (1996).
54. Alessi, D. R., Barry Caudwell, F., Andjelkovic, M., Hemmings, B. A. & Cohen, P. Molecular basis for the substrate specificity of protein kinase B; comparison with MAPKAP kinase‐1 and p70 S6 kinase. *FEBS Letters* **399**, 333–338 (1996).
55. Brunet, A. *et al.* Akt Promotes Cell Survival by Phosphorylating and Inhibiting a Forkhead Transcription Factor. *Cell* **96**, 857–868 (1999).
56. Lützner, N., Kalbacher, H., Krones-Herzig, A. & Rösl, F. FOXO3 Is a Glucocorticoid Receptor Target and Regulates LKB1 and Its Own Expression Based on Cellular AMP Levels via a Positive Autoregulatory Loop. *PLoS ONE* **7**, e42166 (2012).
57. Seoane, J., Le, H.-V., Shen, L., Anderson, S. A. & Massagué, J. Integration of Smad and Forkhead Pathways in the Control of Neuroepithelial and Glioblastoma Cell Proliferation. *Cell* **117**, 211–223 (2004).
58. Joly, J.-S. *et al.* Expression of a zebrafish caudal homeobox gene correlates with the establishment of posterior cell lineages at gastrulation. *Differentiation* **50**, 75–87 (1992).
59. Sunagawa, G. A. *et al.* Mammalian Reverse Genetics without Crossing Reveals Nr3a as a Short-Sleeper Gene. *Cell Reports* **14**, 662–677 (2016).
60. Wu, R. S. *et al.* A Rapid Method for Directed Gene Knockout for Screening in G0

Zebrafish. *Developmental Cell* **46**, 112-125.e4 (2018).

61. Suzuki, H. *et al. De novo* non-synonymous CTR9 variants are associated with motor delay and macrocephaly: human genetic and zebrafish experimental evidence. *Human Molecular Genetics* **31**, 3846–3854 (2022).
62. Kon, S. *et al.* Cell competition with normal epithelial cells promotes apical extrusion of transformed cells through metabolic changes. *Nat Cell Biol* **19**, 530–541 (2017).
63. Sancho, M. *et al.* Competitive Interactions Eliminate Unfit Embryonic Stem Cells at the Onset of Differentiation. *Developmental Cell* **26**, 19–30 (2013).
64. Hu, B. *et al.* Zebrafish eaf1 suppresses foxo3b expression to modulate transcriptional activity of gata1 and spi1 in primitive hematopoiesis. *Developmental Biology* **388**, 81–93 (2014).
65. Gao, L. *et al.* FOXO genes in channel catfish and their response after bacterial infection. *Developmental & Comparative Immunology* **97**, 38–44 (2019).
66. Villa del Campo, C., Clavería, C., Sierra, R. & Torres, M. Cell Competition Promotes Phenotypically Silent Cardiomyocyte Replacement in the Mammalian Heart. *Cell Reports* **8**, 1741–1751 (2014).
67. Ellis, S. J. *et al.* Distinct modes of cell competition shape mammalian tissue morphogenesis. *Nature* **569**, 497–502 (2019).
68. Sun, X.-L. *et al.* Stem cell competition driven by the Axin2-p53 axis controls brain size during murine development. *Developmental Cell* **58**, 744-759.e11 (2023).
69. Adachi-Yamada, T., Fujimura-Kamada, K., Nishida, Y. & Matsumoto, K. Distortion of proximodistal information causes JNK-dependent apoptosis in Drosophila wing. *Nature* **400**, 166–169 (1999).
70. Adachi-Yamada, T. & O'Connor, M. B. Morphogenetic Apoptosis: A Mechanism for Correcting Discontinuities in Morphogen Gradients. *Developmental Biology* **251**, 74–90 (2002).
71. Van Den Brink, G. R. *et al.* Indian Hedgehog is an antagonist of Wnt signaling in colonic epithelial cell differentiation. *Nat Genet* **36**, 277–282 (2004).
72. Farin, H. F. *et al.* Visualization of a short-range Wnt gradient in the intestinal stem-cell

niche. *Nature* **530**, 340–343 (2016).

73. Wang, C. *et al.* Expansion of hedgehog disrupts mesenchymal identity and induces emphysema phenotype. *Journal of Clinical Investigation* **128**, 4343–4358 (2018).
74. Powell, D. R. *et al.* Cdon promotes neural crest migration by regulating N-cadherin localization. *Developmental Biology* **407**, 289–299 (2015).
75. Aoki, K. *et al.* Mechano-gradients drive morphogen-noise correction to ensure robust patterning. *Sci. Adv.* **10**, eadp2357 (2024).
76. Van Der Vos, K. E. & Coffer, P. J. FOXO-binding partners: it takes two to tango. *Oncogene* **27**, 2289–2299 (2008).
77. Daitoku, H., Sakamaki, J. & Fukamizu, A. Regulation of FoxO transcription factors by acetylation and protein–protein interactions. *Biochimica et Biophysica Acta (BBA) - Molecular Cell Research* **1813**, 1954–1960 (2011).
78. Calissi, G., Lam, E. W.-F. & Link, W. Therapeutic strategies targeting FOXO transcription factors. *Nat Rev Drug Discov* **20**, 21–38 (2021).
79. Hagenbuchner, J. & Ausserlechner, M. J. Mitochondria and FOXO3: breath or die. *Front. Physiol.* **4**, (2013).
80. Kinzler, K. W. *et al.* Identification of FAP Locus Genes from Chromosome 5q21. *Science* **253**, 661–665 (1991).
81. Nishisho, I. *et al.* Mutations of chromosome 5q21 genes in FAP and colorectal cancer patients. *Science* **253**, 665–669 (1991).
82. Oro, A. E. *et al.* Basal cell carcinomas in mice overexpressing sonic hedgehog. *Science* **276**, 817–821 (1997).
83. Xie, J. *et al.* Activating Smoothened mutations in sporadic basal-cell carcinoma. *Nature* **391**, 90–92 (1998).
84. Fei, M. *et al.* Low expression of Foxo3a is Associated with Poor Prognosis in Ovarian Cancer Patients. *Cancer Investigation* **27**, 52–59 (2009).
85. Shou, Z., Lin, L., Liang, J., Li, J.-L. & Chen, H.-Y. Expression and prognosis of FOXO3a and HIF-1α in nasopharyngeal carcinoma. *J Cancer Res Clin Oncol* **138**, 585–593 (2012).

86. Willcox, B. J. *et al.* FOXO3A genotype is strongly associated with human longevity. *Proc. Natl. Acad. Sci. U.S.A.* **105**, 13987–13992 (2008).
87. Martins, R., Lithgow, G. J. & Link, W. Long live FOXO : unraveling the role of FOXO proteins in aging and longevity. *Aging Cell* **15**, 196–207 (2016).
88. Timmers, P. R. H. J., Wilson, J. F., Joshi, P. K. & Deelen, J. Multivariate genomic scan implicates novel loci and haem metabolism in human ageing. *Nat Commun* **11**, 3570 (2020).
89. Zhang, W. *et al.* A single-cell transcriptomic landscape of primate arterial aging. *Nat Commun* **11**, 2202 (2020).
90. Liu, X. *et al.* Forkhead Transcription Factor 3a (FOXO3a) Modulates Hypoxia Signaling via Up-regulation of the von Hippel-Lindau Gene (VHL). *Journal of Biological Chemistry* **291**, 25692–25705 (2016).
91. Wada, H. *et al.* Wnt/Dkk Negative Feedback Regulates Sensory Organ Size in Zebrafish. *Current Biology* **23**, 1559–1565 (2013).
92. Sasaki, H., Hui, C., Nakafuku, M. & Kondoh, H. A binding site for Gli proteins is essential for *HNF-3* β floor plate enhancer activity in transgenics and can respond to Shh in vitro. *Development* **124**, 1313–1322 (1997).
93. Shimizu, N., Kawakami, K. & Ishitani, T. Visualization and exploration of Tcf/Lef function using a highly responsive Wnt/β-catenin signaling-reporter transgenic zebrafish. *Developmental Biology* **370**, 71–85 (2012).
94. Taipale, J. *et al.* Effects of oncogenic mutations in Smoothened and Patched can be reversed by cyclopamine. *Nature* **406**, 1005–1009 (2000).
95. Kinzler, K. W., Ruppert, J. M., Bigner, S. H. & Vogelstein, B. The GLI gene is a member of the Kruppel family of zinc finger proteins. *Nature* **332**, 371–374 (1988).
96. Zhang, Y. *et al.* Structural Basis for Cholesterol Transport-like Activity of the Hedgehog Receptor Patched. *Cell* **175**, 1352-1364.e14 (2018).
97. Jia, S., Ren, Z., Li, X., Zheng, Y. & Meng, A. smad2 and smad3 are required for mesendoderm induction by transforming growth factor-beta/nodal signals in zebrafish. *J Biol Chem* **283**, 2418–2426 (2008).

98. Wang, F. *et al.* Structures of KIX domain of CBP in complex with two FOXO3a transactivation domains reveal promiscuity and plasticity in coactivator recruitment. *Proc. Natl. Acad. Sci. U.S.A.* **109**, 6078–6083 (2012).
99. Zhang, J. *et al.* Visualization of caspase-3-like activity in cells using a genetically encoded fluorescent biosensor activated by protein cleavage. *Nat Commun* **4**, 2157 (2013).
100. Bindels, D. S. *et al.* mScarlet: a bright monomeric red fluorescent protein for cellular imaging. *Nat Methods* **14**, 53–56 (2017).
101. Yamamoto, K., Ichijo, H. & Korsmeyer, S. J. BCL-2 Is Phosphorylated and Inactivated by an ASK1/Jun N-Terminal Protein Kinase Pathway Normally Activated at G $_2$ /M. *Molecular and Cellular Biology* **19**, 8469–8478 (1999).
102. Ansai, S. *et al.* Genome editing reveals fitness effects of a gene for sexual dichromatism in Sulawesian fishes. *Nat Commun* **12**, 1350 (2021).
103. Hwang, W. Y. *et al.* Efficient genome editing in zebrafish using a CRISPR-Cas system. *Nat Biotechnol* **31**, 227–229 (2013).
104. Kimura, Y., Hisano, Y., Kawahara, A. & Higashijima, S. Efficient generation of knock-in transgenic zebrafish carrying reporter/driver genes by CRISPR/Cas9-mediated genome engineering. *Sci Rep* **4**, 6545 (2014).
105. Kardash, E. Current Methods in Zebrafish Research. *MATER METHODS* **2**, (2012).
106. Lee, Y. A., Cho, E. J. & Yokozawa, T. Protective Effect of Persimmon (Diospyros kaki) Peel Proanthocyanidin against Oxidative Damage under H2O2-Induced Cellular Senescence. *Biological & Pharmaceutical Bulletin* **31**, 1265–1269 (2008).
107. Thisse, C. & Thisse, B. High-resolution in situ hybridization to whole-mount zebrafish embryos. *Nat Protoc* **3**, 59–69 (2008).
108. Brend, T. & Holley, S. A. Zebrafish whole mount high-resolution double fluorescent in situ hybridization. *J Vis Exp* 1229 (2009) doi:10.3791/1229.
109. Tsuneoka, Y. & Funato, H. Modified in situ Hybridization Chain Reaction Using Short Hairpin DNAs. *Front. Mol. Neurosci.* **13**, 75 (2020).
110. Prieto, C. & Barrios, D. RaNA-Seq: interactive RNA-Seq analysis from FASTQ files to

functional analysis. *Bioinformatics* **36**, 1955–1956 (2020).

111. Behringer, R. *Manipulating the Mouse Embryo: A Laboratory Manual*. (Cold Spring Harbor Laboratory Press, Cold Spring Harbor, New York, 2014).
112. Hao, Y. *et al.* Integrated analysis of multimodal single-cell data. *Cell* **184**, 3573-3587.e29 (2021).

Acknowledgements

I would like to express my gratitude to my supervisors, Professor Tohru Ishitani and Dr. Yuki Akieda, for their continuous guidance and unwavering support throughout my research. I am very thankful for the opportunity you have given me.

My special thanks to Dr. Yukinari Haraoka for performing Foxo3-related work in zebrafish, and Professor Hiroshi Sasaki and Mr. Naoki Hirono for the invaluable advice and cooperation during the mouse experiments.

I would also like to acknowledge Prof. Dr. Kenji Matsuno and Prof. Dr. Asako Shindo for critically reading this dissertation and for their valuable discussions.

Many thanks to my family and friends for their love and continuous support. Despite the challenges of this journey, it would have been insurmountable without each and every one of them over these past five years.

Last but not least, I would like to express my appreciation to Japan Science and Technology Agency (Grant-in-Aid for JST SPRING) and the Japan Society for the Promotion of Science (Grant-in-Aid for JSPS Fellows, Grant No. 24KJ1617) for their wonderful support throughout my doctoral study.